

# Hot Forming of Boron Steels with Tailored Mechanical Properties

## Experiments and Numerical Simulations

by  
Ryan George

A thesis  
presented to the University of Waterloo  
in fulfillment of the  
thesis requirement for the degree of  
Master of Applied Science  
in  
Mechanical Engineering

Waterloo, Ontario, Canada, 2011

© Ryan George 2011

I hereby declare that I am the sole author of this thesis. This is a true copy of the thesis, including any required final revisions, as accepted by my examiners.

I understand that my thesis may be made electronically available to the public.

## Abstract

Hot forming of boron steels is becoming increasingly popular in the automotive industry due to the demands for weight reduction and increased safety requirements for new vehicles. Hot formed components offer a significant increase in strength over conventional cold-formed steels, which has allowed for reductions in material thickness (and thus weight) while maintaining the same strength. Hot formed components are typically used in structural applications to improve the integrity of the vehicle's cabin in the event of a collision. It has been suggested, however, that the crash performance of certain hot formed parts may be increased by locally tailoring their mechanical properties to improve their energy absorption. The final microstructure of a hot formed part is driven by the rate at which it is cooled within the tooling during the forming and quenching process. By controlling the cooling rate of the part, it is possible to control the final microstructure, and thus the final mechanical properties.

This thesis outlines the experimental and numerical studies that were performed for the hot forming of a lab-scale B-pillar. A hot forming die set was developed which has both heating and cooling capabilities to control the local cooling rate of the blank as it is formed and quenched. The first aspect of this research is to produce a hot formed part which is representative of an industrial component, and then to numerically model the process to predict the final mechanical properties. The second aspect is to produce a hot formed part with tailored mechanical properties, such that there are regions of the part with very high strength (very hard) and other regions with increased ductility (softer). By tailoring the microstructure to meet the performance requirement of a hot formed part, it may be possible to optimize its crash behavior and also reduce the overall weight.

Cartridge heaters were installed into sections of the tooling allowing it to reach a maximum temperature of 400°C. Cooling channels are used in other sections to maintain it at approximately room temperature. Experiments were performed on 1.2 mm Usibor® 1500P steel at heated die temperatures ranging from 25°C to 400°C. In the fully cooled region, the Vickers hardness of the blank was measured to be 450 – 475 HV, on average. As the temperature of the heated region was increased, a significant softening trend was observed in the areas of the blank that were in contact with the heated tool. The greatest levels of softening occurred in the 400°C heated die trial. Hardness measurements as low as 234 HV were recorded, which represents a reduction in hardness of 49% compared to the fully cooled trials.

Numerical models of the experiments were developed using LS-DYNA and use of its advanced hot forming material model which allows for microstructure and hardness prediction within the final part. The numerical models have shown promising results in terms of predicting the hardness trends as the temperature of the die increases.

Thermal expansion of the tooling resulted in local changes in the geometry of the tooling which proved to be problematic during the forming and quenching stages of the process. The expansion caused unexpected changes in the part-die contact, and the resulting microstructures were altered. These thermal expansion issues were addressed in the current work by shimming the tooling; however, in future work the tooling should be designed to account for this expansion at the desired operating temperature.



## **Acknowledgements**

I would like to thank my supervisor, Dr. Michael Worswick, for giving me the opportunity to work within his elite group of researchers on this very exciting and fulfilling project. It has been an excellent learning experience and I feel that it has helped me a great deal to prepare myself for the “real world” of engineering.

This project has been generously supported by several industrial partners, including: Honda R&D North America, Promatek Research Center (MAGNA), and ArcelorMittal/Dofasco. Additional funding was also provided by: Initiative for Automotive Manufacturing Innovation (IAMI) / Ontario Research Fund (ORF), and the Natural Sciences and Engineering Research Council (NSERC).

I would like to thank Alex Bardelcik for his guidance and knowledge of all things “grad student” related. He has been a great role model throughout my time here as a masters student and I have learned a lot from him. My office mates Brock, Jason, Jenn, and Jon, have all made life in E3-3101G that much more entertaining. The homebrew that Andrew and I developed has also been essential for surviving grad school and the “difficulties” that arise. I would also like to thank Jill Redman for her endless motivation for me to finish my thesis and her constant reminding me of how much smarter she thinks she is.

Andy Barber, Eckhard Budziarek, and Tom Gawel have all given tremendous amounts of time in the lab dealing with the equipment and the many problems that always occur... Their support and experience have been invaluable for me to finish the many hours of experiments.

Finally, I would like to thank my parents for their unconditional support and motivation throughout my time here.

*To my parents*

# Contents

Author’s Declaration.....	ii
Abstract.....	iii
Acknowledgements.....	v
Dedication.....	vi
List of Figures .....	x
List of Tables .....	xiii
1 Introduction & Background .....	1
1.1 Hot Forming Die Quenching.....	1
1.2 Hot Forming Material.....	4
1.3 Blank Heating Technologies .....	6
1.3.1 Convection Furnace .....	6
1.3.2 Conduction/Resistance Heating.....	6
1.3.3 Induction Heating.....	6
1.4 Tailored Properties.....	7
1.4.1 Tailor Welded Blanks .....	7
1.4.2 Partial Austenizing in Furnace.....	8
1.4.3 Post Tempering .....	9
1.4.4 Die Materials with varying Thermal Conductivity.....	9
1.4.5 Partially Heated Dies .....	9
1.5 Numerical Modeling.....	10
1.5.1 Material Models.....	11
1.5.2 Heat Transfer Coefficient (HTC) .....	11
1.6 Current Work .....	12
2 Equipment and Experimental Methods.....	15
2.1 Material.....	15
2.2 Tooling.....	16
2.3 Furnace.....	18
2.4 Transfer System .....	20
2.5 Press & Hydraulics.....	21
2.6 Part Design & Geometry .....	22
2.7 Areas of Interest.....	23

2.8	Sample Preparation .....	24
3	Experiments .....	28
3.1	Die Alignment.....	30
3.2	Experimental Results.....	31
3.2.1	Baseline – Die Fully Cooled .....	31
3.2.2	Heated Die Results – 100°C.....	33
3.2.3	Heated Die Results – 200°C.....	35
3.2.4	Heated Die Results – 300°C.....	37
3.2.5	Heated Die Results – 350°C.....	39
3.2.6	Heated Die Results – 400°C.....	41
3.3	Thermal Expansion of the Tooling .....	43
3.3.1	Heated Die Results – 400°C with Shimmed Tooling.....	45
4	Numerical Modeling.....	48
4.1	Tooling Mesh and Configuration.....	49
4.1.1	Steady-State Thermal Distribution.....	51
4.1.2	Material Properties and Definitions.....	53
4.2	Blank Design and Definition.....	53
4.2.1	Blank Material Model & Validation.....	55
4.3	Free Cooling Validation .....	57
4.4	Heat Transfer Coefficient.....	59
4.4.1	HTC Study .....	59
4.5	Numerical Results .....	63
4.5.1	Die Fully Cooled – 25°C .....	64
4.5.2	Heated Die – 100°C .....	65
4.5.3	Heated Die – 200°C .....	67
4.5.4	Heated Die – 300°C .....	69
4.5.5	Heated Die – 350°C .....	71
4.5.6	Heated Die – 400°C .....	73
4.5.7	Heated Die 400°C with Shim .....	75
4.6	Thermal Expansion.....	76
4.6.1	300°C.....	78
4.6.2	350°C.....	79

4.6.3	400°C .....	81
5	Summary of Results .....	83
6	Discussion, Conclusions, and Recommendations .....	88
6.1	Discussion.....	88
6.2	Conclusions .....	89
6.2.1	Experiments .....	89
6.2.2	Simulations.....	90
6.3	Recommendations .....	90
6.3.1	Experiments .....	90
6.3.2	Simulations.....	91
	References .....	93
	Appendices	
	Appendix A – Usibor® 1500P CCT .....	96
	Appendix B – LS-DYNA Material Model .....	98
	Appendix C – Press Modification CAD .....	108
	Appendix D – Press Operation Procedures.....	113
	Appendix E – LS-DYNA Simulation Steps.....	120
	Appendix F – Convection and Radiation Parameters .....	122

## List of Figures

Figure 1 - Typical Steels used in the Automotive Industry, adapted from [1].	2
Figure 2 - Common Hot Formed Structural Components [1]	2
Figure 3 - Direct and Indirect Hot Forming [6]	3
Figure 4 - CCT Diagram for Usibor® 1500P [16]	5
Figure 5 – Regions of tailored mechanical properties [7]	7
Figure 6 - Example of Tailor Welded Blanks, adapted from [14]	8
Figure 7 – (a) Simple die with embedded heating and cooling (b) Effect of die temperature on the cooling rates [26]	10
Figure 8 - Mechanical, thermal, and microstructural interactions, adapted from [28]	11
Figure 9 - Typical contact zone for blank-tool heat exchange	12
Figure 10 - Automotive and University of Waterloo B-Pillars	14
Figure 11 - Schematic of tooling	16
Figure 12 - Location of the cartridge heaters	17
Figure 13 - Approximate shim thickness versus temperature	18
Figure 14 - Press & Furnace Layout	19
Figure 15 - Heating of Instrumented Blank	19
Figure 16 - Transfer Mechanism	20
Figure 17 - Press Actuator Modifications	21
Figure 18 - Final Part Geometry	22
Figure 19 - Tooling cross section & draw bead	23
Figure 20 - Sample Locations	24
Figure 21 - Laser-cut samples	24
Figure 22 - Vickers Microhardness (a) Schematic of indenter (b) Sample micrograph of a Vickers microhardness test	25
Figure 23 - Sample preparation (H1 - H4)	26
Figure 24 - H1 to H4 measurement details	26
Figure 25 - Sample preparation (a) H5, (b) H6	27
Figure 26 - H5 & H6 orientation and reference positions	27
Figure 27 - Process flow-chart	29
Figure 28 - Typical punch force & displacement	30

Figure 29 - Die Alignment .....	31
Figure 30 - Baseline experimental results (H1 - H4) .....	32
Figure 31 - Baseline experimental results (H5 & H6).....	33
Figure 32 – Experimental results 100°C (H1-H4) .....	34
Figure 33 – Experimental results 100°C (H5 & H6) .....	35
Figure 34 – Experimental results 200°C (H1-H4) .....	36
Figure 35 - Experimental results 200°C (H5 & H6).....	37
Figure 36 - Experimental results 300°C (H1-H4) .....	38
Figure 37 - Experimental results 300°C (H5 & H6).....	39
Figure 38 - Experimental results 350°C (H1-H4) .....	40
Figure 39 - Experimental results 350°C (H5 & H6).....	41
Figure 40 - Experimental results 400°C (H1-H4) .....	42
Figure 41 - Experimental results 400°C (H5 & H6).....	43
Figure 42 - (a) Thermal expansion of the die (b) Rotation of slide/upper tooling.....	44
Figure 43 - Shims installed .....	45
Figure 44 - 400°C (H1-H4) shimmed die .....	46
Figure 45 - 400°C (H5 & H6) shimmed die .....	47
Figure 46 - Half-symmetry model .....	49
Figure 47 - Insulation & air gap model.....	50
Figure 48 - Coarse solid mesh .....	50
Figure 49 - Tied surfaces for forming.....	51
Figure 50 - Cartridge Heater Locations .....	51
Figure 51 - Thermal Boundary Conditions .....	52
Figure 52 - Temperature Distribution (350°C) .....	52
Figure 53 - Blank Mesh.....	54
Figure 54 - Adaptive Meshing .....	54
Figure 55 - Material Model Numerical Validation .....	55
Figure 56 - Hardness Validation .....	56
Figure 57 - Perfectly linear cooling (solid lines) and constant flux cooling (dotted lines).....	57
Figure 58 - Free Cooling Validation.....	58
Figure 59 - HTC Study - Graph.....	60

Figure 60 - HTC Study - Hardness Contour Plots for selected trials at 300°C to 400°C, showing effect of HTC on resulting predicted hardness.....	60
Figure 61 - HTC Study - Hardness comparison.....	61
Figure 62 - Air cooling compared to 400°C die quenching .....	62
Figure 63 - Hardness Contour Plot (25°C) .....	64
Figure 64 - Numerical Results (25°C) .....	65
Figure 65 - Hardness Contour Plot (100°C) .....	66
Figure 66 - Numerical Results (100°C) .....	67
Figure 67 - Hardness Contour Plot (200°C) .....	68
Figure 68 - Numerical Results (200°C) .....	69
Figure 69 - Hardness Contour Plot (300°C) .....	70
Figure 70 - Numerical Results (300°C) .....	71
Figure 71 - Hardness Contour Plot (350°C) .....	72
Figure 72 - Numerical Results (350°C) .....	73
Figure 73 - Hardness Contour Plot (400°C) .....	74
Figure 74 - Numerical Results (400°C) .....	75
Figure 75 - Numerical Results (400°C) with shim.....	76
Figure 76 - Thermal Expansion (a) Uniform die scaling, (b) Addition DOF .....	77
Figure 77 - Hardness Contour Plot (300°C) Thermal Die Expansion .....	78
Figure 78 - Numerical Results (300°C) Thermal Die Expansion .....	79
Figure 79 - Hardness Contour Plot (350°C) Thermal Die Expansion .....	80
Figure 80 - Numerical Results (350°C) Thermal Die Expansion .....	80
Figure 81 - Hardness Contour Plot (400°C) Thermal Die Expansion .....	81
Figure 82 - Numerical Results (400°C) Thermal Die Expansion .....	82
Figure 83 - Experimental Summary (H1-H4) .....	84
Figure 84 - Numerical Summary (H1-H4) .....	85
Figure 85 - Transition Zone Width Description .....	86
Figure 86 - Transition Zone Width .....	87



## List of Tables

Table 1 - Material Composition .....	15
Table 2 – Test Matrix .....	28
Table 3 - Mass Scaling Factors .....	49
Table 4 - Material Thermal Properties.....	53
Table 5 - Heat Transfer Coefficients.....	63

# 1 Introduction & Background

The demand for weight reduction in the automotive industry has led to the development and implementation of new lightweight materials and manufacturing processes. The growing concern for occupant safety also leads to the adoption of materials which improve the integrity of the vehicle during a crash while also improving the energy absorption and crash deformation predictability. A process known as Hot Forming Die Quenching (HFDQ) (also *hot stamping* or *press hardening*) uses boron steel sheets to create stamped components with Ultra High Strength Steel (UHSS) properties, with tensile strengths up to 1,500 MPa. This is accomplished by in-die quenching of a pre-heated blank as it is being formed which causes a solid-state phase transformation from austenite to martensite. The increase in strength allows for a thinner gauge material to be used, which results in a weight savings over conventionally cold-stamped mild steel components.

The objectives of this research were to design and implement a lab-sized tool used for Hot Forming Die Quenching (HFDQ) experiments, and to develop a computer model using LS-DYNA to predict the forming behavior and as-formed mechanical properties of the parts. HFDQ is a process which relies on the simultaneous rapid quenching of the heated boron steel as it is being formed within the tooling. The high cooling rates trigger a phase transformation from austenite to martensite, which is very hard and strong and is suitable for anti-intrusion structural components in an automotive unibody. Particular grades of boron steel are developed by steel manufacturers specifically for the use in HFDQ applications.

Another significant component of this work is to investigate the feasibility of producing a hot-formed part with tailored mechanical properties (regions of high strength and other regions of increased ductility), in an effort to improve the crash performance of certain structural HFDQ members.

## 1.1 Hot Forming Die Quenching

There are several types of steel commonly used in the automotive industry, which cover a wide range of mechanical properties. A particular grade of steel may be chosen for its strength or ductility, depending on the application. Figure 1 compares the total elongation vs. tensile strength for common steels used in the automotive industry. Mild and low strength steels are able to deform to quite high levels of strain before failure, which is beneficial for both energy absorption and the forming of complicated geometries. The trade-off with using mild or low strength metals is their low tensile strength, which requires a much thicker gauge to be used for structural applications. The quenched martensitic steels

used in this research have considerably higher strengths; however, their low ductility tends to limit their use in crush structures and other energy-absorbing components.

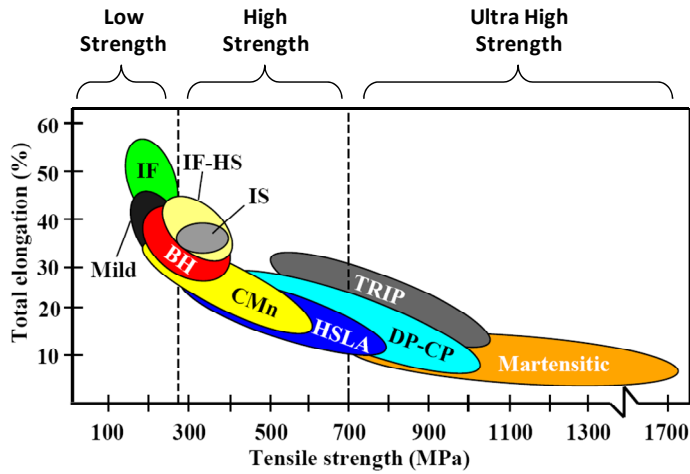
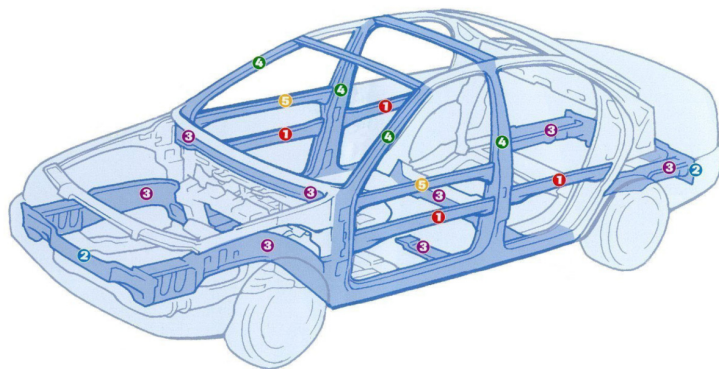


Figure 1 - Typical Steels used in the Automotive Industry, adapted from [1].

Hot formed parts are becoming more common in vehicles today due to their excellent strength and formability. Many structural members which were traditionally cold formed from mild steel, are being replaced with hot formed equivalents. Typical parts which are manufactured using the HFDQ process include: door beams, bumper beams, cross/side members, A/B pillar reinforcements, and waist rail reinforcements (Figure 2).



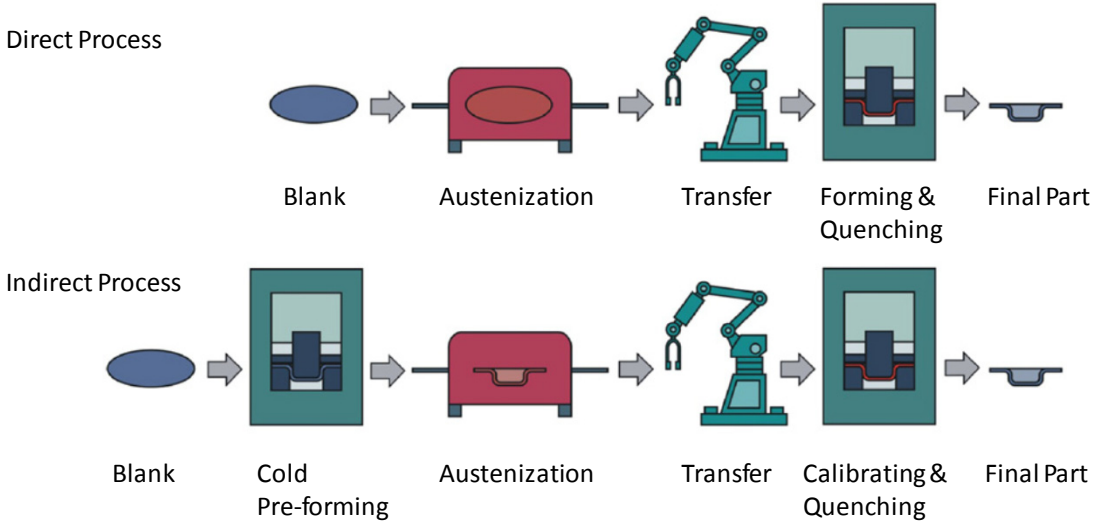
1. Door Beam
2. Bumper Beam
3. Cross / Side Members
4. A/B Pillar Reinforcements
5. Waist Rail Reinforcements

Figure 2 - Common Hot Formed Structural Components [1]

Hot forming is a well-understood process which was developed and patented in 1974 by NJA Steel Works in Luleå, Sweden, which merged to SSAB Hardtech and is known today as Gestamp Hardtech [2].

A hot formed part is produced by heating a boron-steel blank to 900-950°C for 3-10 minutes such that

the microstructure becomes fully austenized [3-5]. The blank is then rapidly formed and quenched at a rate greater than 30°C/s which transforms the austenite into 100% martensite. There are two general classifications of hot forming: direct and indirect (Figure 3, adapted from [6]).



**Figure 3 - Direct and Indirect Hot Forming [6]**

In the direct forming method, a furnace is used to heat the blank to the austenizing temperature for the required time. The hot blank is quickly transferred from the furnace to the press where it is simultaneously formed and quenched using a cooled die set. The cooled part is then removed and may be trimmed or punched to produce the final part. The increased ductility and reduced flow stress of the hot blank allows for excellent formability and the ability to form complex parts with a single stroke. The direct forming method is used for the experiments in this work.

The indirect forming method involves a cold-forming operation first, where a room temperature blank is stamped to 90-95% of its final shape. It is then transferred to the furnace and continues exactly the same as the direct forming method.

A component with a fully martensitic microstructure is generally desirable for its high strength and intrusion resistance. The high strength-to-weight ratio of these parts allows for a lighter gauge material to be used, which can offer a significant weight reduction over conventional cold formed parts. These hot formed parts, however, offer very low levels of ductility and energy absorption in the as-formed condition. It may be possible to introduce softer regions within a single part to improve the ductility and energy absorption in key areas, while maintaining the required high strength and intrusion resistance in

other regions. By tailoring the microstructure and mechanical properties of certain structural parts, it may be possible to improve overall energy absorption and maintain structural integrity during a crash situation [7].

## **1.2 Hot Forming Material**

The material used for this research is USIBOR® 1500P, manufactured by ArcelorMittal. This material has an aluminum-silicon coating which prevents oxidation and decarburization of the base metal during the hot stamping process [8]. The as-received microstructure of boron steels is typically composed of ferrite and pearlite and has an Ultimate Tensile Strength (UTS) of approximately 400 - 600 MPa and elongation of 20% [9-11].

The process of creating a hot formed part is fairly simple and consists of three major steps: heating, holding/soaking, and quenching. The first stage involves heating the blank above the austenization temperature, which is typically done at 900°C – 950°C. Holding at this temperature allows the microstructure to transform to homogeneous austenite, which requires approximately 3-10 minutes. The final step in hot forming is to quench the austenized blank; the rate at which it is quenched will determine the final microstructure.

In addition to the desirable high strength and hardness of a hot formed part, there are other benefits to the actual forming of the parts using this process. When boron steels are heated to the austenitic state (>850°C) the flow stress dramatically decreases and allows for greater forming limits and strains prior to failure [3,12]. This increased ductility allows for the forming of complex geometries in a single operation. Another benefit over conventionally cold-stamped high strength steels is the reduction in forming forces and significant reduction in springback as a result of the residual stresses being relieved during the solid-state transformation of austenite to martensite [7,8,11,13,14].

A Continuous Cooling Transformation (CCT) diagram (Figure 4) is often used to illustrate the effect of cooling rate on the final microstructure of a material that undergoes phase transformations during cooling. Depending on the cooling rate of the material from the austenization temperature, different microstructures will be formed as the material is cooled to room temperature. The final microstructure can be approximated by examining the CCT for a given line of constant cooling rate and observing which microstructure “windows” the line passes through. The CCT diagram is determined by performing dilatometer tests, in which a small sample is precisely cooled at a controlled rate and its exact change in

length is measured [15]. The decomposition of austenite into the other phases causes a change in crystal structure which each have a characteristic volume that can be measured as a change in length. These length changes indicate when a microstructural transformation is occurring and a point on the CCT can be generated. Figure 4 displays the CCT diagram for Usibor® 1500P, showing lines of constant cooling rates and the measured Vickers hardness (HV) after cooling to room temperature. This particular figure has been adapted from a CCT diagram supplied by ArcelorMittal [16], found in Appendix A. The critical cooling rate of approximately 30°C/s is shown which is the minimum cooling rate required to obtain a final microstructure that is 100% martensite.

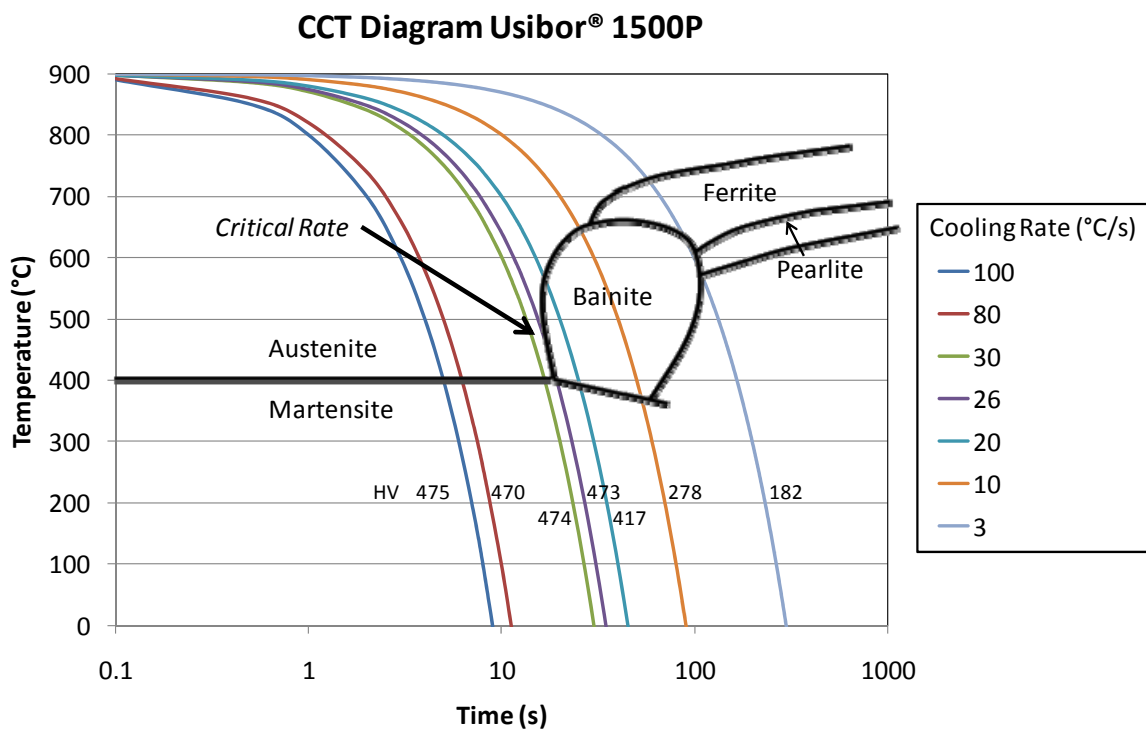


**Figure 4 - CCT Diagram for Usibor® 1500P [16]**

The term “boron steel” is used because of the additions of boron to the base steel composition, which improves the hardenability of the steel. Hardenability is defined as the ease in which steels can be quenched to form martensite; more specifically, the critical cooling rate which is necessary to form a fully martensitic microstructure [17]. A more hardenable steel has a slower critical cooling rate.

## **1.3 Blank Heating Technologies**

There are several methods of heating a steel blank to its austenization temperature for the purposes of hot forming. This section outlines several common heating methods and their suitability for an industrial application.

### **1.3.1 Convection Furnace**

The conventional blank heating method used by many original equipment manufacturers (OEM) involves long furnaces where the blanks are fed into one end and continue along rollers through to the other side. These are commonly known as roller-hearth furnaces and are typically 30-40 meters in length [6]. As the blank travels through the furnace it is heated to its austenization temperature and held for a length of time such that the microstructure transforms to 100% austenite. The length of the furnace is dictated both by the required through-put of the stamping line and the residence time of the blank inside the furnace. Several temperature stages can be built into the furnace to control the heat-up rate of the blank. It has been recommended that heating rates of around 12°C/s are to be used to avoid melting of the aluminum-silicon surface coating and to improve the diffusion of iron into this layer [5].

### **1.3.2 Conduction/Resistance Heating**

Conduction heating is achieved by passing an electric current through the blank to generate internal heat through resistance heating, as described by Joule's Law. The heat generation in the material is directly proportional to the power that is applied and is highly dependent on the geometry of the blank and the placement of the electrodes. It is also possible for "hot-spots" to form, where defects or irregularities in the sheet result in a higher current density. It is difficult to evenly heat a blank with complicated geometry, as the current will favor a path with the shortest distance between the electrodes [5,18,19]. Although the space requirement for a conductive heating line is considerably less than that of a roller-hearth furnace, it is due to these short-comings that this heating method does not have any large-scale industrial adoption for HFDQ. Experiments in [20] make use of a resistance heating system for hot forming of simple rectangular strips and showed no detrimental effects on the final specimens by using this heating method.

### **1.3.3 Induction Heating**

Induction heating is commonly used in several industrial applications, such as tempering and heat treating metals. Similar to resistive heating, induction heating requires very little time to fully heat the material. As the blank is passed through the inductor, current is induced in the bulk of the blank material

and heat is generated. The frequency of the inductor is one of the parameters which can control the depth of the heat generated in the part. There is currently no industrial use of induction heating for hot stamping, although significant research is being done by Kolleck and Merklein *et al* [5] at the University of Graz and University of Erlangen-Nuremberg.

## 1.4 Tailored Properties

Traditionally, hot formed parts are designed to have a fully martensitic microstructure such that the maximum strength and anti-intrusion performance can be achieved. It has been suggested, however, that some hot-formed parts may benefit from regions of lower strength and increased ductility for crash performance [7,21]. A hot formed B-Pillar, for example, could be improved by reducing the martensite content at one or both ends to improve the deformation and energy absorption, while maintaining a fully martensitic microstructure through the center section where intrusion resistance is essential [14].

Figure 5 illustrates this concept.

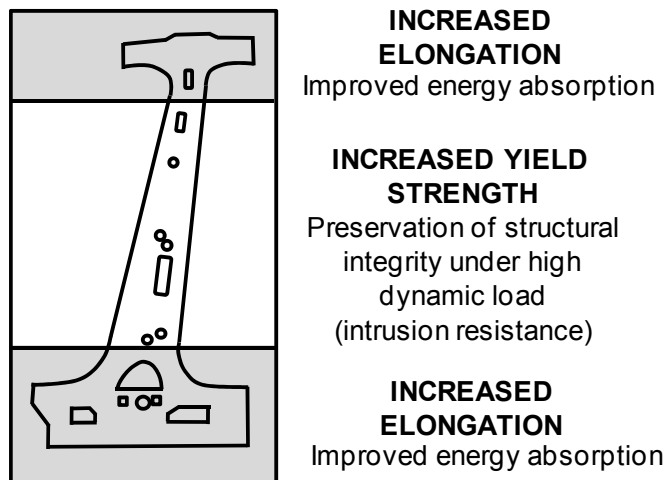


Figure 5 – Regions of tailored mechanical properties [7]

There are several existing methods for controlling the properties of a hot formed part, each with their own benefits and drawbacks:

### 1.4.1 Tailor Welded Blanks

ArcelorMittal produces tailor-welded blanks (TWB) which consist of USIBOR® 1500P and a new material called DUCTIBOR® 500P. The DUCTIBOR® is a hot stamping material which is designed to maintain high ductility after forming and quenching, with a UTS of 500 MPa and elongation at fracture over 15% [8,14].



The combination of the two steel grades produces a part with both high strength and high ductility regions. Figure 6 shows a comparison of a rear frame rail which has been produced from a tailor welded blank. Work presented by Múnera, *et al* [21,22] has shown significant weight savings by the use of TWB while maintaining or improving the crash response of the components that were examined. The drawback of TWB is the need for an additional processing step and increased complexity of the blanks.

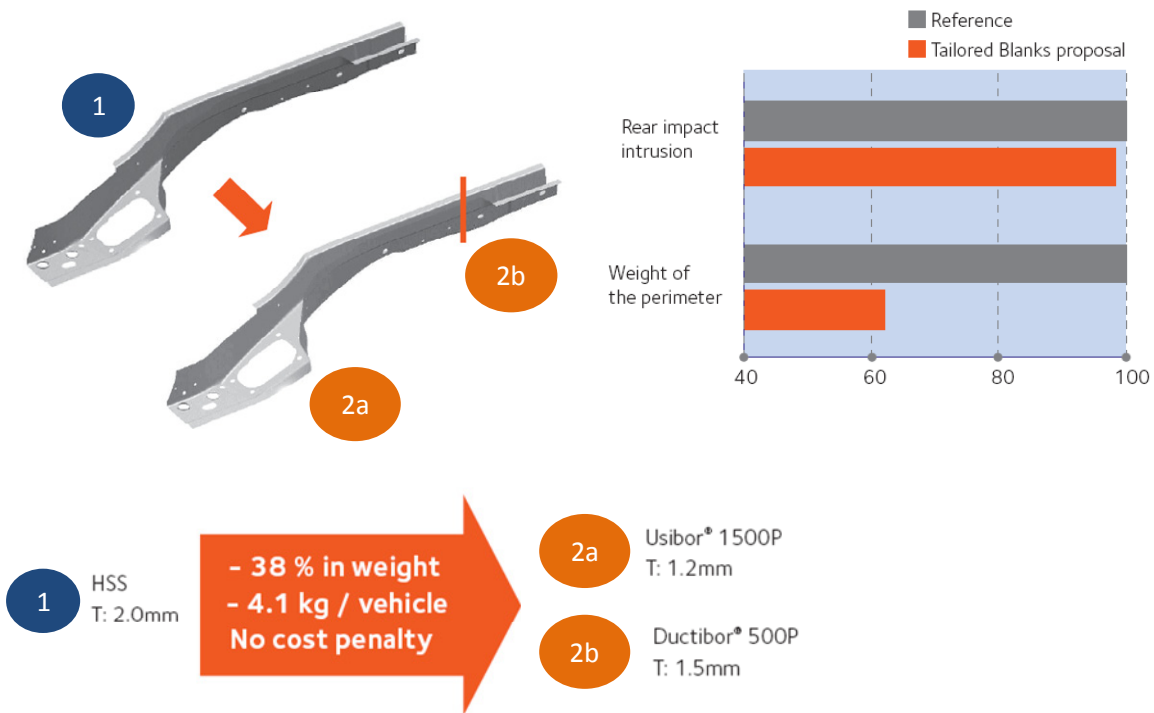


Figure 6 - Example of Tailor Welded Blanks, adapted from [14]

#### 1.4.2 Partial Austenizing in Furnace

It is possible to partially austenize portions of the blank while in the furnace, to prevent 100% martensite from forming after the quenching operation. Partial austenizing may be done using a furnace with independently controlled temperature zones, where it is possible to control the temperature distribution across the blank. Work presented in [23] consists of experiments done by heating specimens to furnace temperatures of 775°C, 825°C, and 950°C. The experiments have shown a decrease in hardness to below 300 HV at 775°C, compared to 440 HV at 825°C and 950°C. These lower hardness values are due to the ferritic-martensitic microstructure that exists from a combination of the as-received properties (ferrite, pearlite) and martensite which was formed from the partial austenizing.

### **1.4.3 Post Tempering**

A fully martensitic hot formed part can be locally tempered to modify the mechanical properties and create more ductile zones. The increased ductility is achieved through the formation of tempered martensite. Tempering at temperatures above 450°C for 30 minutes can reduce the hardness of the material by over 30% [24]. This tempering process comes at an additional cost in terms of cycle time and equipment.

### **1.4.4 Die Materials with varying Thermal Conductivity**

The primary mechanism for blank quenching is the contact with the die surface and the heat transfer through the die to the cooling channels. Hot forming dies used in production are often machined from 4140 steel, which has a thermal conductivity of 42 W/mK. It is possible to machine certain parts of the die from a tool steel with a lower thermal conductivity to reduce the heat transfer in that region. A reduction in thermal conductivity can effectively reduce the cooling rate of the blank in these parts, in order to form the softer phases [7,14,25]. It is, however, difficult to modify and fine tune the cooling rates in these areas, as new tooling would need to be machined to make any process changes.

### **1.4.5 Partially Heated Dies**

Another method to reduce the effective heat transfer from the blank to the tooling is to reduce the temperature difference between the two surfaces in contact. The reduction in temperature difference can be achieved by increasing the die temperature in local regions by use of a heat source, such as embedded cartridge heaters. By locally heating the die, it is possible to sufficiently reduce the cooling rate of the blank in these regions below the critical rate of 30°C/s, such that the softer phases are formed [14]. This method, accompanied with cooling channels, could produce a very controllable temperature distribution across the die, which would allow for very fine tailoring of the microstructures. A simplified example of this can be seen in Figure 7a, where a simple die was modeled with cartridge heaters at one end and a cooling system at the other. This creates a temperature gradient across the die which will induce varying cooling rates across the blank. Figure 7b shows the cooling rates of four elements which are evenly spaced across the length of the blank, each of which are in contact with areas of the tool at different temperatures. These cooling curves illustrate the ability to have significantly different cooling rates within a single part due to the die temperature control.

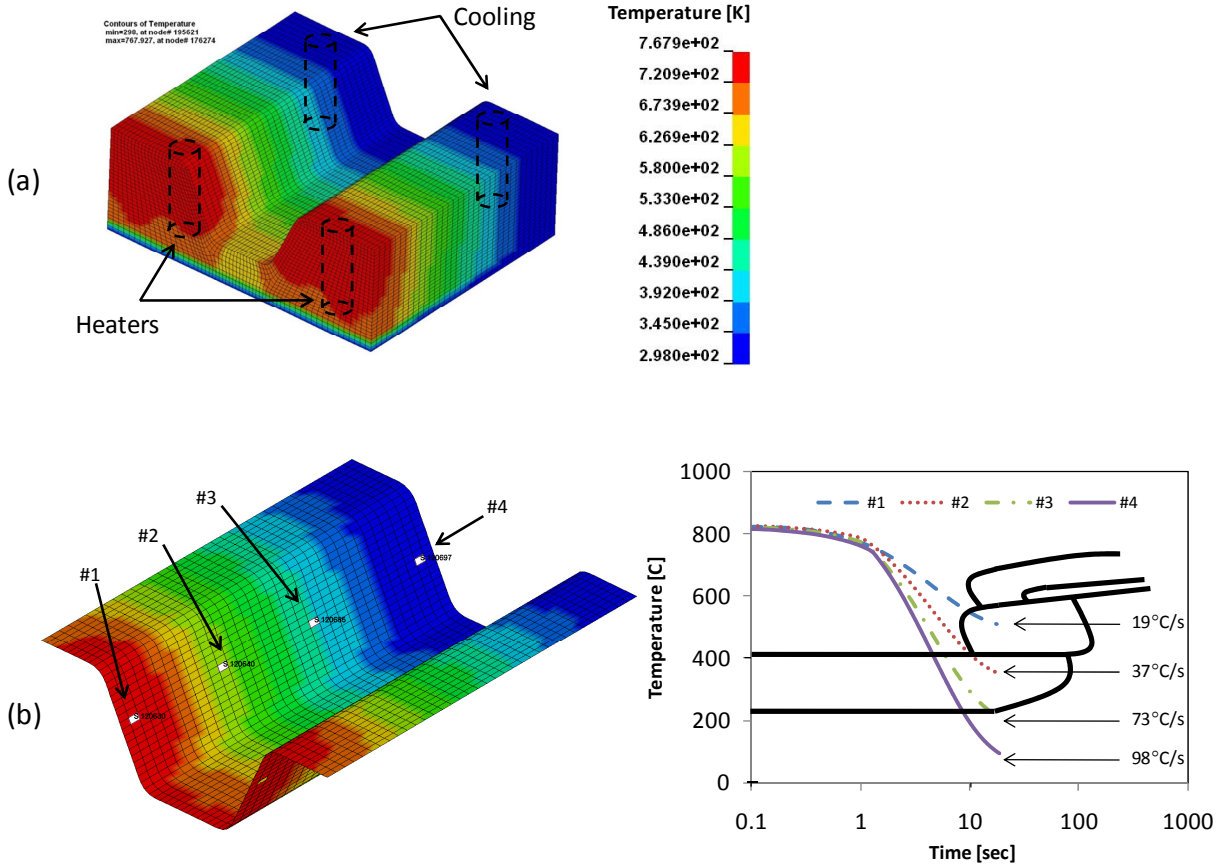


Figure 7 – (a) Simple die with embedded heating and cooling (b) Effect of die temperature on the cooling rates [26]

## 1.5 Numerical Modeling

There have been many improvements over the last few years with respect to the numerical modeling of the hot forming process. The use and development of explicit dynamic finite element (FE) code such as LS-DYNA [27] has also allowed for a significant improvement in the modeling accuracy of these processes. This forming process becomes more difficult to numerically solve when compared to conventional cold-stamping, due to the fact that the mechanical properties of the material vary over time due to the change in temperature and microstructure. Figure 8 outlines the interaction of these properties during the simulation.

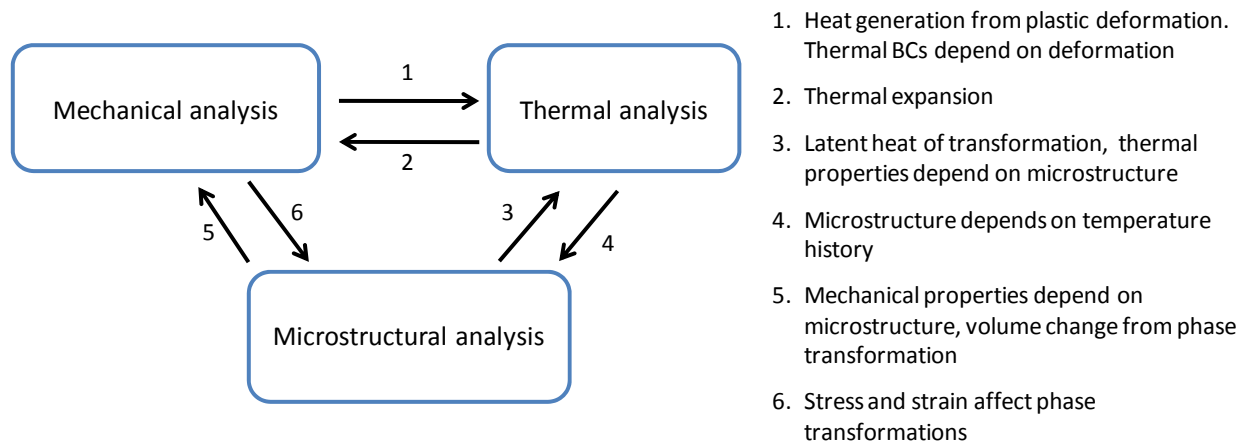


Figure 8 - Mechanical, thermal, and microstructural interactions, adapted from [28]

### 1.5.1 Material Models

The material models required for a hot forming simulation are considerably more complicated and computationally expensive than standard cold forming models. There are two common material models used in LS-DYNA for hot forming. The most basic model is Material #106, which is an elastic viscoplastic material with temperature dependency. This model allows material effective stress vs. effective plastic strain to be defined at various temperatures, as well as Young's modulus, Poisson's ratio, and viscous parameters [27]. This model does not account for microstructural changes or influences and thus has limited accuracy.

A new material model for LS-DYNA (\*MAT\_244 or \*MAT\_UHS\_STEEL) was developed in part by Paul Åkerström at the Luleå University of Technology for his PhD thesis [1] which accounts for, and predicts, the microstructural phases during the forming and quenching simulation. The decomposition of austenite into the daughter phases (martensite, bainite, ferrite, pearlite) is modeled and used to calculate the final Vickers microhardness of the elements. Latent heat of decomposition of austenite into the daughter phases is also included. The definition of this material requires an extensive list of parameters which are defined in Appendix B. These parameters were supplied by Arthur Shapiro at Livermore Software Technology Corporation (LSTC) [29].

### 1.5.2 Heat Transfer Coefficient (HTC)

The heat transfer between the blank and the tooling is one of the primary factors that determines the cooling rate of the blank as it is formed and quenched. The purpose of the tooling is to both form and quench the blank. As such, it is necessary to fully understand the thermal mechanisms and interactions during this process. At a microscopic level, the surfaces of both the blank and tooling are not flat; rather,

they are composed of hills and valleys as represented in Figure 9. As the two surfaces come into contact, there will be some areas with direct contact, where conduction will occur through spot contact. The primary heat transfer mechanism here is based on the thermal conductance of the two materials. In areas where there is not direct contact there will be heat transfer through the gas barrier (air) and also a radiation exchange between the exposed surfaces, which transmits significantly less heat than full spot conduction. As pressure is applied the hills start to deform and the contact patches begin to grow. This increases the amount of surface area in direct contact; increasing the overall heat transfer and ultimately increasing the cooling rate of the blank.

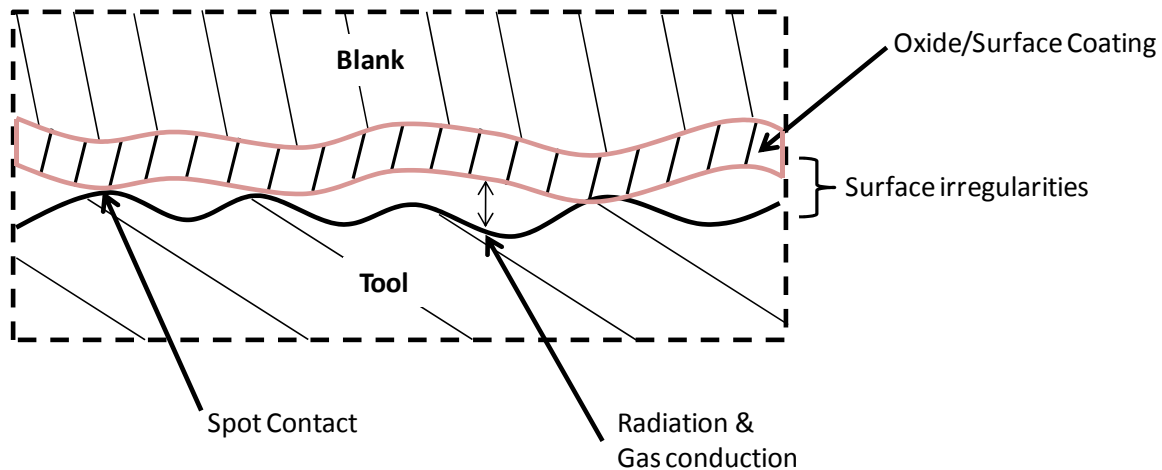


**Figure 9 - Typical contact zone for blank-tool heat exchange**

The heat transfer between these interfaces is dependent on many factors. As previously stated, the normal pressure applied to the surfaces will cause the hills/valleys to deform and increase the overall heat transfer. Similarly, the roughness of the tooling, its hardness, modulus of elasticity, temperature, and emissivity all affect the total heat transfer that occurs [10]. Significant work in [10] has shown an approximately linear increase in average HTC with respect to interface pressure, ranging from approximately 700 – 3000 W/m<sup>2</sup>K from pressures of 0 – 40 MPa. They have also shown a dependence of the instantaneous HTC with respect to the blank temperature.

## 1.6 Current Work

There is a significant knowledge base in current literature regarding hot forming and the parameters required for producing fully martensitic parts. There is also considerable documentation on the forming limits, frictional behavior, heat transfer characterization, material coatings, and numerical modeling, pertaining to the forming of fully martensitic parts. The process of hot forming a part with tailored

mechanical properties is, however, not fully understood. Work has been done using TWB [21], partial austenizing [23], and various die materials [25], however, there is little published work regarding the use of heated tooling to control the cooling rate of the blank. Additionally, there is limited experience using both heated and cooled tooling segments simultaneously to produce a single part with a large gradient of mechanical properties. The current research serves to address these deficiencies.

A large component of the current work is to design a lab-sized tool used for hot forming and to develop a computer model using LS-DYNA to predict the forming behavior and as-formed mechanical properties of the parts. The tooling and process is designed to replicate an industrial hot-forming process such that the results from these experiments can be carried over to an industrial application.

Another significant component of this work is to investigate the feasibility of producing a hot-formed part with tailored mechanical properties (some regions of high strength and other regions of increased ductility), in an effort to improve the crash performance of certain structural hot-formed members. There are several different approaches to achieve these tailored properties, each with their own benefits and draw-backs. The method considered here is to control the cooling rate of various regions of the blank during the forming and quenching stage of the manufacturing process. By controlling the cooling rate, it is possible to control the microstructure that is formed and thus control the final mechanical properties of the entire part. The cooling rate is controlled by heating sections of the die with electrical cartridge heaters, while other sections are cooled with chilled water. As the temperature of the tooling is increased, the heat transfer and cooling rate are decreased. Experiments are performed at various die temperatures and quench durations to determine the parameters for which softening occurs and also to determine the trends which exist with respect to microhardness versus die temperature.

The part geometry chosen for this work is a simplified B-pillar, which has been scaled down to a more manageable size to accommodate the existing press and equipment. The tooling for this geometry was designed such that the heated (locally soft) region is at the “T” section where it would typically be welded to a lower sill member in an automotive unibody. Figure 10 shows an automotive B-pillar compared to the lab-scale B-pillar developed for this research.



Automotive B-Pillar

UW Lab-Scale B-Pillar

**Figure 10 - Automotive and University of Waterloo B-Pillars**

The remainder of this thesis is organized as follows. Chapter 2 describes the equipment and tooling that was used for the experiments. Chapter 3 outlines the experimental procedures and the experimental results for the various die temperatures and quench durations. Chapter 4 discusses the numerical modeling techniques, validation, and the numerical simulation results. Chapter 5 summarizes the numerical and experimental results for easy comparison. Chapter 6 contains the discussions, conclusions, and recommendations for further work which were drawn from this research.

## 2 Equipment and Experimental Methods

### 2.1 Material

The material used in these experiments is Usibor<sup>®</sup> 1500P; a boron steel manufactured by ArcelorMittal specifically for hot forming. This material has an Aluminum-Silicon (Al-Si) coating which prevents oxidation of the surface as it is heated. The nominal thickness of this material, including the coating, is 1.2 mm. The chemical composition given from the manufacturer is shown below (Table 1).

Table 1 - Material Composition

Element	Composition (weight %)
Carbon (C)	0.22
Manganese (Mn)	1.23
Phosphorus (P)	0.008
Sulfur (S)	0.001
Silicon (Si)	0.25
Copper (Cu)	0.03
Nickel (Ni)	0.02
Molybdenum (Mo)	0.02
Chromium (Cr)	0.20
Columbium (Cb)	0.008
Vanadium (V)	0.008
Aluminum (Al)	0.03
Tin (Sn)	0.01
Titanium (Ti)	0.037
Nitrogen (N)	0.044
Boron (B)	0.004
Iron (Fe)	<i>Remaining</i>

The CCT diagram for this particular material was shown previously in Figure 4. From this diagram, the critical cooling rate of approximately 30°C/s, which results in a 100% martensitic microstructure, has a Vickers hardness of 474 HV. Previous work by Bardelcik, *et al* [30] has shown that for the critical cooling rate of 30°C/s the Vickers microhardness was measured to be approximately 450 HV. Measurements from literature indicate a large range of hardness values for a fully martensitic microstructure; typically ranging from 450 – 500 HV [5,7,10]. For this report, measured hardness levels in excess of 450 HV will indicate a fully martensitic microstructure.



## 2.2 Tooling

The tooling shown in Figure 11 has been designed to represent a cut-down B-pillar, with geometries and features that are similar to that seen in a production part. Each upper and lower tool is actually composed of two separate parts, one cooled and the other either heated or cooled. A small air gap is introduced between the heated and cooled sections, which has been proven to be a very effective insulation method. The air gap produces a very abrupt temperature change across the boundary which is designed to induce an immediate change in cooling rate of the blank across that gap. A numerical study on this approach was presented in [26] and compared different methods for insulating the heated and cooled tool sections. It was found that using air as an insulation barrier was more effective than a physical piece of ceramic insulation between the sections.

Between the tooling and the bolster plates is a layer of 19 mm ( $\frac{3}{4}$ " ) thick structural ceramic insulation. This insulation is in place so that the entire press is not heated by the cartridge heaters, and also to improve the temperature uniformity of the dies and reduce electrical power requirements. A very strong and durable insulation had to be selected, because the entire press load is transmitted through these plates. The insulation used here is Zircal-95, manufactured by ZIRCAR Refractory Composites, Inc. (Florida, NY). This particular insulation was chosen for its high compressive strength (450 MPa), its low thermal conductivity (0.27 W/mK @ 400°C), and its relatively low cost. The dies are clamped to bolster plates using brackets (not shown in Figure 11) which are then fixed to the press bed and slide using T bolts.

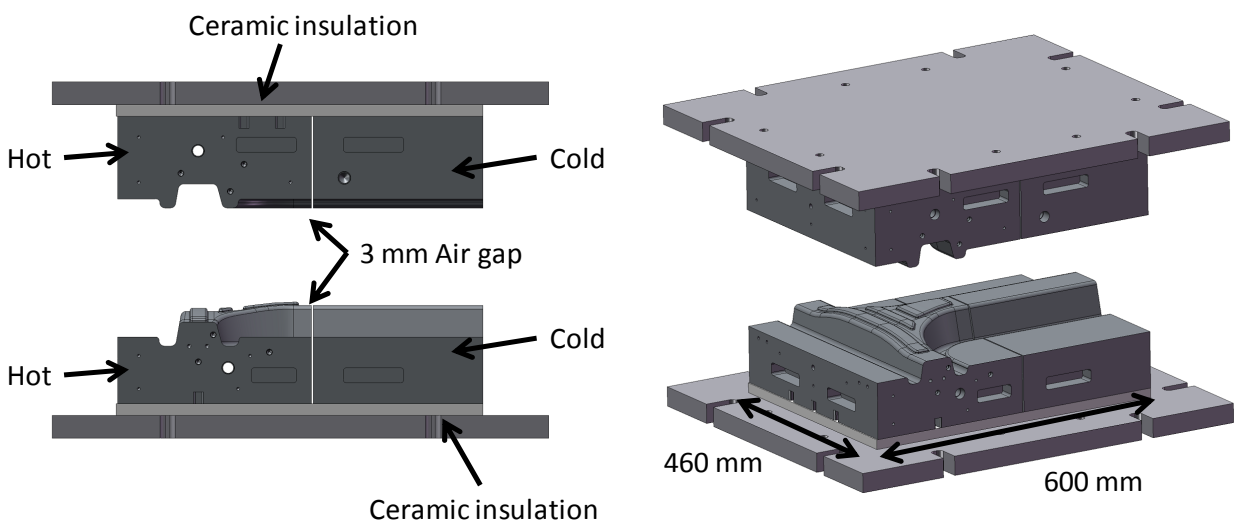
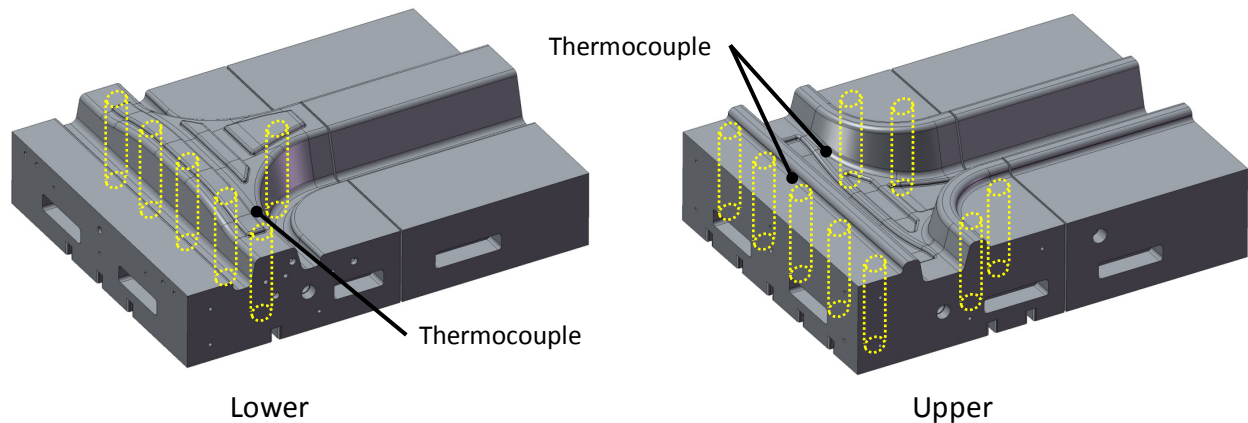


Figure 11 - Schematic of tooling

A total of 15 cartridge heaters are installed in the tooling: six in the lower tooling and nine in the upper. The electrical service available in the lab was rated for 30 A at 208 V, with one circuit available for each tool. It was desired to take full advantage of this electrical power and size heater wattage accordingly. The circuit with the largest load is the upper tool, with a total of nine cartridge heaters. For each 30 A circuit it was recommended to have a current draw below  $\sim 25$  A for continuous use, which equals approximately 2.8 A (577 W) per heating element. Based on the tooling geometry, heaters of dimensions  $\varnothing 19.05$  mm x 101.6 mm ( $\varnothing 3/4$ " x 4") were chosen, which corresponds to a heat flux (also referred to as Watt Density) of  $61.3$  W/in<sup>2</sup>. Watt Density for these cartridge heaters is determined by the total power divided by the cylindrical surface area of the heaters. A standard watt density from the manufacturer of  $60$  W/in<sup>2</sup> was chosen, which equates to 575 W per heater, for a total combined power input of 8.6 kW. Figure 12 shows the layout of the cartridge heaters in the tooling. These heaters are divided into three control groups for more precise and uniform heating. The lower tool has its own controller for the six elements and the upper tool has two controllers for the group of five and group of four. The controller feedback thermocouples are embedded into the tooling within 5-10 mm of the die surface to control the surface temperature as accurately as possible. The nominal die clearance between the forming surfaces is approximately 110% of the sheet thickness, or 1.30 mm total.



**Figure 12 - Location of the cartridge heaters**

The tooling did not incorporate geometric corrections for thermal expansion. This was not possible since the experimental design (Section 3) considered a range of initial die temperatures in the heated section of the tooling, ranging from room temperature to 400°C. In some of the experiments it was observed that thermal expansion did alter the part-tooling contact locally and directly affected the quench rate and resulting local part hardness. Accordingly, subsequent experiments were performed utilizing the

highest heated die temperature of 400°C that incorporated shim stock between the cooled die components and the ceramic insulator block. The shim thicknesses were 0.63 mm (0.025”) for the lower die and 0.41 mm (0.016”) for the upper die. More details regarding the thermal expansion can be found in Section 3.3. Figure 13 shows the approximate required shim thickness as a function of temperature for the upper and lower tooling. This figure can serve as a guideline for any future work with this tooling for installing shims at temperatures other than 400°C.

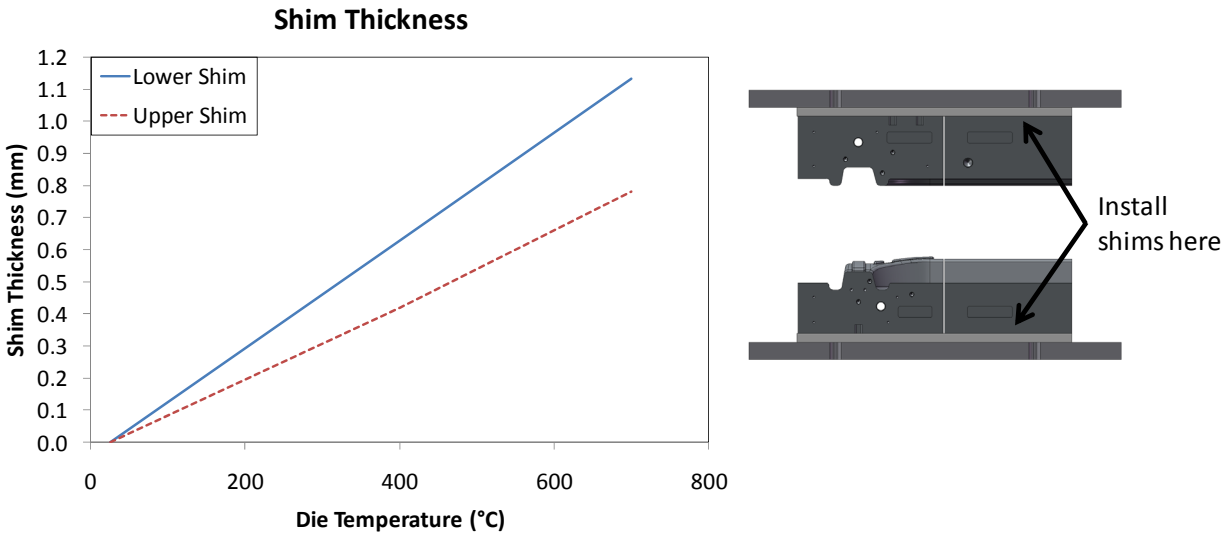
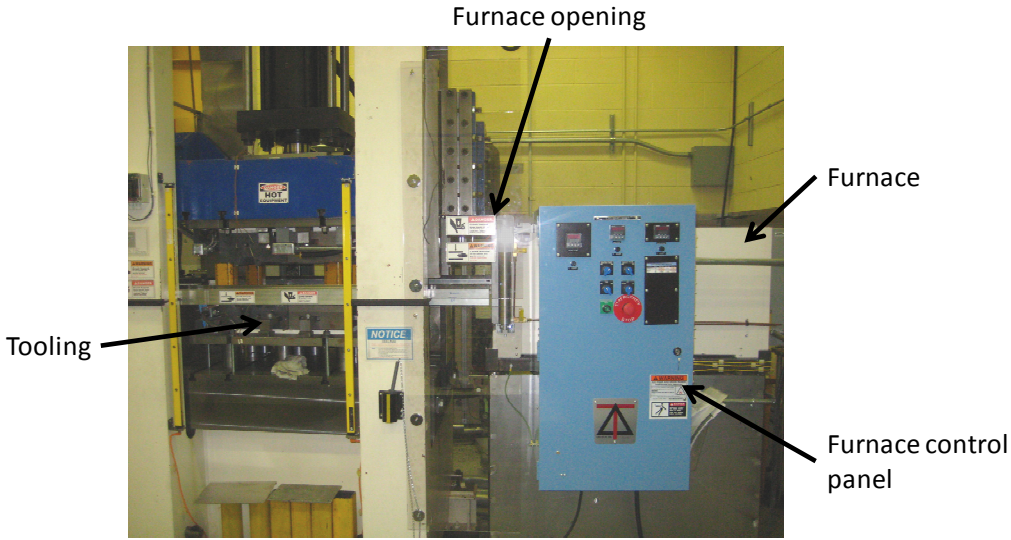


Figure 13 - Approximate shim thickness versus temperature

## 2.3 Furnace

The furnace used for the experiments was custom built by Deltech, Inc. (Denver, CO). The furnace has internal dimensions of 610 mm x 915 mm x 203 mm (24” x 36” x 8”) and a heating capacity of 18 kW. It has a total of six heating elements, three on the top and three on the bottom, which fill the entire 610 mm x 915 mm (24” x 36”) area. There are three separate control groups for the furnace, allowing different temperatures to be defined for the front, middle, and back of the furnace. The multiple controllers are currently only used to ensure that there is even heating within the furnace. Creating an actual multi-zone furnace would require the installation of baffles/screens to prevent heat transfer between the zones. A foot pedal is used to remotely open and close the furnace door for ease of operation. Figure 14 shows the layout of the furnace with respect to the press and die. It has been placed as close as possible to the press to minimize the handling distance of the hot blank as it transfers from the furnace into the tooling.



**Figure 14 - Press & Furnace Layout**

Figure 15 shows the temperature-time history of a blank as it is placed into the 930°C furnace. Thermocouples were welded to the blank in three different locations to monitor the temperature across the whole blank and ensure that there is uniform heating within the furnace. The blank is held in the furnace for a total of 5 minutes to fully austenize the microstructure before forming and quenching.

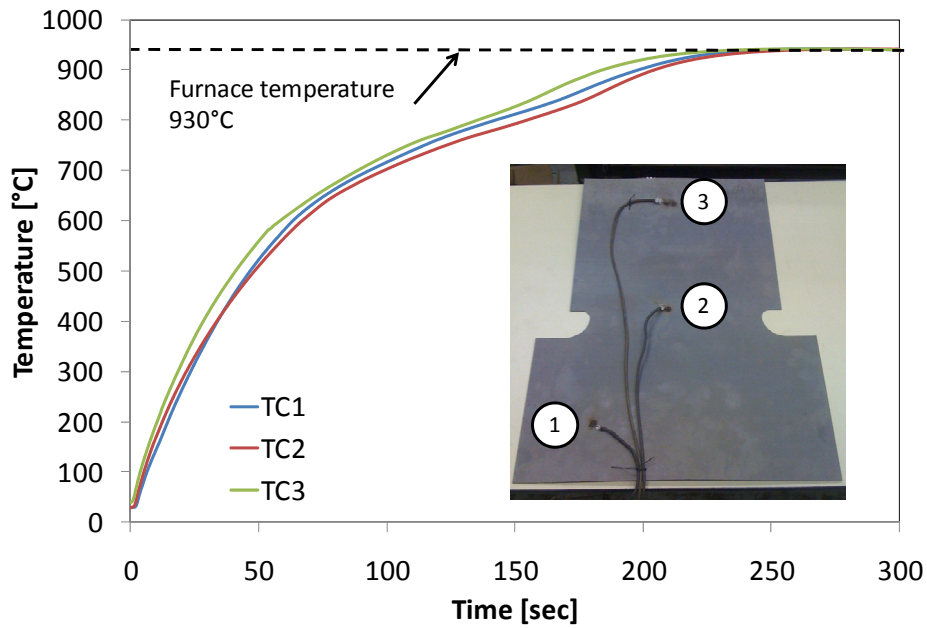


**Figure 15 - Heating of Instrumented Blank**

## 2.4 Transfer System

In a production environment, an automated robotic transfer system is used to transport the heated blanks from the furnace to the press. Automation ensures fast, accurate, and repeatable results. In a prototyping environment, where the size and shape of blanks is constantly changing, the transfer process is often done by hand. Transferring the blank manually is a very low-cost solution that is adaptable to different tooling configurations and blank sizes. However, the timing and repeatability of this fully manual process can vary, and consistent results may be difficult to achieve. Furthermore, there is an element of risk that is associated with moving large blanks at high temperature by hand. For these experiments, a compromise was made between the repeatability of an automated system and the ease of implementation of a manual system. A cart was designed that travels along linear bearings within the press bed and is able to reach into the furnace to grip the blank and position it onto the tooling. The gripper head is controlled by a push-pull cable that is manually operated and has ceramic gripping surfaces which minimize heat loss during contact. Figure 16 shows the transfer system installed within the press. A rail system is used to support the blank between the furnace and the tooling to prevent sag and deformation during the transfer process. The rails are insulated with ceramic insulation to avoid heat loss at the points of contact during transfer.

This semi-manual system is very easy to control and has shown very repeatable results in terms of timing and blank positioning. It also sets the operator at least 50 inches away from the hot blank when in operation.

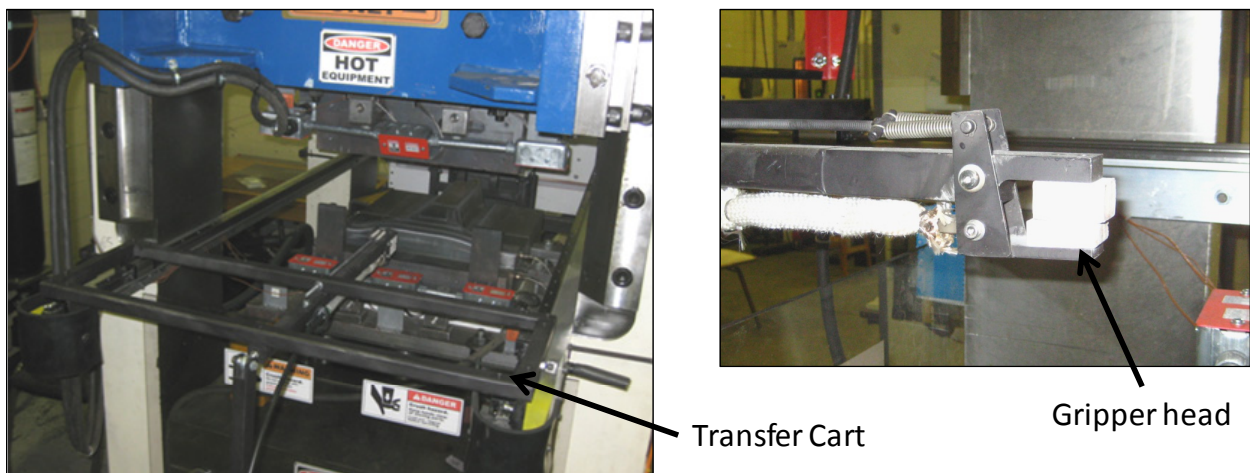


Figure 16 - Transfer Mechanism

## 2.5 Press & Hydraulics

The press used for these experiments is manufactured by Macrodyne Technologies Inc., which was originally configured with a 1000 ton actuator and a stroke of 12". It has a total bed size of 54" x 30", which was used as a main constraint for determining the size of the part and tooling. The original 1000 ton actuator was designed for use in previous hydroforming projects where the punch speed was not important. However, for these experiments, it was necessary to significantly increase the punch speed so that the forming stage is completed before the blank cools too much and begins to form martensite. As part of this work the press was reconfigured to utilize a smaller, 120 ton actuator (an existing end-feed actuator from hydroforming). To mount this new actuator within the press several new adapters and couplers were fabricated (Figure 17). CAD drawings for these components can be found in Appendix C.

In addition, a 100 GPM servo valve and a pair of 15 gallon hydraulic accumulators were added to the hydraulic circuit used to power the press. This new system allowed a maximum punch speed of approximately 10 inch/sec. With this configuration the blank is fully formed in less than 2 seconds, which is more than adequate for this research.

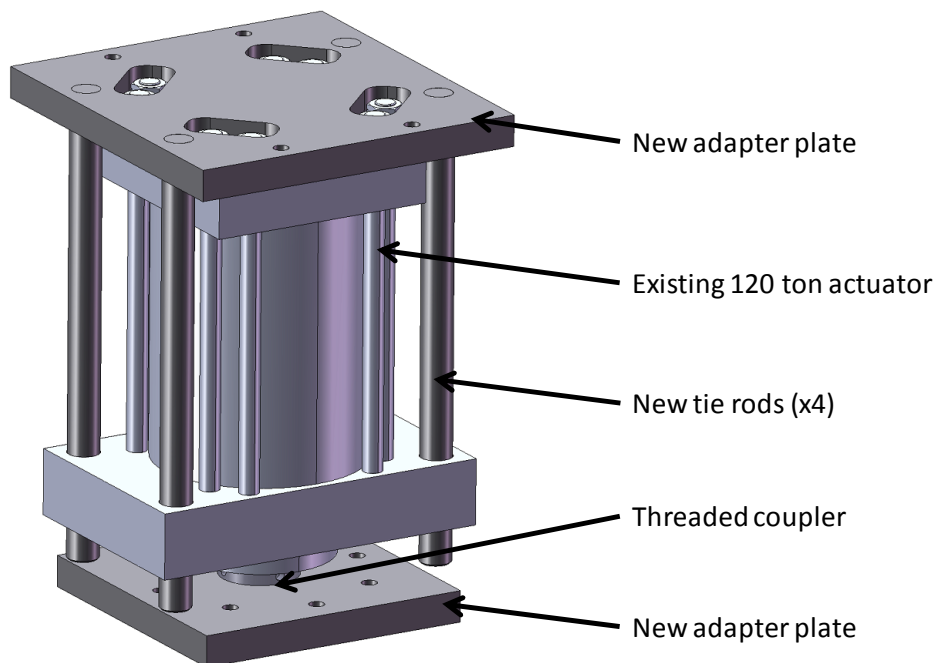


Figure 17 - Press Actuator Modifications



The press utilizes closed-loop position control via an MTS FlexTest servo controller with program signals generated by a PC-based Digital-to-Analog card driven by a custom LabView program. The punch is instrumented with a string potentiometer to measure the displacement and for closed-loop displacement control. For load measurement there is a pressure transducer at the oil inlet and outlet of the actuator which is used to calculate the total force based on the difference in pressures and the cylinder areas. Data acquisition is performed using Analog-to-Digital channels on the same card. Tooling temperature is recorded using the thermocouples described in Section 2.2.

## 2.6 Part Design & Geometry

A laboratory-scale B-pillar was developed for the experiments to represent a part that is currently hot-formed by several OEMs. The B-pillar is also the focus of efforts by many researchers investigating the implementation of tailored properties in a hot-formed part. Due to size limitations of the press, a full-sized B-pillar could not be created. Rather, it has been reduced in length to capture roughly one-half of the vertical structure and the T profile section where it would be connected to a lower sill. Figure 18 shows the final part with overall dimensions, also showing the location of the air-gap within the tooling. Three bosses were designed into the tooling to take up additional material to prevent wrinkles.

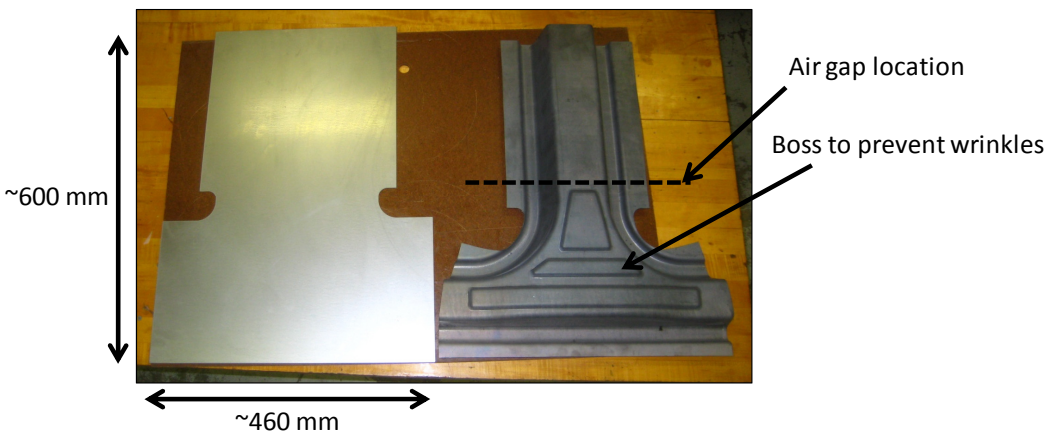


**Figure 18 - Final Part Geometry**

To simplify the tooling, a blank holder or “binder” is not used to form this part. Thus only upper and lower tools are used, as is common practice in some commercial hot stamping operations. It was, however, necessary to develop another method to restrain the blank to increase the degree of material stretching and eliminate wrinkles. A feature similar to a draw-bead was designed into the tooling to engage the blank in the final stages of the forming stroke. Figure 19 shows a cross-sectional view of the

tooling and highlights the draw-bead feature. Design consulting was provided in part by Promatek Research Centre, who also performed all of the manufacturing and machining. The size and shape of the draw-bead was optimized by performing a series of forming simulations in LS-DYNA to increase the stretch and draw behavior of the blank.

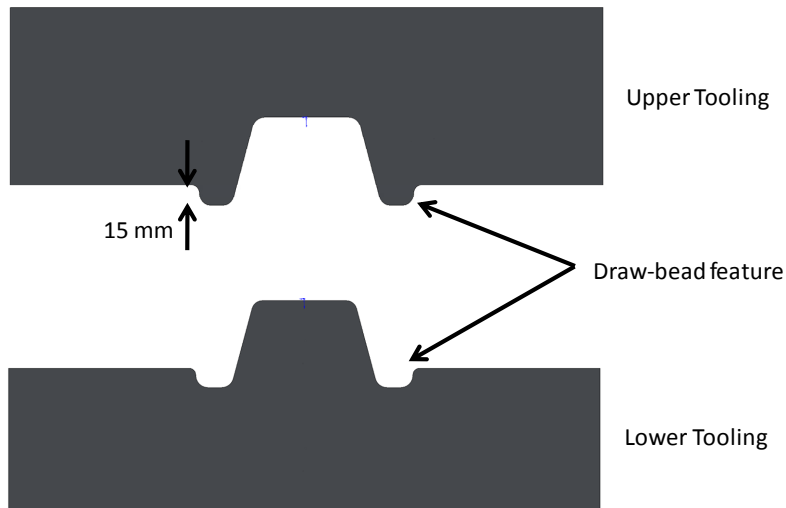


**Figure 19 - Tooling cross section & draw bead**

The blanks were cut using a water-jet cutting system which produces no heat-affected zone (HAZ).

## **2.7 Areas of Interest**

After the parts are formed, smaller samples are cut from the parts to measure the Vickers microhardness. Hardness measurements are taken at six locations across the part: two in the cooled section (H1 & H2), two in the heated section (H3 & H4), and two across the transition zone (H5 & H6) (Figure 20). Measurement locations H1, H3, and H5 are on the top face, and locations H2, H4, and H6 are on the side wall.



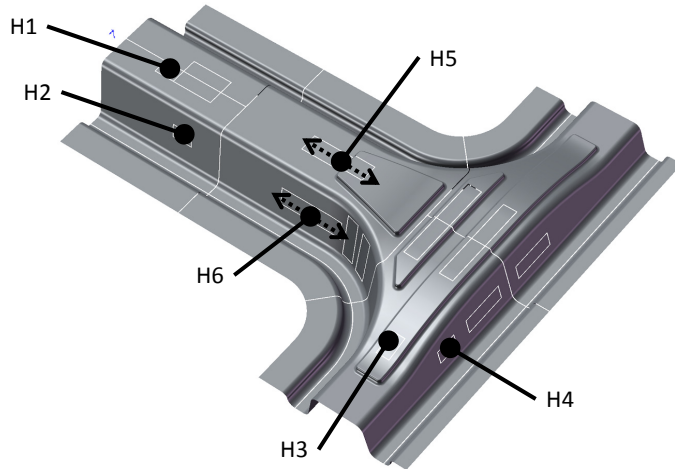


**Figure 20 - Sample Locations**

The samples were laser-cut from the parts using the facilities at Promatek Research Center. The 5-axis laser cell is able to produce very clean and repeatable cuts across this complicated geometry, with minimal HAZ. Small tabs were left on each sample so that they could be punched out from the parts and labeled at a later time (Figure 21).

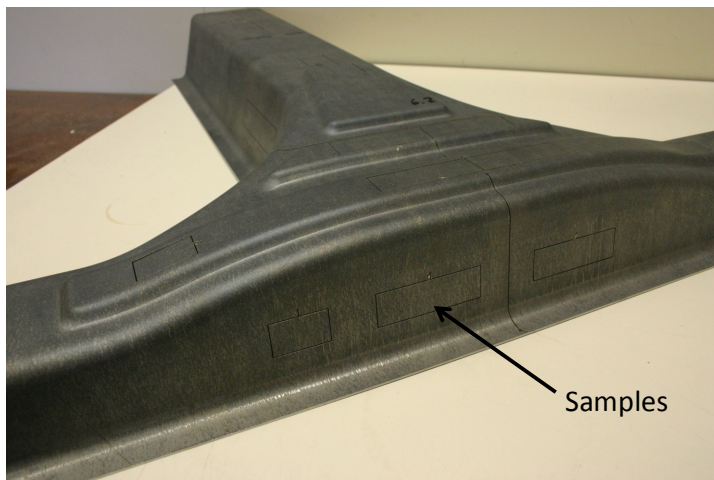


**Figure 21 - Laser-cut samples**

## **2.8 Sample Preparation**

Hardness measurements were taken using a Vickers microhardness machine. Vickers microhardness is measured by indenting the sample with a diamond indenter at a known force. The size of the impression that is left in the sample is measured under a microscope and is used to calculate the hardness (Figure

22). This equation is shown in Figure 22, where  $F$  is the load [kg] and  $d$  is the average length of  $d1$  and  $d2$  [mm]. Typical measurements for  $d$  are on the order of 0.1 - 0.4 mm.

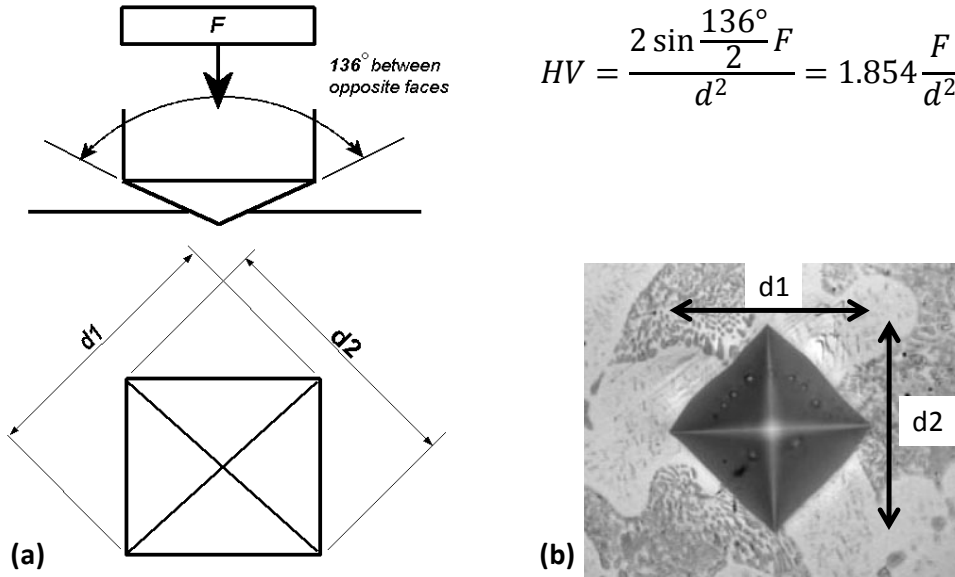


**Figure 22 - Vickers Microhardness (a) Schematic of indenter (b) Sample micrograph of a Vickers microhardness test**

For these measurements it is required that the samples are mounted in an epoxy “puck” and polished to achieve accurate results. Each sample removed from the formed parts was cut in half with an abrasive wet saw. This additional cutting step is to expose an edge for hardness measurement that wasn’t laser-cut, to avoid the HAZ. To minimize the number of pucks which needed to be prepared, hardness locations H1 – H4 were mounted in the same puck. A binder clip was used to hold all of the samples together and a brass shim was installed to provide a reference point (Figure 23). Measurements taken for H1 – H4 represent an average of three through-thickness measurements at each location (shown in Figure 24).

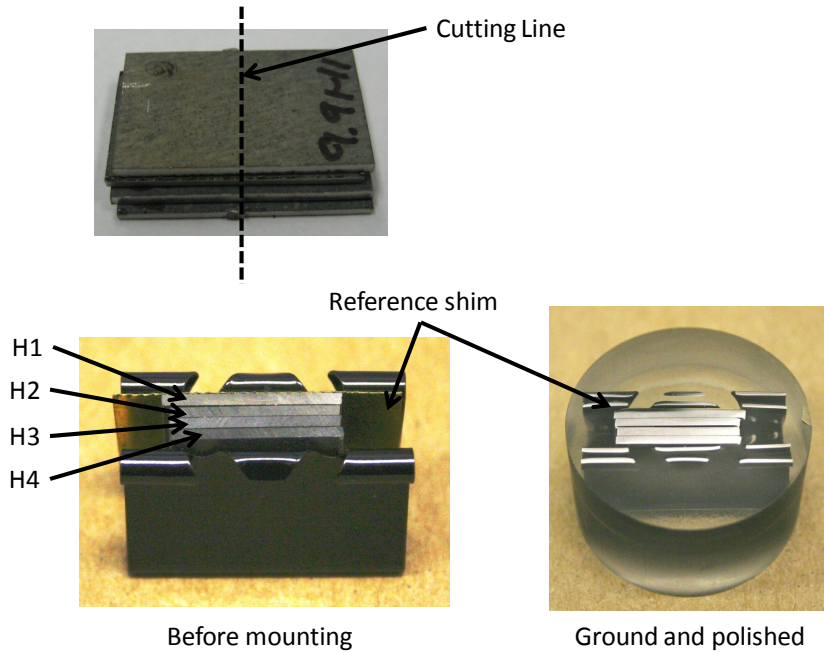


**Figure 23 - Sample preparation (H1 - H4)**

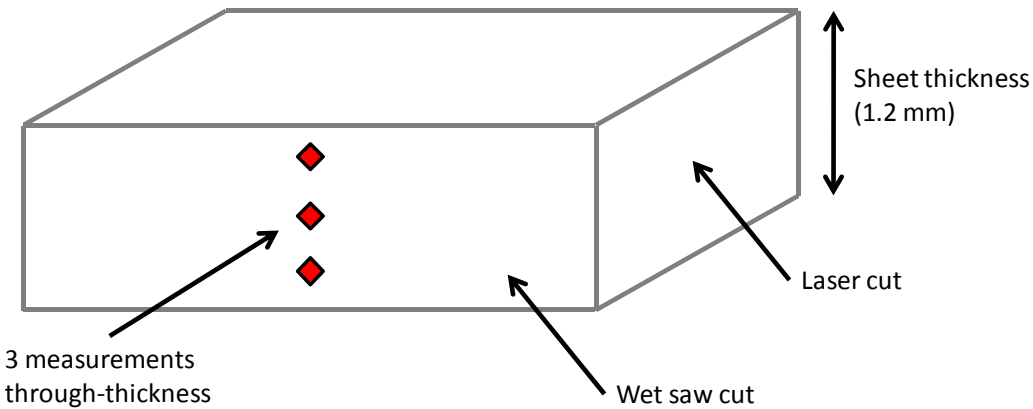


**Figure 24 - H1 to H4 measurement details**

Hardness samples #5 and #6 have a total length of 80 mm, which is too large to mount as-is in the  $\varnothing 25$  mm pucks. To accommodate this, these samples were cut using the wet saw into 4 sections of 20 mm each and then cut in half again to expose the measurement edge. Reference marks were drawn to ensure that the sections could be reorganized in the proper location and orientation when mounting in the pucks (Figure 25). For H5 and H6, measurements are taken along the through-thickness centerline every 2.5 mm – 5.0 mm (0.10" to 0.20") and are recorded left to right, top to bottom for each puck. The

reference shim indicates the location of the first section. Figure 26 shows the orientation of the H5 and H6 samples. Position = 0 mm is in the heated region, and position = 80 mm is in the cooled region.

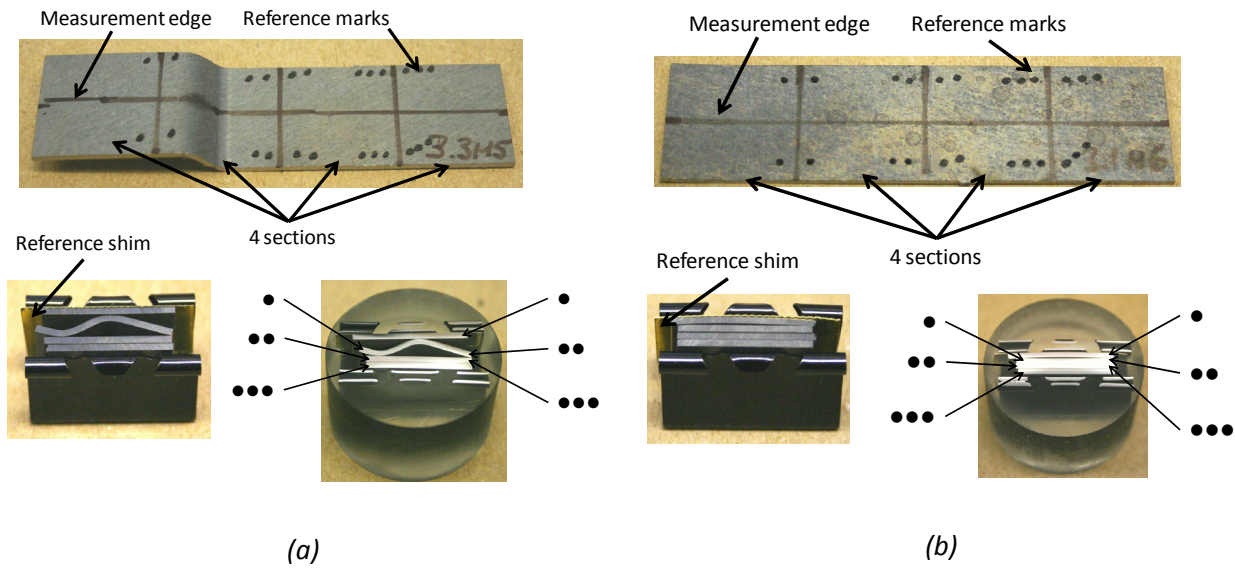


Figure 25 - Sample preparation (a) H5, (b) H6

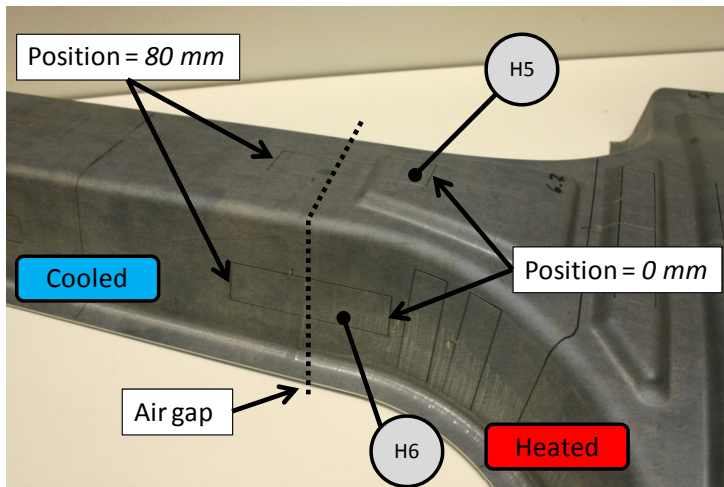


Figure 26 - H5 & H6 orientation and reference positions

All samples were mounted in a cold-setting epoxy, rather than a heated mounting which may affect the microstructure and hardness of the samples. All of the samples were ground and polished in four stages up to 4000 grit, which produces a mirror-finish that is acceptable for these microhardness measurements.

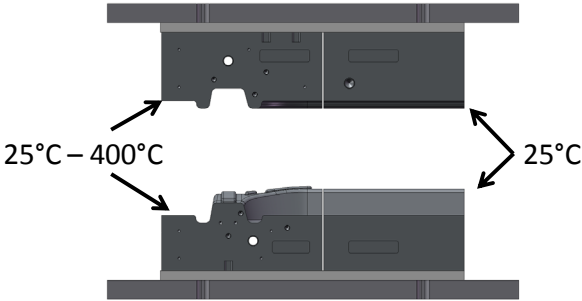
### 3 Experiments

Please refer to Appendix D for thorough instructions of the operation of the press.

The hot forming experiments were performed at various hot die temperatures (25°C to 400°C) while maintaining the cold half of the die at or near room temperature with the chilled water circulation. Two quench durations were also used for each of the die temperatures (4 s and 10 s). Refer to Table 2 for the complete test matrix.

Table 2 – Test Matrix

Heated Die Temperature [°C]	Quench Duration [seconds]
25	4
	10
100	4
	10
200	4
	10
300	4
	10
350	4
	10
400	4
	10



The process to form a part is as follows (also refer to Figure 27):

- The blank is loaded into the furnace and held for 5 minutes to fully transform the microstructure to austenite
- The blank is removed from the furnace, rests for 5 seconds, and is then transferred into the die. This step takes 10 seconds in total.
- Once the blank is placed into the die and the transfer cart has cleared the press, the punch is automatically activated and the part is formed (2 seconds).
- Depending on the test, the part is quenched with the die fully closed and maximum tonnage applied for 4 or 10 seconds.
- When the die opens, the part is manually stripped from the tool and is set aside to air cool naturally.

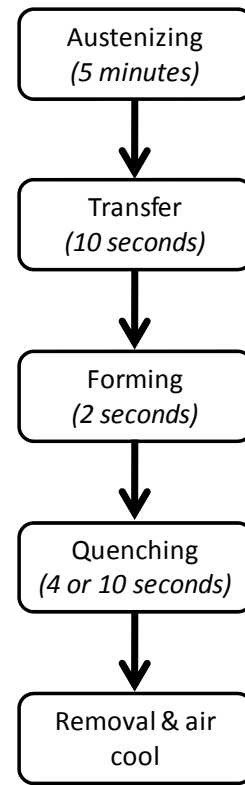


Figure 27 - Process flow-chart

Figure 28 shows a typical punch force and displacement plot which was recorded from an experiment. The part is formed in 1.6 seconds and requires approximately 900 kN of force. A free-fall of 150 mm is necessary for clearing the transfer system and the working stroke is 68 mm.

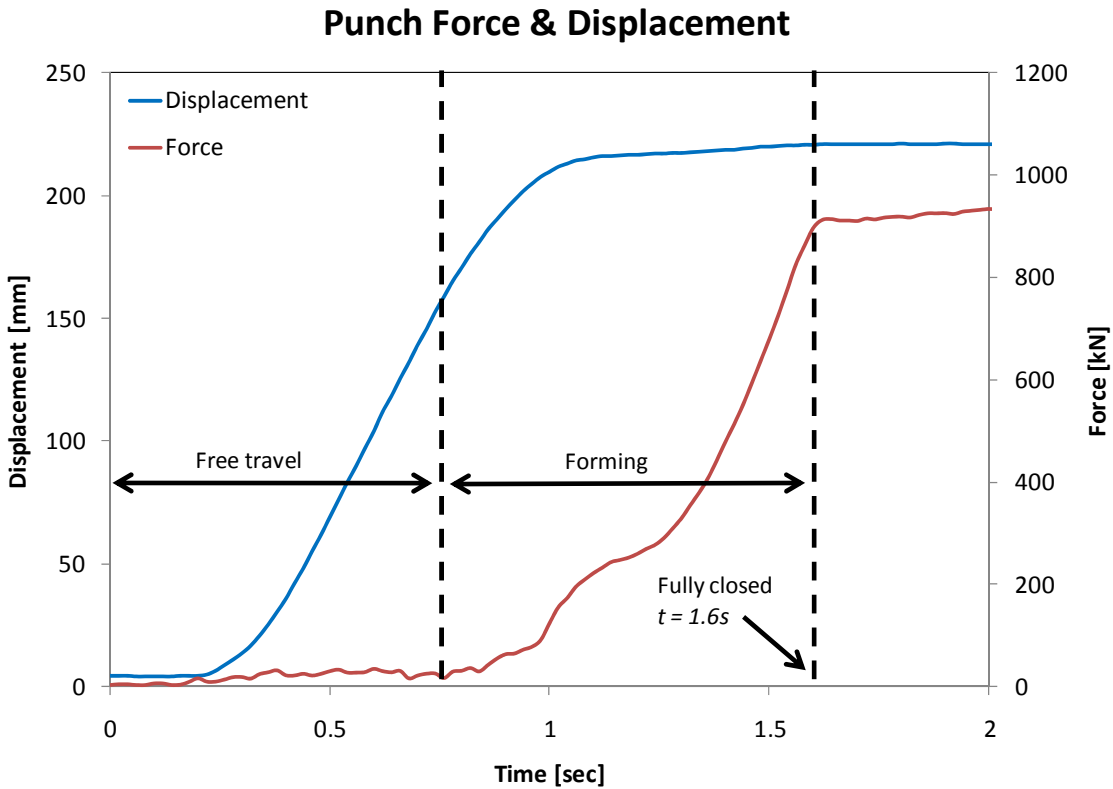


Figure 28 - Typical punch force & displacement

### 3.1 Die Alignment

When the tooling is heated it will deform due to thermal expansion. This deformation and expansion causes the heated tools to come out of alignment with the cooled tools. Due to this movement, it is necessary to re-align the tooling each time the tooling is heated or allowed to cool. When the tooling has reached the specified temperature, the lower heated section is unclamped and aligned to the lower cooled section. This is done by measuring the clearance on the sides between the hot and cold tools, which is generated due to thermal expansion, with a straight edge and feeler gauges. The hot side is repositioned until the clearance on both sides is equal, which means that the centerline of the tools are in line (Figure 29). After the lower tooling is aligned, a previously formed part is placed onto the tool. The upper heated section is loosened slightly and lowered until it comes into contact with the lower die. The formed part is in place to ensure the two die halves align with proper internal clearance. The punch is manually cycled approximately 1" several times to ensure the upper tool has shifted and aligned with the lower tool. After this process it is re-tightened and the die set is now aligned.

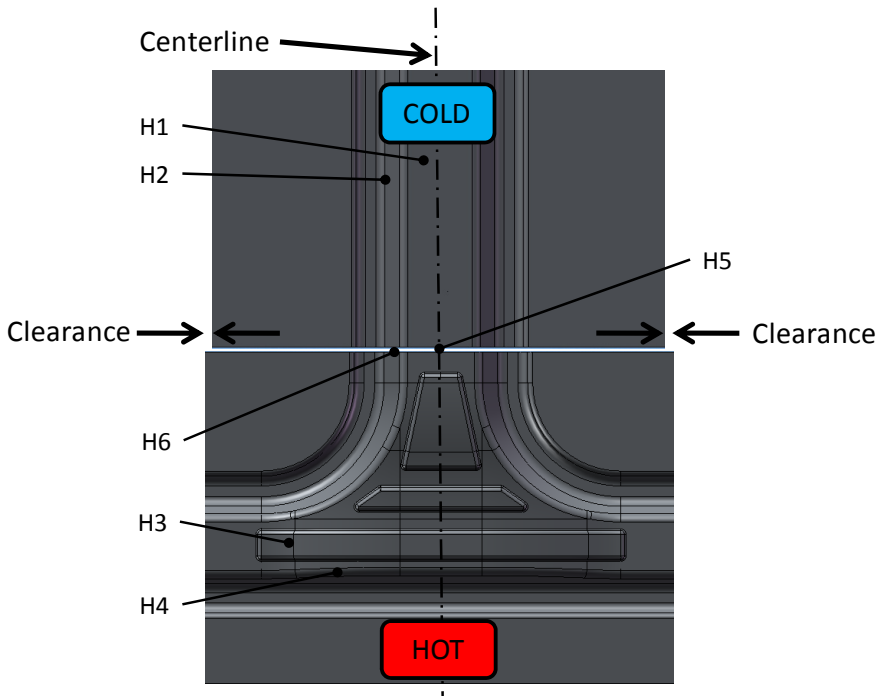


Figure 29 - Die Alignment

## 3.2 Experimental Results

Section 3.2 describes the experimental results from the experiments without shims to compensate for thermal expansion effects in the heated section of the tool. The results for the experiments with shimming are provided in Section 3.3.

### 3.2.1 Baseline – Die Fully Cooled

A set of baseline parts, in which both sections of the tooling are cooled, were formed and measured to characterize this particular tool, part geometry, and process. These tests were performed with a uniform die temperature of room temperature (approximately 25°C). Refer back to Figure 20 for details of the measurement locations. Figure 30 shows the results at locations H1 – H4 at the two different quench times. A total of four parts were measured at each test case and each data point represents the average of those four parts. The error bars indicate the maximum and minimum measured values. From these measured values, it is apparent that the microstructure is 100% martensite at positions H1, H2, and H3. However, there is a significant difference in hardness at H4, which is approximately 350 HV. At this die temperature, it is expected that the entire part should have a martensitic microstructure. The measurements at H4 are very repeatable with minimal scatter, which suggests a more fundamental reason for this drop. This drop may be due to the reduced contact pressure along the walls, and also the



deformation during quenching. Work done by [11] has shown that deformation during quenching can cause a shift in the CCT diagram and allows bainite to form at cooling rates greater than 30°C/s.

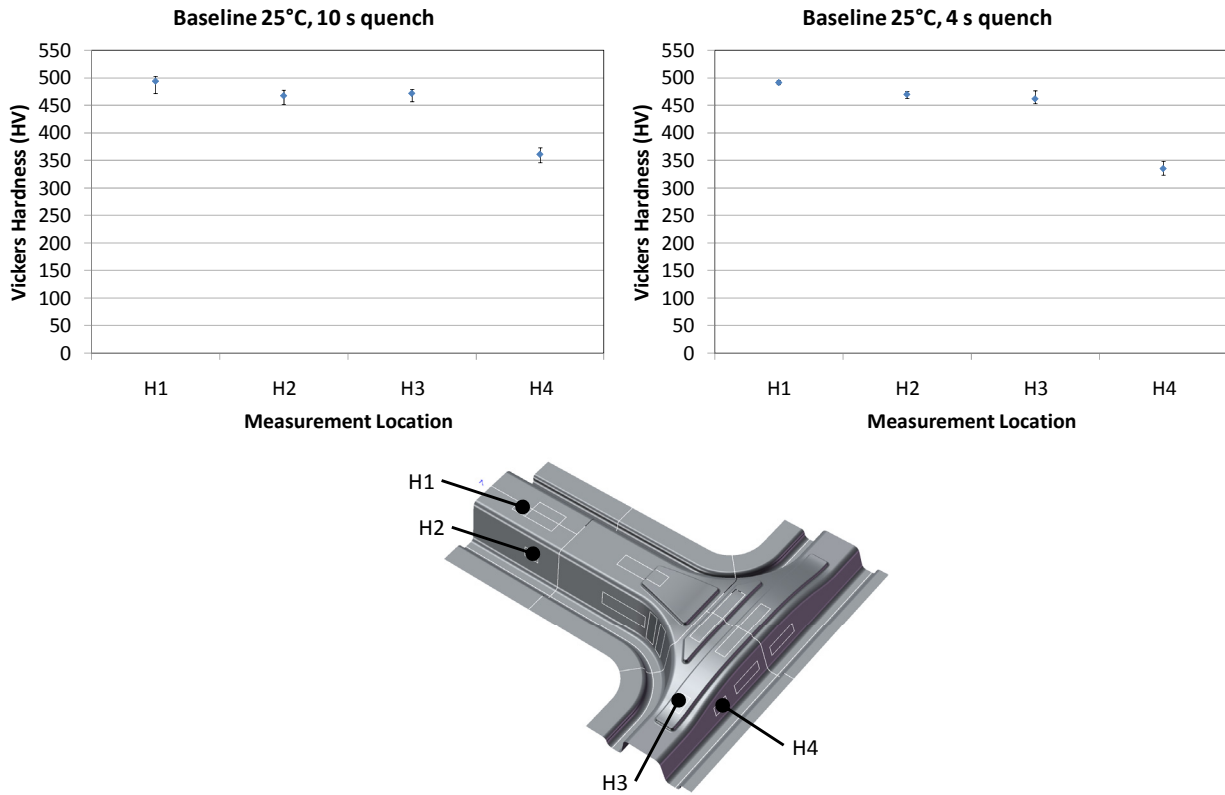


Figure 30 - Baseline experimental results (H1 - H4)

Figure 31 shows the transition zone hardness profiles (H5 and H6) for the baseline cases. The three lines on each plot represent three different parts that were measured for each case. There is minimal scatter between the three data sets for each test case. The profiles are fairly uniform, with a hardness of approximately 450 HV, on average.

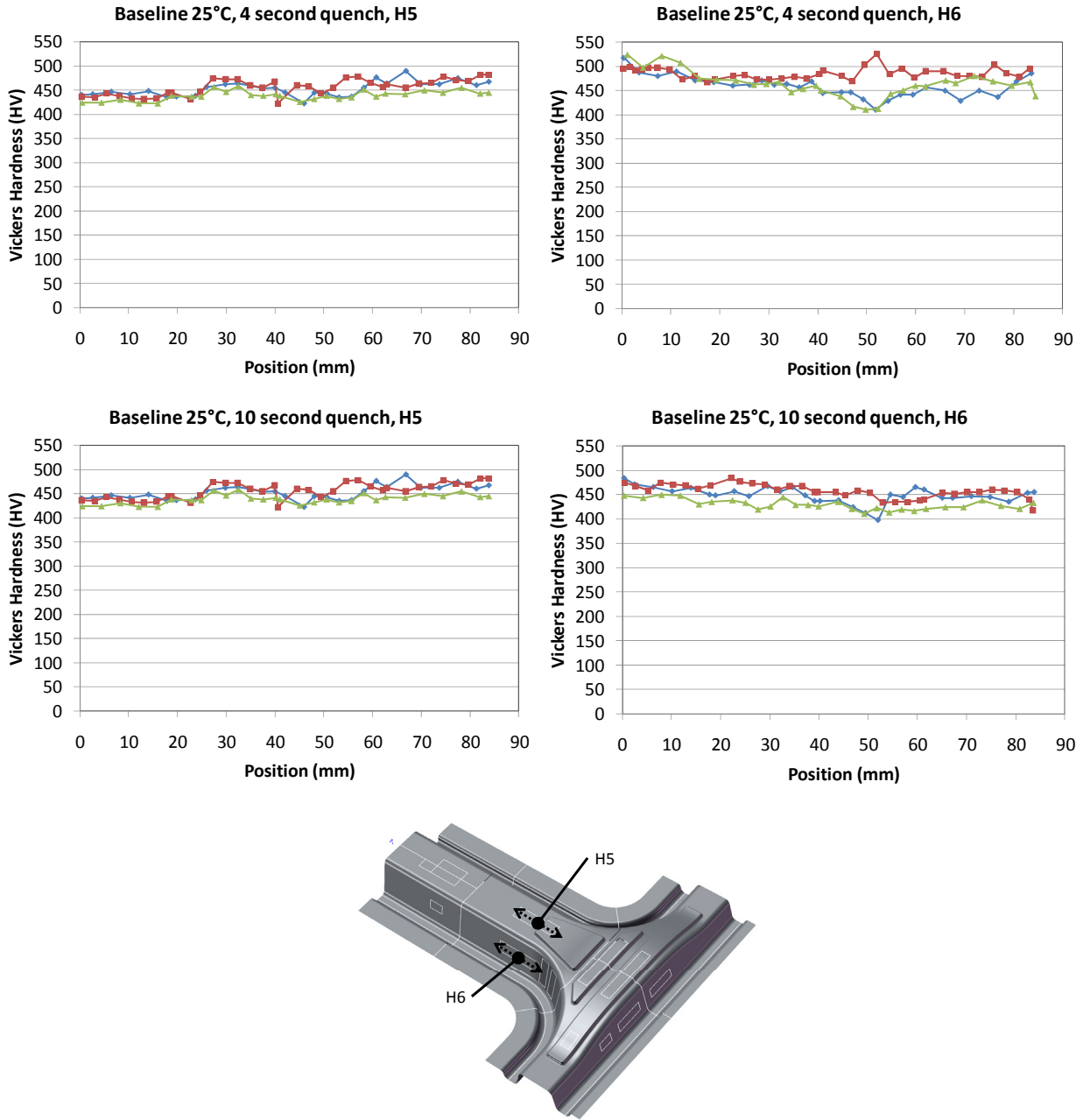


Figure 31 - Baseline experimental results (H5 & H6)

### 3.2.2 Heated Die Results – 100°C

A die temperature of 100°C is not expected to produce results much different than a room temperature die. In many industrial applications, the dies typically operate at 80°C – 100°C due to the large throughput of parts which inherently heat the tooling to a steady state temperature. Figure 32 shows the results for positions H1 to H4. As expected, the measured hardness for this die temperature is very similar to the results from the baseline case.

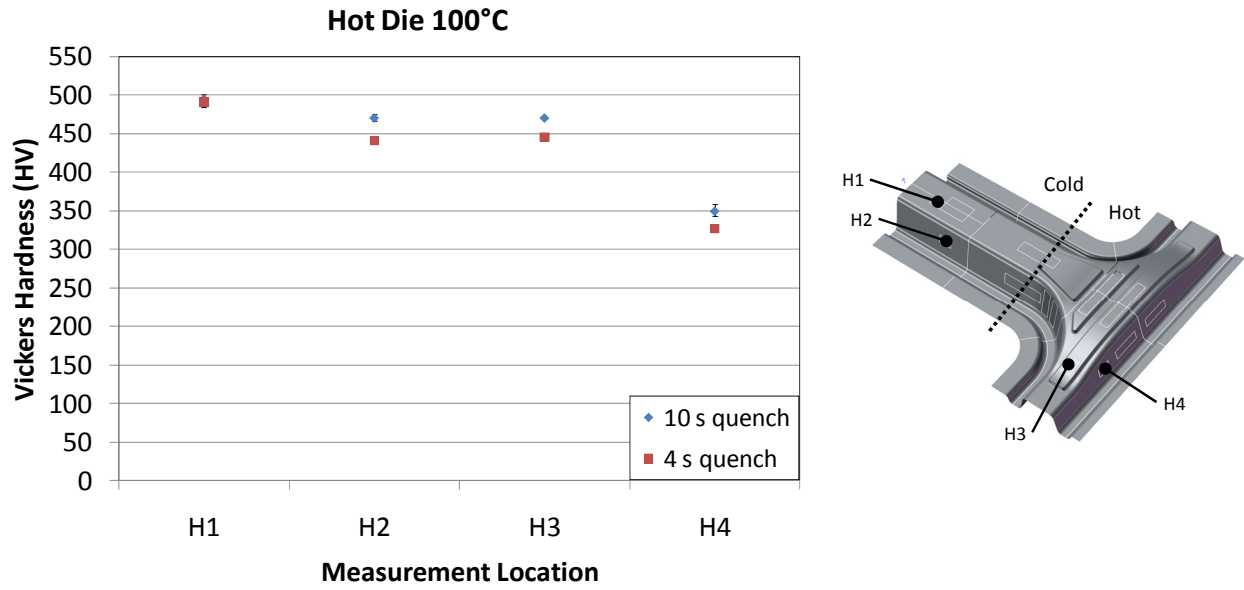


Figure 32 – Experimental results 100°C (H1-H4)

Figure 33 displays the results across the transition for a ten and four second quench. These results are also very similar to the baseline case, with no apparent trends when moving from the heated side to the cooled side.

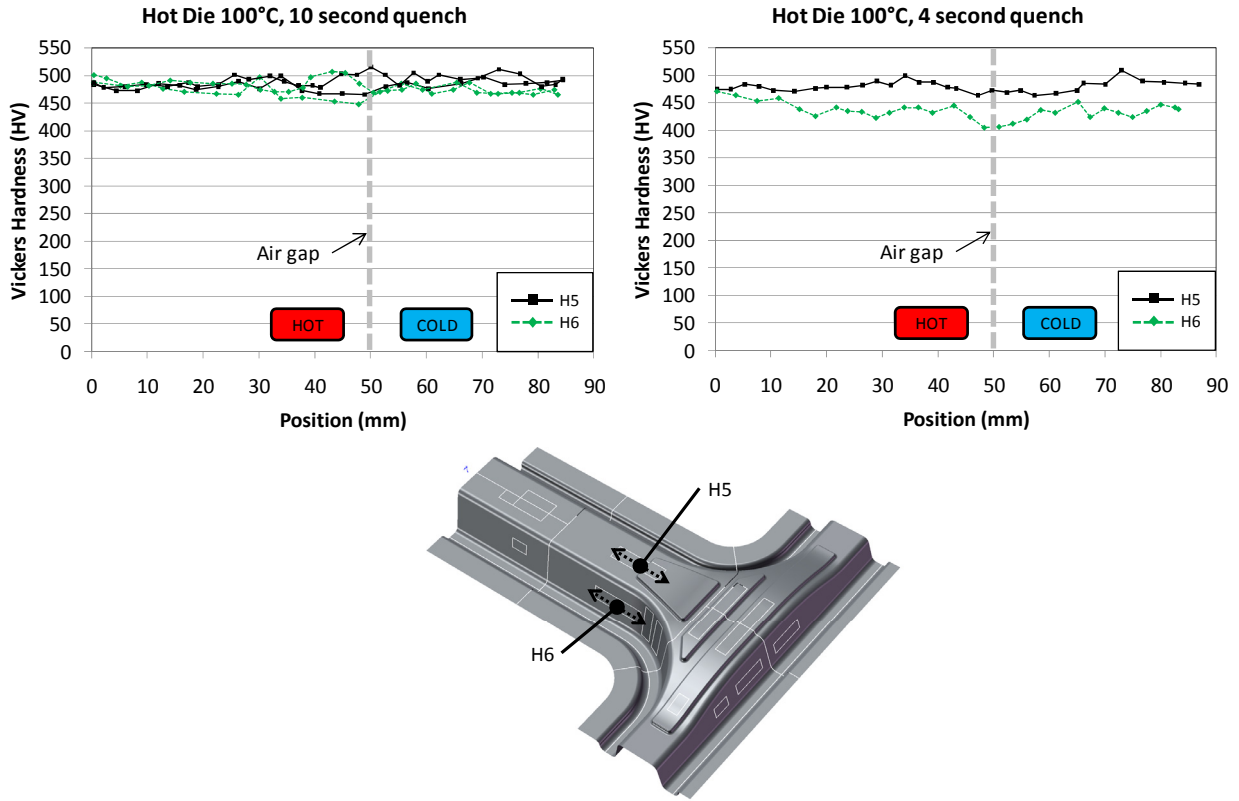


Figure 33 – Experimental results 100°C (H5 & H6)

### 3.2.3 Heated Die Results – 200°C

Figure 34 shows the hardness measurements for locations H1 through H4 for a heated die temperature of 200°C. The hardness at H3 has dropped from 470 HV and 446 HV (at a die temperature of 100°C) to 453 HV and 402 HV, for the ten and four second quench, respectively. At these hardness levels, the microstructure is still expected to be mostly martensite. At location H4, the hardness has dropped by approximately 30 HV for both quench durations. There is a slight drop in hardness at H2, which is in the cooled part of the tool and is not expected to be affected by the heated side. A drop of 20 HV and 25 HV is seen for the four second and ten second quench, respectively.

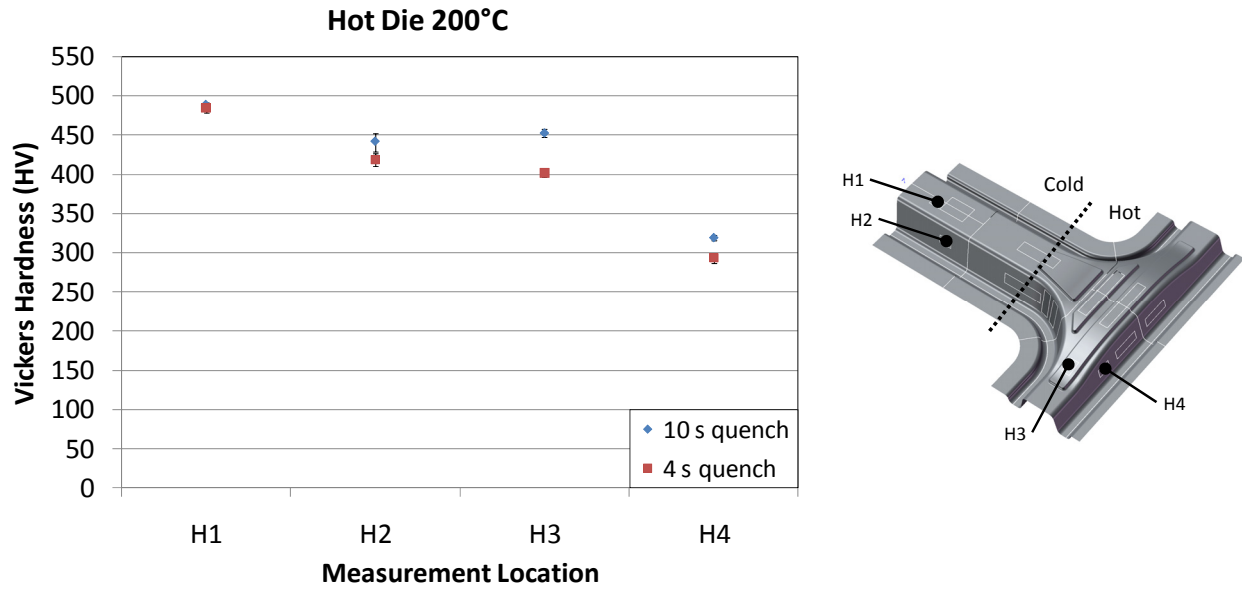


Figure 34 – Experimental results 200°C (H1-H4)

Figure 35 displays the hardness plots for H5 and H6, for both quench durations. The curves for the ten second quench have not changed significantly and the effect of the heated die is not yet apparent. There is some additional softening at the H6 position for the four second quench. At either end of the curve (position = 0 mm and position = 90 mm), the hardness indicates that the microstructure is still fully martensitic.

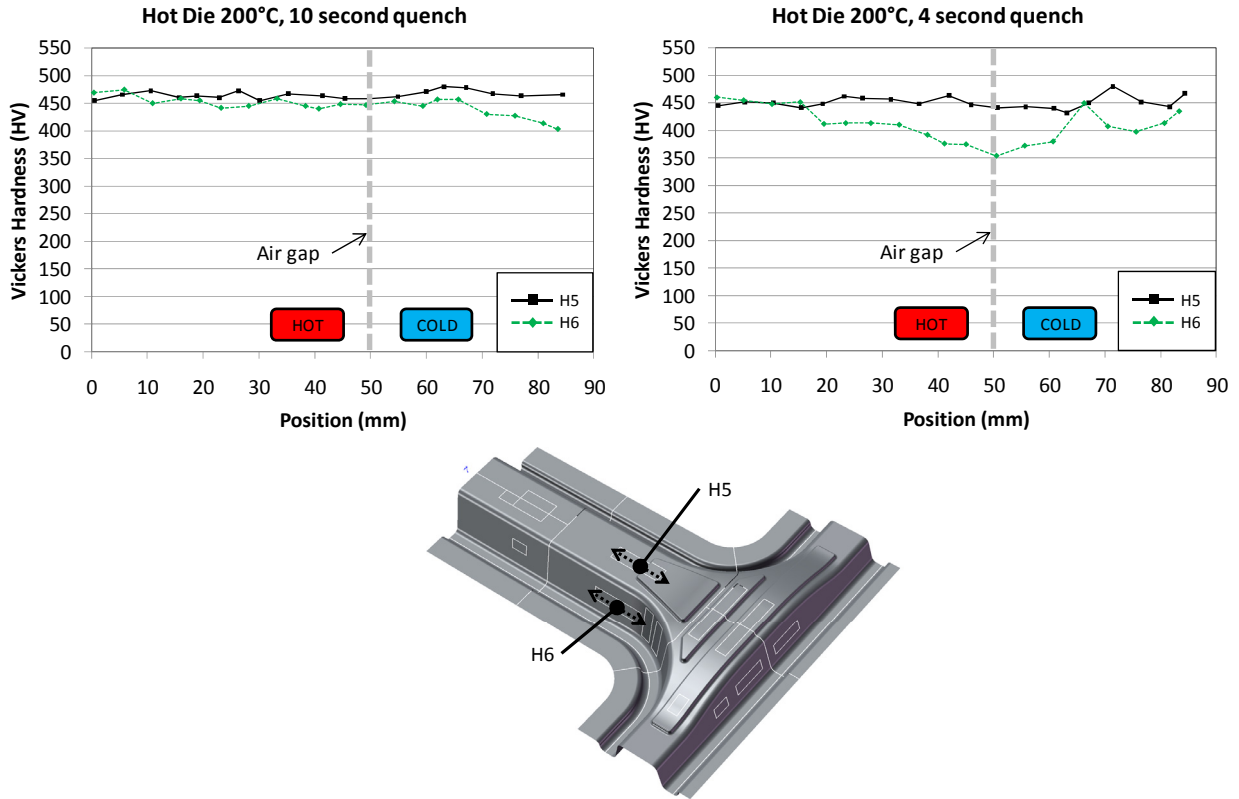


Figure 35 - Experimental results 200°C (H5 & H6)

### 3.2.4 Heated Die Results – 300°C

At a heated die temperature of 300°C, significant softening occurs in the heated regions compared to the baseline case. Measurement H4, which is the softest measured location, has dropped to 272 HV with a ten second quench, and 254 HV with a four second quench (Figure 36). However, there is now an unexpected drop in hardness at H2; which is in the fully cooled region and is expected to be fully martensitic. It has dropped to 432 HV and 395 HV for the ten second and four second quench, respectively.

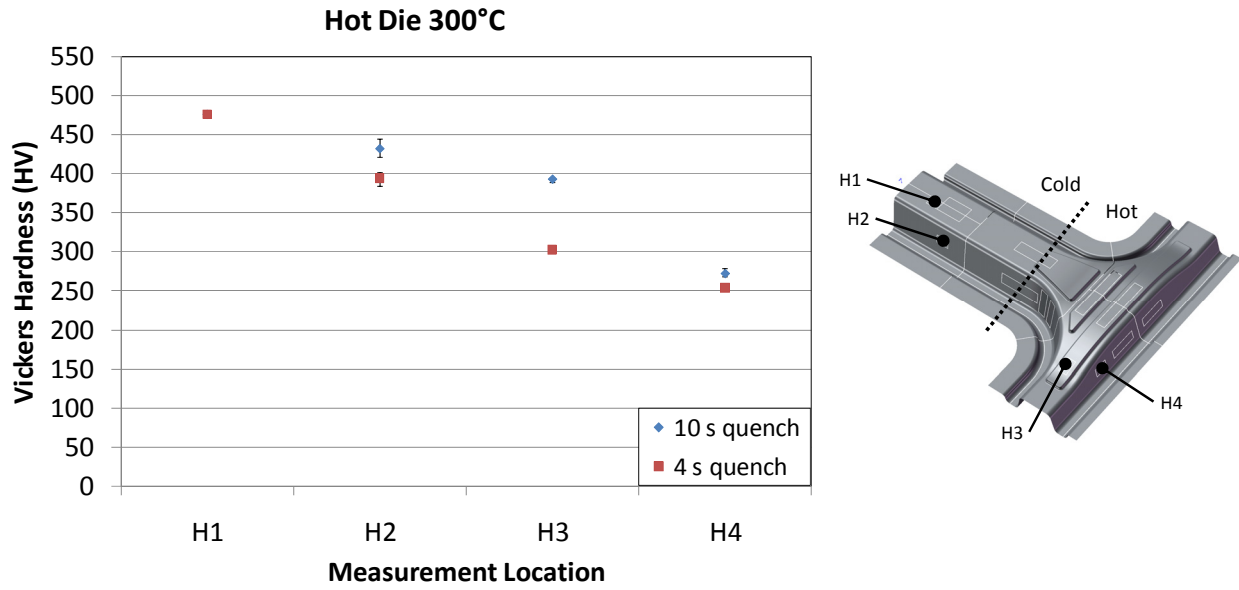


Figure 36 - Experimental results 300°C (H1-H4)

Figure 37 shows the hardness plots across the H5 and H6 transitions for the two different quench times. For the ten second quench the hardness profiles are very uniform, ranging from 400-450 HV at H5 and 350-425 HV at H6. It was expected that given the results from H3 and H4, there would be a noticeable difference between the heated and cooled sides. For the four second quench, however, some trends begin to emerge. Looking at the H6 hardness lines, there is a moderate hardness difference between the hot and cold sides. As expected, the material is softer in the heated zone and harder in the cooled zone. The H5 line, however, shows an opposite and unexpected trend. The cooled side of the part along the top face is showing a decrease in hardness compared to the heated side, which is counter-intuitive. Possible reasons for this response are discussed in later sections of this thesis.

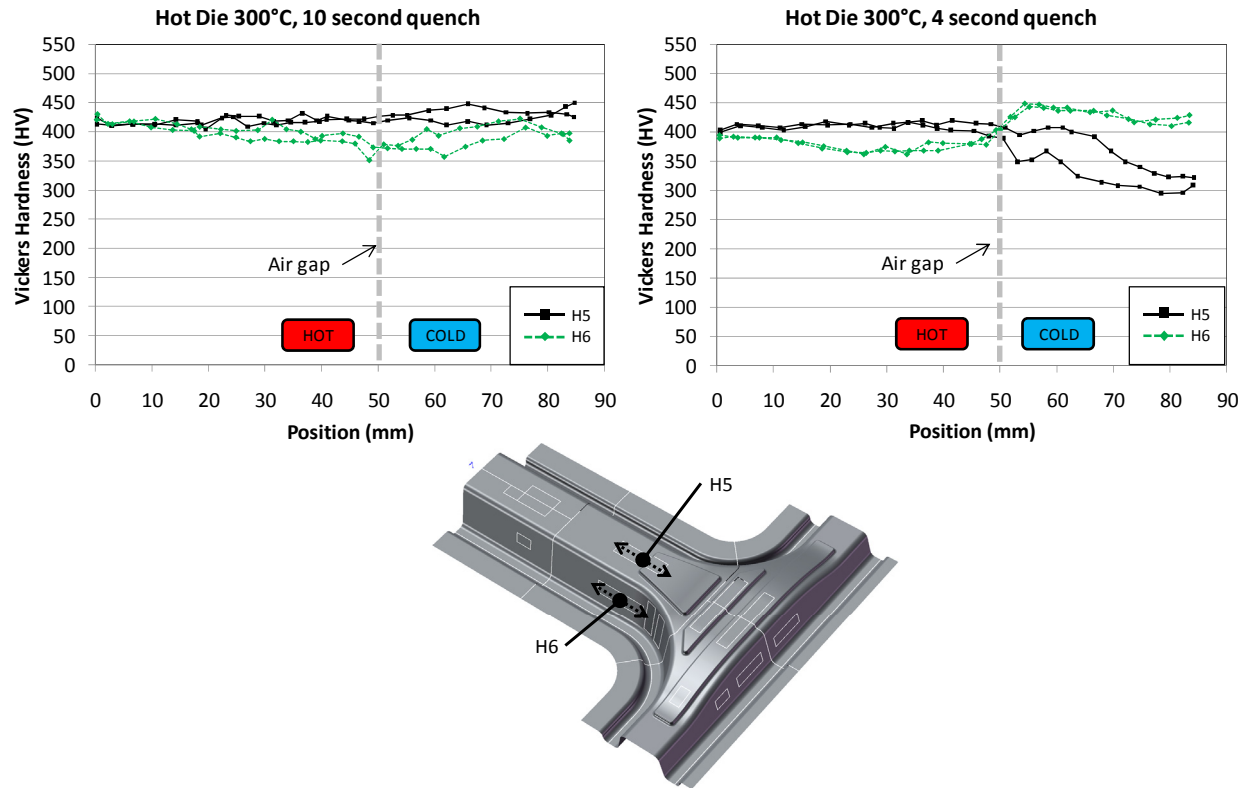


Figure 37 - Experimental results 300°C (H5 & H6)

### 3.2.5 Heated Die Results – 350°C

At a heated die temperature of 350°C, even more softening is seen in the heated areas of the part (Figure 38). Measurement H4 has dropped to 250 HV for the ten second quench and 238 HV for the four second quench. The measurements at H3 have also dropped and the spread between them has reduced to 47 HV. Similar to the 300°C experiments, there is now a drop in hardness at H1 for the four second quench, which is in the fully cooled region and is expected to be fully hardened.



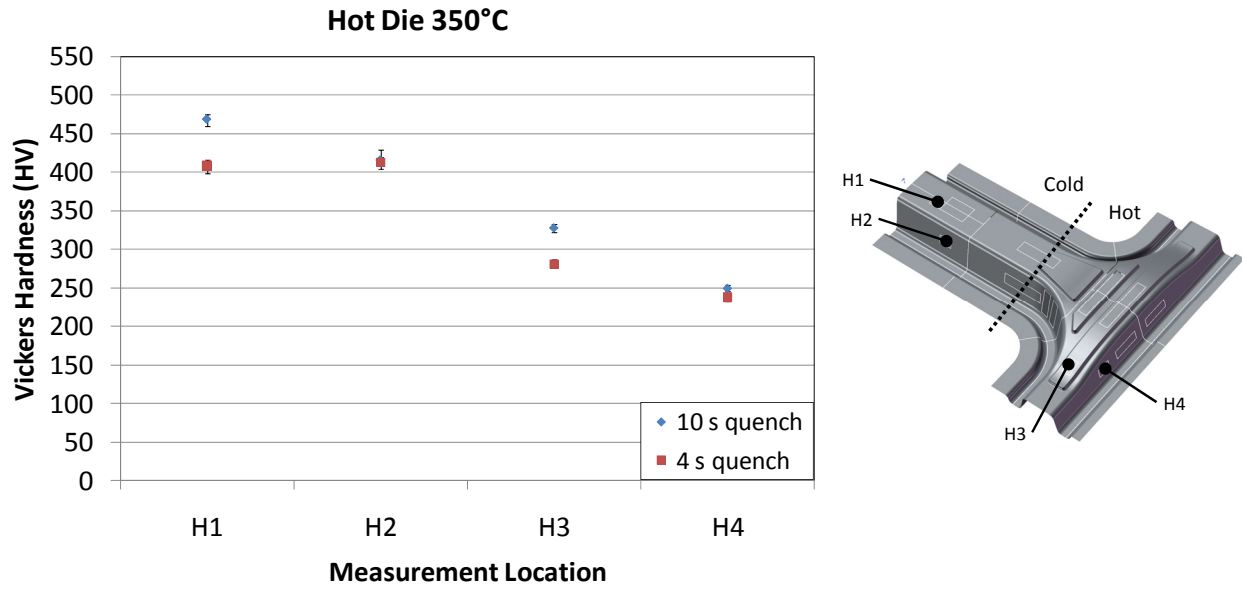


Figure 38 - Experimental results 350°C (H1-H4)

Figure 39 shows plots for the ten second and four second quench durations. Similar to the 300°C results, the H5 location with a ten second quench shows very little difference in hardness across the examined length, but with a slight downward shift from the previous case. The profile at location H6 with the ten second quench is starting to show an upward trend in hardness from the hot to the cold section of the tooling.

The four second quench in Figure 39 is showing very similar trends compared to the 300°C results. The hardness measurements at H6 are moving in an upward trend from hot to cold; however, the H5 measurements are still showing a similar decrease in hardness from hot to cold. Both curves have shifted downward approximately 50 HV compared to the previous 300°C results.

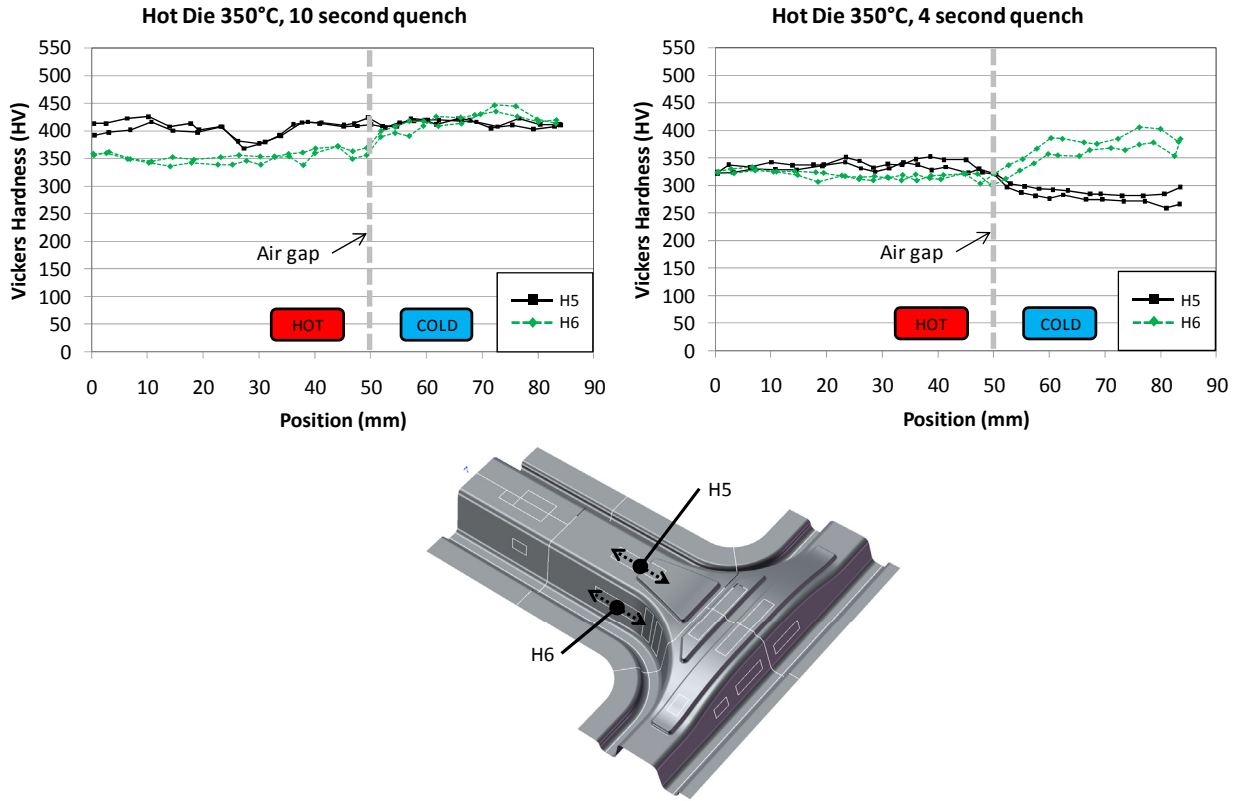


Figure 39 - Experimental results 350°C (H5 & H6)

### 3.2.6 Heated Die Results – 400°C

At a heated die temperature of 400°C there is some additional softening throughout the part. Figure 40 shows the results for locations H1 to H4. The softest location, H4, has not changed significantly compared to the die temperature of 350°C. The hardness at H3 has dropped to 299 HV and 265 HV, for the ten second and four second quench, respectively.

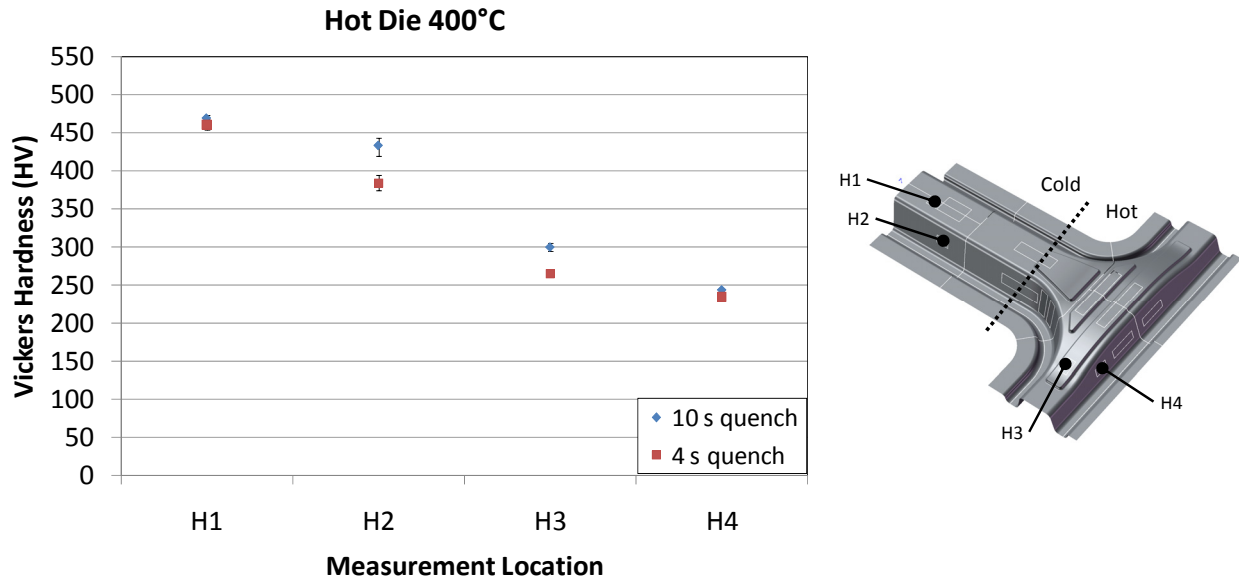


Figure 40 - Experimental results 400°C (H1-H4)

Figure 41 displays the H5 and H6 hardness profiles for the two quench durations. The plot for the ten second quench is now showing some more obvious trends than the previous results for 350°C. There is a noticeable increase in hardness at H6 ranging from approximately 300 HV in the heated area to 450 HV in the cooled area. There is a similar, although less significant, rise in hardness at the H5 location as well.

The four second quench is showing similar, but more defined, trends with H5 and H6 compared to the previous 350°C results.

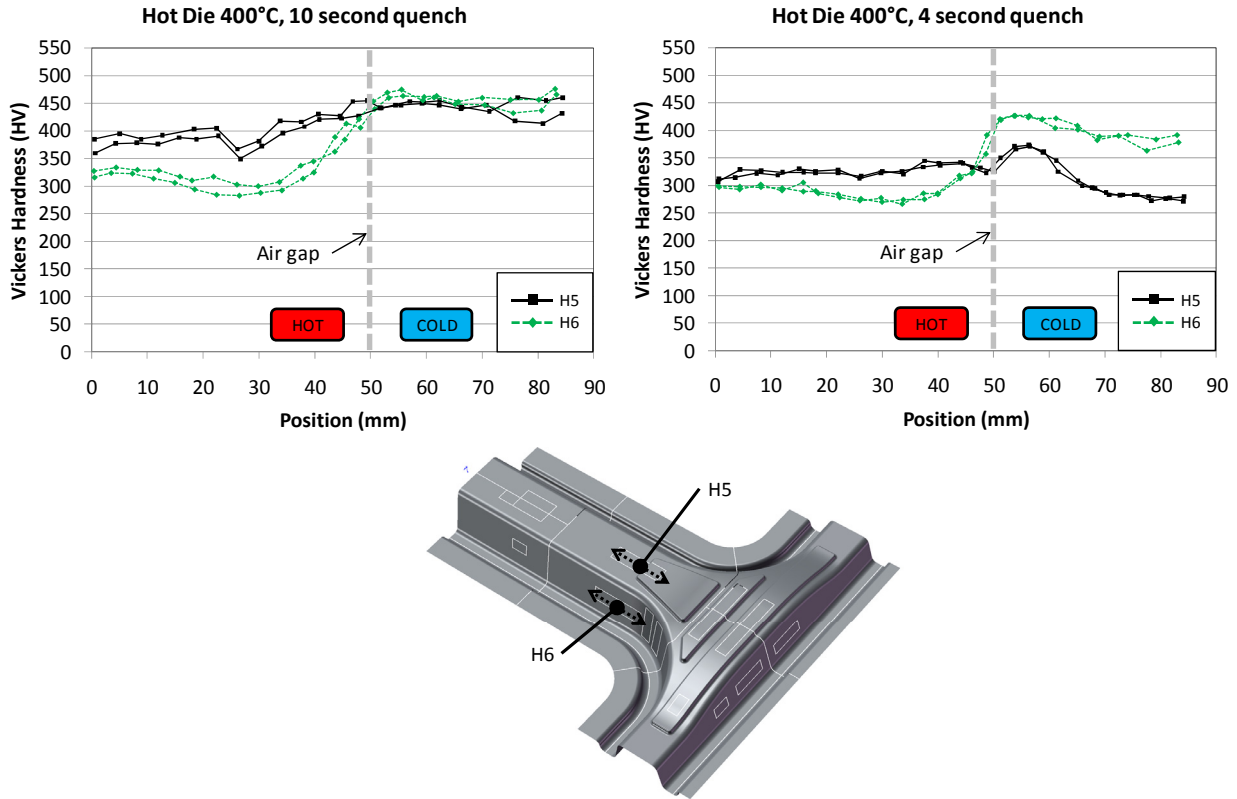


Figure 41 - Experimental results 400°C (H5 & H6)

### 3.3 Thermal Expansion of the Tooling

The measured hardness data at the locations remote from the transition zone between the heated and cooled tools exhibited the expected trends of high hardness in the cooled region and reducing hardness in regions where the die temperature was increased. The measurements located near the transition zone exhibited an anomalous hardness distribution in that the hardness was lower on the cooled side of the air gap. As discussed in the following, this behavior was attributed directly to the thermal expansion of the heated portion of the die. As noted in Section 2.2, thermal compensation of the tooling geometry was considered impractical in the initial design of experiments since a range of die temperatures were considered. As the dies were heated to the highest temperatures, it was noticed that there was a significant change in height of the heated portion of the die with respect to the cooled part of the die. An exaggeration of this is shown in Figure 42a. As the tooling comes to a close, the heated sections will come into contact first and the cooled sections will still have clearance between them. This clearance in the cooled section means that there will be a variation in the interfacial contact pressure between the blank and the tooling during the quenching stage. This reduction in contact pressure will reduce the heat

transfer and the part will not have uniform mechanical properties within each zone of the die. Figure 42b is an illustration of what happens during the experiments when the die is fully closed and the tonnage is applied. Since there is extra clearance on the cooled side of the tooling, as the hydraulic cylinder acts downward on the press slide it forces the entire slide and tooling to rotate slightly until contact is made between the cooled surfaces. This creates a very non-uniform pressure distribution across the blank which may explain some of the non-intuitive results from the previous sections.

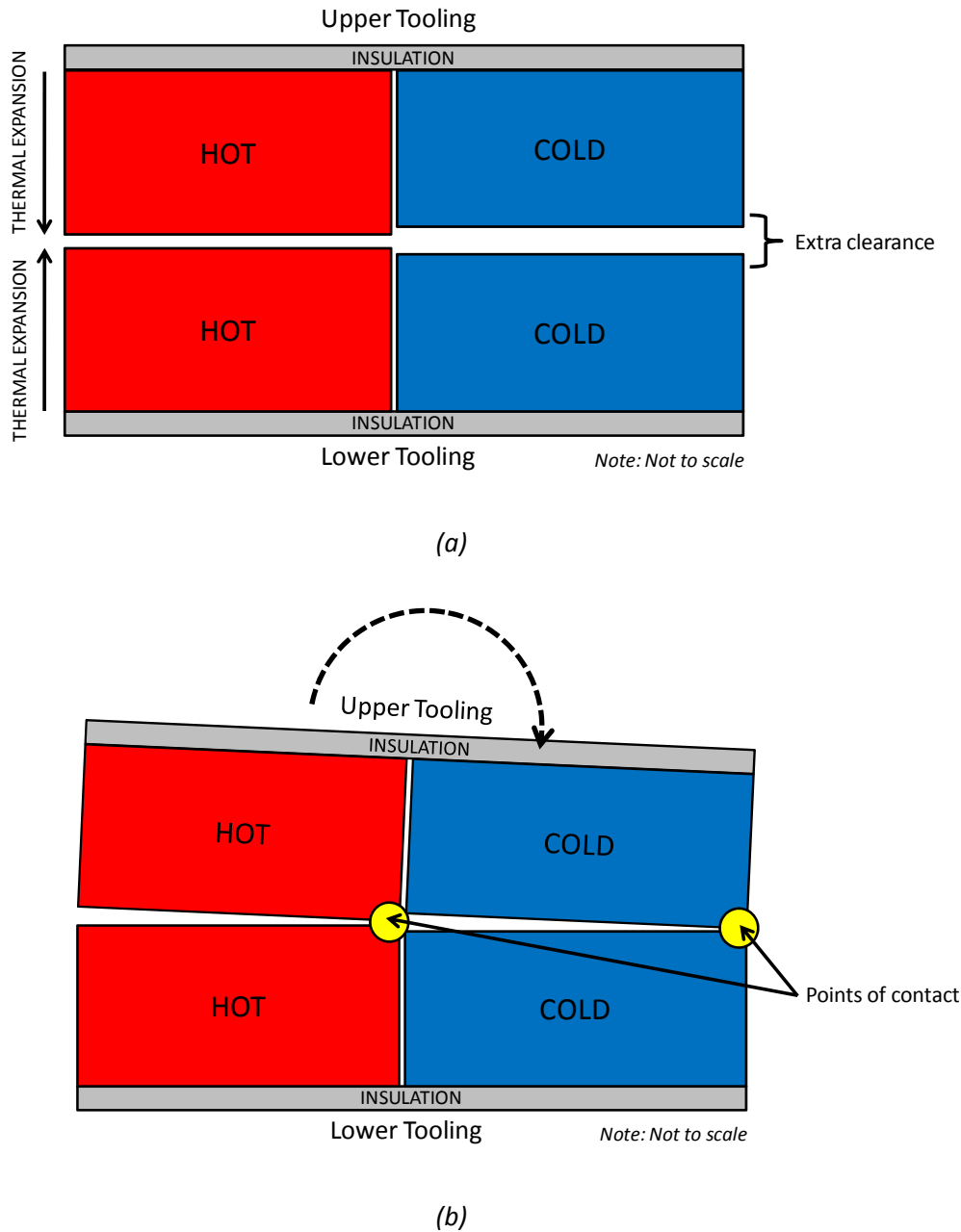
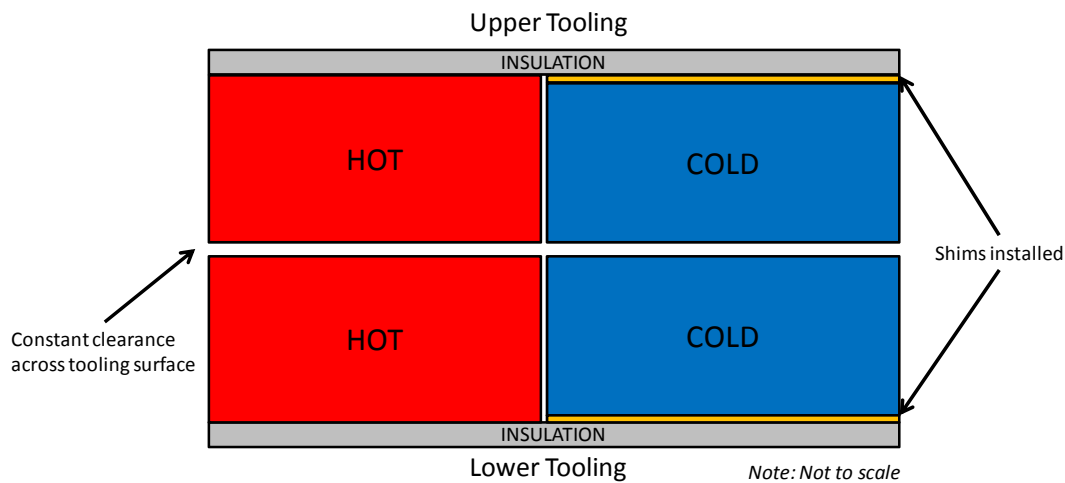


Figure 42 - (a) Thermal expansion of the die (b) Rotation of slide/upper tooling

To account for the thermal expansion in the vertical direction (along the line of the punch stroke), shims were installed underneath the cold tooling to bring the contact surfaces in-line with the heated sections (Figure 43). The required shim thickness is determined by the temperature of the heated die. To determine the effects of the shim, the highest die temperature was examined. The die temperature was set at 400°C and the initial clearance was measured. The shims required to align the contact surfaces of the tooling were 0.016" and 0.025" for the upper and lower tooling, respectively. Experiments at 400°C with the shimmed tool were then performed. Note that thermal expansion effects will still result in geometric differences in the lateral dimensions of the tooling (measured perpendicular to the direction of the punch stroke); however, these were judged as less significant for the current study but could be corrected by re-machining the tooling to compensate for the thermal expansion effect.



**Figure 43 - Shims installed**

### 3.3.1 Heated Die Results – 400°C with Shimmed Tooling

The 400°C experiments were repeated with the shimmed tooling to determine if the thermal expansion of the die was causing the unexpected results from the 300°C, 350°C, and 400°C test cases. Figure 44 shows the previous results (left) compared to the new results with the shimmed tooling (right). The results at H3 and H4 are very similar, and no significant difference is noticed. The main difference between the two occurs at locations H1 and H2, where in the previous results there was a softening behavior at these locations. With the shims installed, the hardness at these locations is the same as the baseline case, which is as expected.

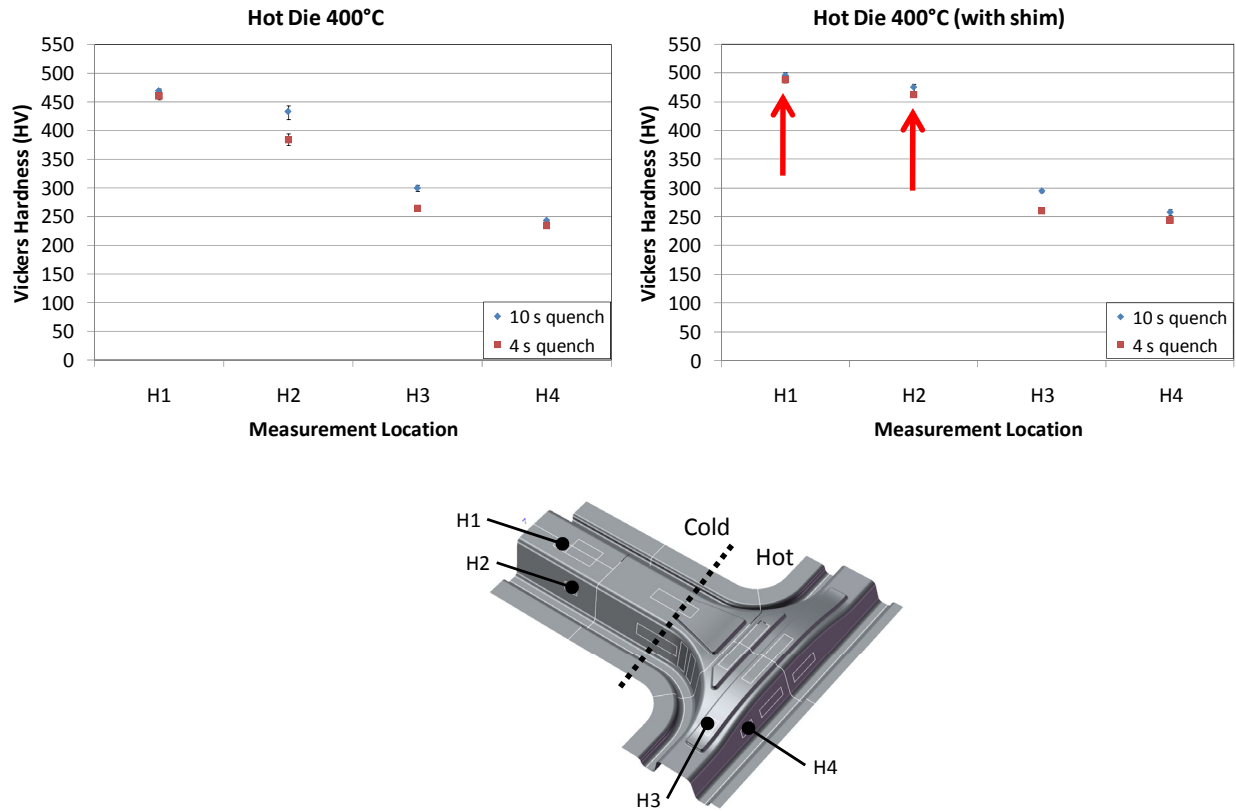


Figure 44 - 400°C (H1-H4) shimmed die

Figure 45 shows four plots which compare the shimmed tooling to the previous results. To simplify the graphs, only one curve from the previous results is shown. The results for the four second quench at H5 and H6 show a significant improvement in terms of the hardness difference between the heated and cooled regions. The ten second quench shows little difference between the two cases, only with a slight improvement at H5.

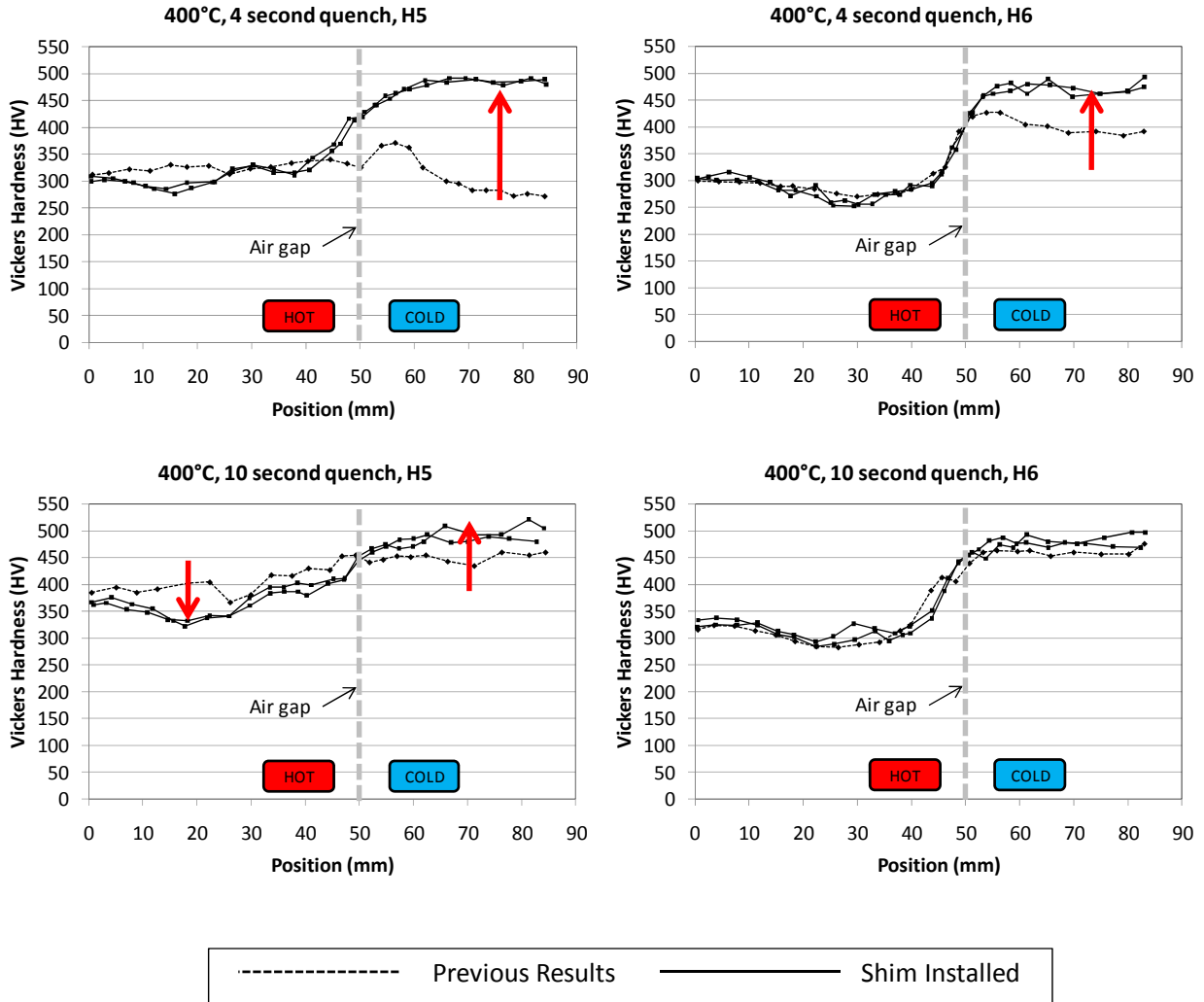


Figure 45 - 400°C (H5 & H6) shimmed die

Shimming the tooling to account for the thermal expansion has improved the response of the measurements to align with the behavior that is expected. This shows the importance of thermal expansion and taking it into account when designing a tool similar to this. In practice this approach should be possible assuming that the operating temperatures in the various regions of the die are predetermined based upon results such as those provided in this study.



## 4 Numerical Modeling

The Finite Element (FE) model for these experiments was solved using the explicit dynamic formulation within LS-DYNA Version 971 revision 5 [27]. The hot forming process is composed of five main steps, as outlined previously in Figure 27. To model the entire process, a similar break-down was performed for the models. A total of four models are run to simulate the hot forming process from start to finish. The purpose for this was to reduce the total computing time necessary, by individually mass-scaling each simulation depending on the nature of the simulation step while still maintaining reasonable accuracy. Information is passed from one simulation to the next using the DYNAIN input/output files. Refer to Appendix E for more details on the several simulation steps.

Mass-scaling is a common numerical technique which is used to reduce the total computation time of a simulation that uses explicit time integration. The timestep of an explicit simulation must be small enough such that it satisfies the Courant criterion [31]. For shell elements, the maximum timestep can be defined by the following equation, where  $L_s$  is the minimum characteristic element length in the model and  $c$  is the speed of sound in that material [31]:

$$\Delta t_{max} = \frac{L_s}{c}$$
$$c = \sqrt{\frac{E}{\rho(1 - \nu^2)}}$$

It is possible to increase the timestep to reduce the number of computations, thus reducing the overall computation time, by artificially increasing the density,  $\rho$ , by several orders of magnitude. This must be performed with caution, as inertial effects may become significant due to the elevated mass of the parts.

For example, during the forming stage, the blank undergoes significant deformation. Heavily mass-scaling the blank during this stage would result in significant inertial effects and the formed part in the model would not represent the actual strains and strain-rates which are encountered in the experiments. However, during the cooling stage where the only deformation is due to thermal contraction, mass scaling can be increased by many orders of magnitude without ill-effects. A summary of the four simulation steps and their respective mass scaling factors are shown in Table 3. Although the mechanical density is scaled in all of the simulations, the thermal density (used for the thermal

calculations) is always maintained at the actual physical value. This ensures that there is no additional thermal mass as the mechanical mass increases.

**Table 3 - Mass Scaling Factors**

Process Step	Duration (sec)	Mass scaling factor
Transfer	10	100
Forming	1.6	100
Quenching	4 or 10	100,000
Final Air Cooling	500	100,000,000

### 4.1 Tooling Mesh and Configuration

All of the meshing was performed using Altair Hypermesh 10. Due to the symmetry of the tooling, all of the models were created as half-symmetry models. An example of this can be seen in Figure 46 with the half-model of the lower tooling shown. Typically in metal-forming operations the tooling is modeled with shell elements, which greatly improves the calculation time. However, the tooling here was modeled with solid elements to capture the rise in surface temperature of the tool as it comes into contact with the hot blank, and also the heat transfer from the surface through to the rest of the tooling.

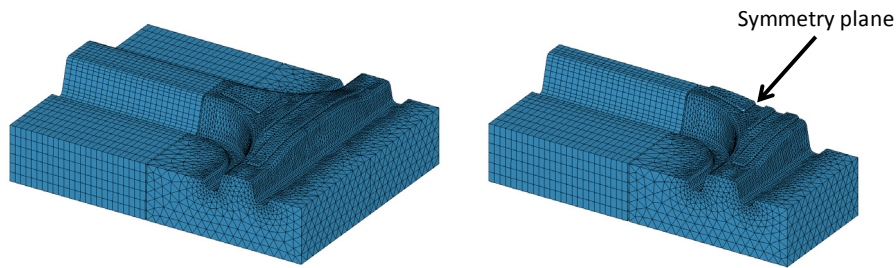


**Figure 46 - Half-symmetry model**

To model the experiment as closely as possible, the ceramic insulation between the tooling and the bolster plates was modeled to get the appropriate temperature distributions within the tooling. For purposes of modeling the heat conduction from the heated section to the cooled section through the air gap, the gap was modeled with solid elements (Figure 47).

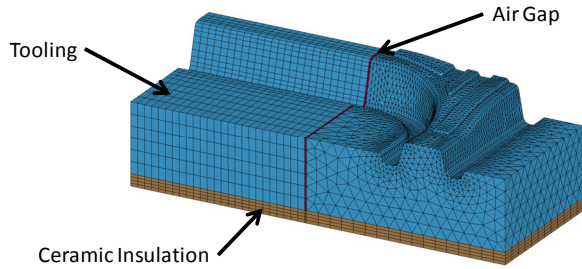


**Figure 47 - Insulation & air gap model**

To minimize the computation time, a coarse mesh was used for the solid tooling, with an element size ranging from approximately 5 – 30 mm. This does, however, create a problem for forming simulations when coarse elements on the tool radius come into contact with the blank with relatively small elements (Figure 48). To accommodate this, the tooling surface which comes into contact with the blank is meshed again with shell elements, and their size is reduced to capture the finer geometry of the tooling. It is placed over top of the existing solid elements (Figure 49). The surfaces are connected together (both thermally and mechanically) in LS-DYNA using the keyword \*CONTACT\_TIED\_SURFACE\_TO\_SURFACE. In this configuration, only the shells are defined to have mechanical and thermal contact with the blank. There is a very high thermal conductivity defined between the shells and solids, as they are essentially acting as a zero-thickness interface between the blank and tooling. The heat then travels through the tooling and captures the temperature rise from the hot blank.

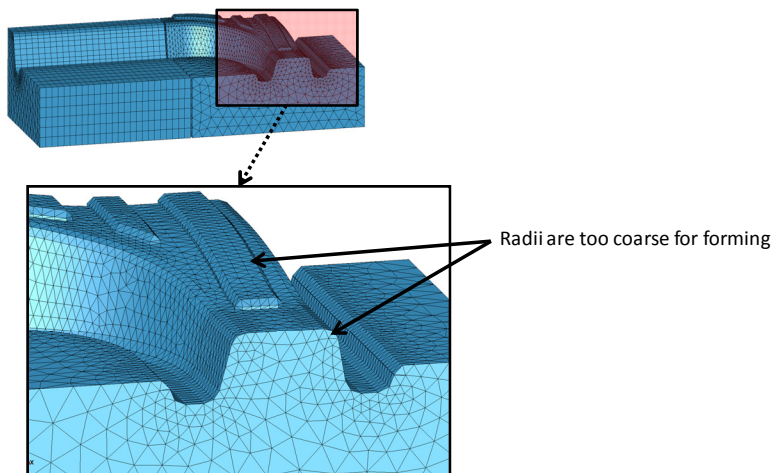


**Figure 48 - Coarse solid mesh**

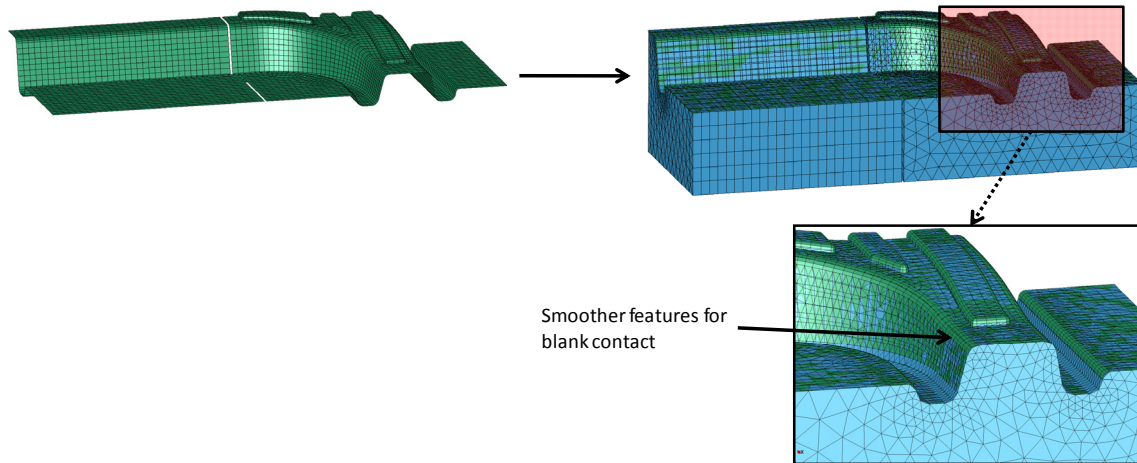


Figure 49 - Tied surfaces for forming

#### 4.1.1 Steady-State Thermal Distribution

To model the hot forming process with a heated die, it is necessary to get the initial thermal state for the tooling first. This is done with a steady-state thermal model with all heat sources (cartridge heaters) and heat sinks (conduction, convection, radiation). The cartridge heaters mount from the underside of each tool (Figure 50). There are three groups of heaters which have their own PID control system: one group in the lower tool (6 heaters), and two groups in the upper tool (5 along the back edge, and 4 at the “T”). Surface segments are defined across the cylindrical surface area of each of these holes and grouped based on their control group.

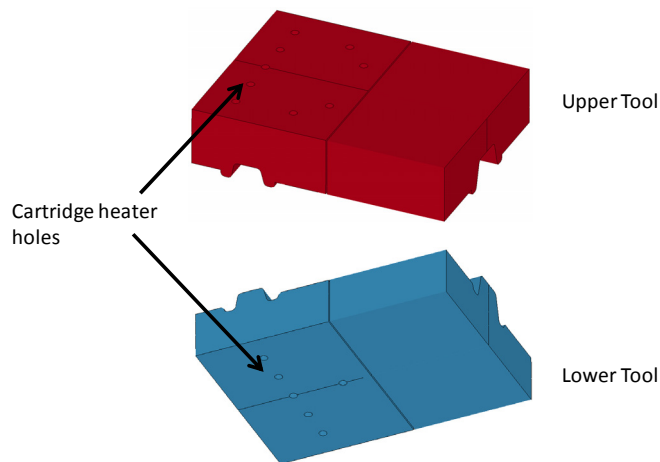
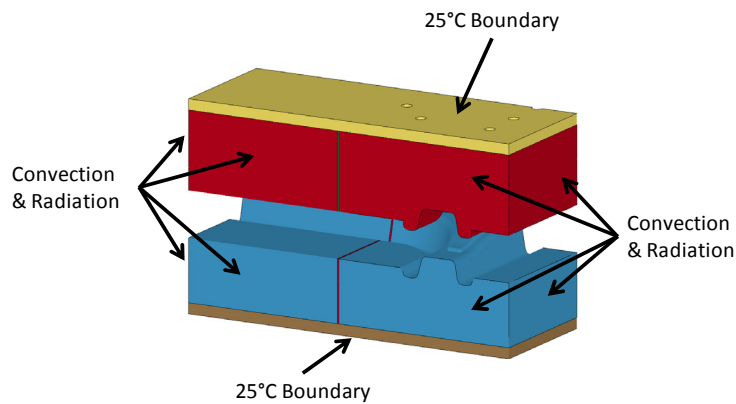


Figure 50 - Cartridge Heater Locations

Convection and radiation boundary conditions are applied to all of the outside faces of the tooling. Free convection is assumed with an ambient temperature of 25°C. The faces of the insulation plates which

mount against the press/bolster are assumed to stay constant at 25°C. This is illustrated in Figure 51. Heat transfer from the hot side to the cold side occurs through the air gap from conduction through the air and also radiation exchange between the surfaces. The conduction was modeled by meshing elements which represent the air with the thermal properties of air. A radiation exchange was modeled between the hot and cold faces to account for this heat transfer mode. The water cooling channels were modeled by placing 25°C boundary conditions on the nodes where the water channels run through the tool.



**Figure 51 - Thermal Boundary Conditions**

Figure 52 shows a steady state thermal distribution (half symmetry) for the tooling and insulation. The cartridge heater flux has been input by trial and error until the die surface temperature reaches the approximate target temperature, in this case 350°C. One of these simulations is performed for each heated die temperature. The tooling and all insulation is rigid and thermal expansion is not considered.

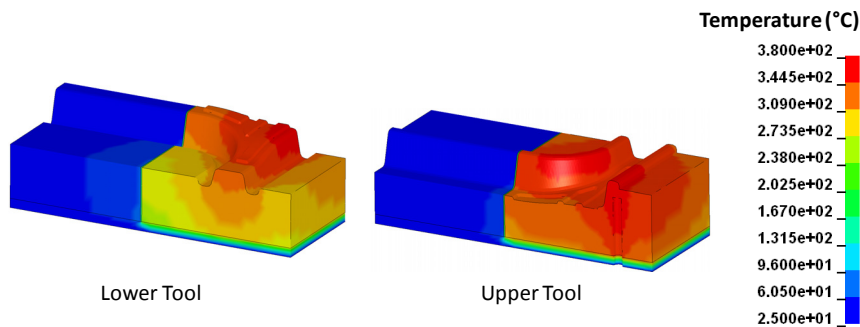


**Figure 52 - Temperature Distribution (350°C)**

After the steady state thermal simulations are performed, the final nodal temperatures are used as an initial condition for the remaining forming and quenching simulations.

The power input for the steady-state thermal simulations is approximately 70% of the average recorded power consumption from the experiments at a die temperature of 400°C. This discrepancy suggests that there is a need to improve the assumptions and boundary conditions for these models.

#### 4.1.2 Material Properties and Definitions

A total of four materials are used to define the experimental setup in these simulations. Their thermal properties are listed below in Table 4. The tooling, ceramic, and air gap were all defined as the same rigid material with density, modulus of elasticity, and Poisson’s ratio to be 7890 kg/m<sup>3</sup>, 100 GPa, and 0.3, respectively.

**Table 4 - Material Thermal Properties**

Part	Actual Material	LS DYNA Material	Heat Capacity [J/kgK]	Thermal Conductivity [W/mK]
Tooling	4140 steel	*MAT_RIGID	460	24
Ceramic Insulation	Zircal 95	*MAT_RIGID	1172	0.6
Air Gap	n/a	*MAT_RIGID	1022	0.03
Blank	Usibor® 1500P	*MAT_UHS_STEEL	650	32

## 4.2 Blank Design and Definition

The blank is meshed with quadrilateral shell elements with 4 mm average length and is shown below in Figure 53. The blank shape was determined through a trial-and-error system using LS-Dyna to develop a geometry which minimized wrinkling potential and prevented tearing or other failures. The initial shell thickness is set to 1.21 mm, which is the nominal thickness plus thermal expansion at 930°C.

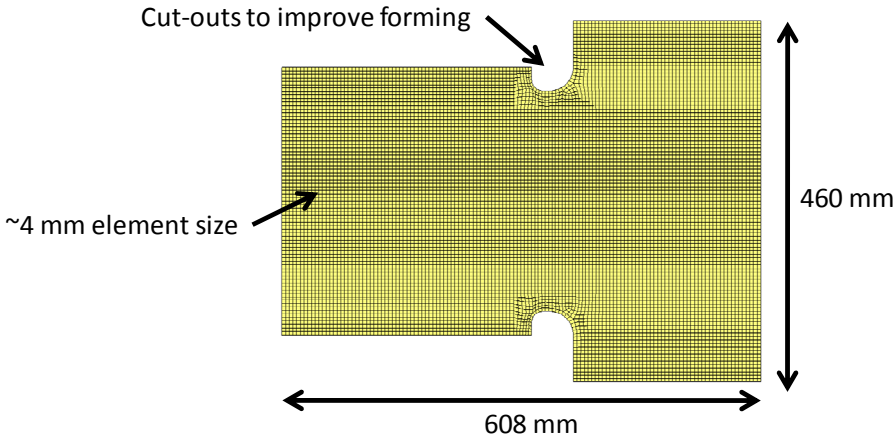


**Figure 53 - Blank Mesh**

A mesh size of approximately 4 mm was chosen because it is a representative length of some of the die features and radii. However, to more accurately model the deformation of the blank and punch forces, smaller elements are required along the small radii and other regions which undergo significant bending. An adaptive meshing scheme was implemented during the forming phase of the process, where elements which have undergone significant deformation due to bending are split into smaller elements. The remeshing is shown in Figure 54 where the blank is remeshed automatically during heavy deformation. The purpose of using adaptive meshing, rather than starting the simulation with a much finer mesh, is to reduce computation time and number of elements.

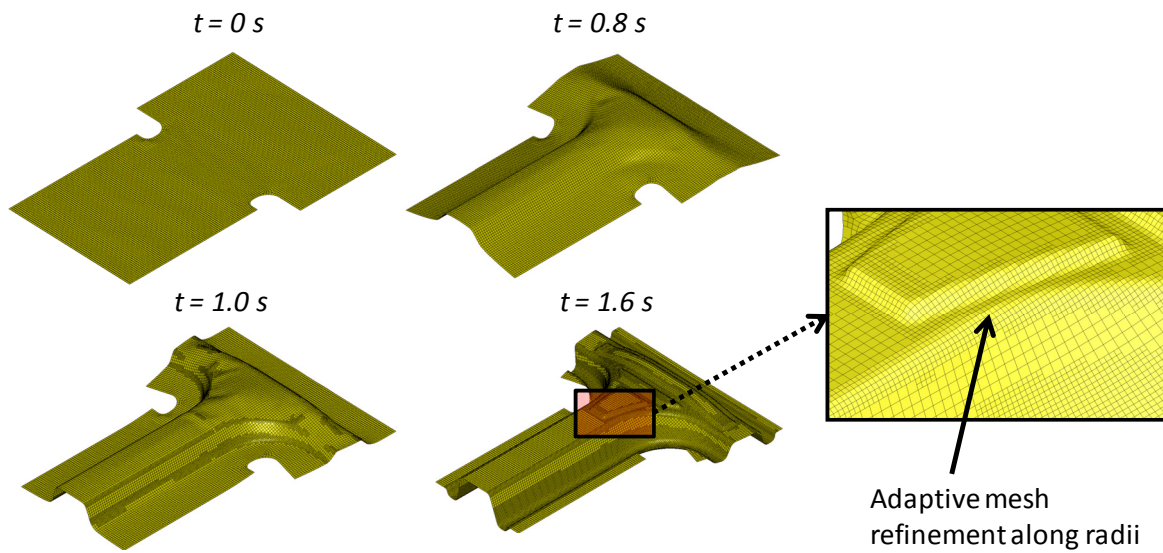


**Figure 54 - Adaptive Meshing**

### 4.2.1 Blank Material Model & Validation

The material model used for the blank is a hot-forming model which is used to predict the microstructure evolution, Vickers hardness, and yield strength after forming and quenching. The material definition is \*MAT\_UHS\_STEEL and is available in LS-DYNA version 971 revision 5. The development of this model was performed by Paul Åkerström and colleagues at the University of Luleå, Sweden [1]. The material card definition is very elaborate and requires inputs such as chemical composition, phase activation energies, latent heat of decomposition, and flow curves for all of the phases. The card definition and input file used for the simulations is available in Appendix B. The input parameters were supplied by Arthur Shapiro at LSTC [29].

Figure 55 shows the material model validation using a single element which has a prescribed constant flux imposed on it. Cooling rates of 100°C/s to 3°C/s were modeled and the temperature-time history is plotted. The CCT diagram from Appendix A has been superimposed on these results to see where the inflections occur with respect to the CCT lines. It is possible to see the change in slope of the predicted cooling curves as heat is released during the austenite phase decomposition.

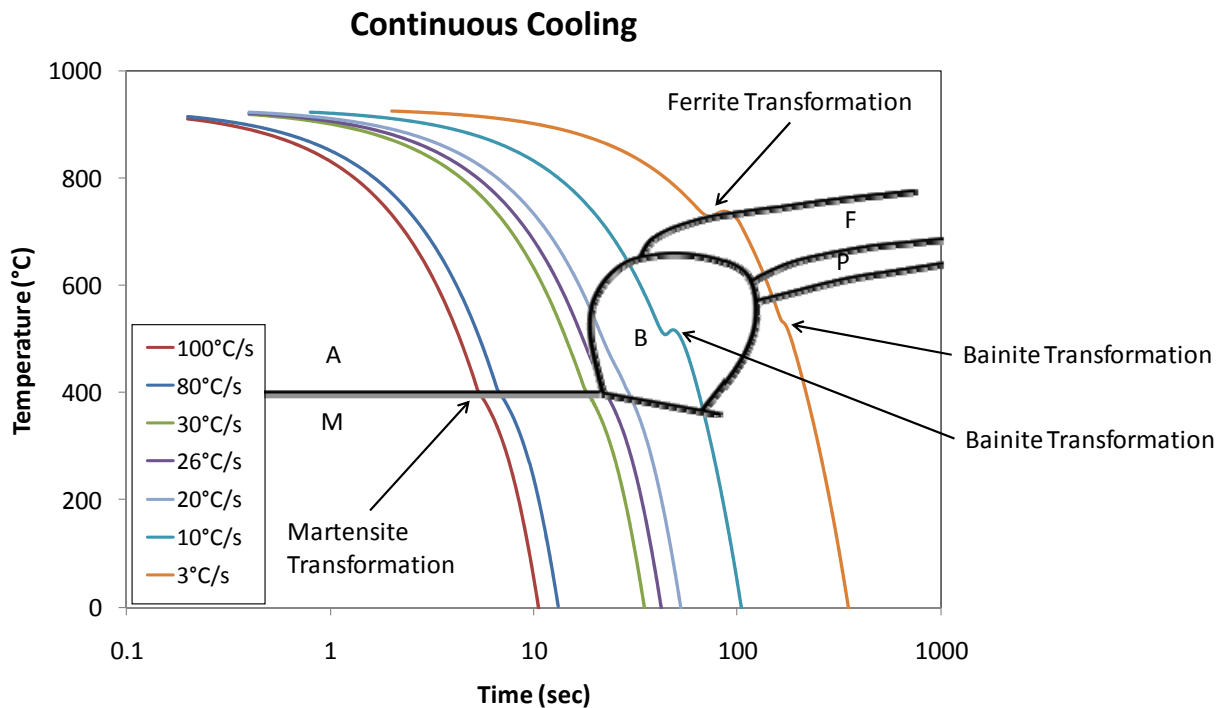


Figure 55 - Material Model Numerical Validation



Figure 56 shows a comparison between the predicted and measured hardness values listed on the CCT diagram from ArcelorMittal (shown previously in Figure 4). There is very good agreement between these curves, with only some minor differences seen near the critical cooling rate. It is possible that the differences observed here are due to slightly different interpretations of a “constant cooling rate”. The CCT testing performed by ArcelorMittal utilizes a perfectly linear cooling rate, where  $dT/dt$  is constant. The heat release during phase transformation does not affect the linear temperature-time relationship which has been imposed on the samples. However, the numerical validation shown here imposes a constant flux to cool the blank. Differences exist between these two methods due to the latent heat release as austenite is transformed to the daughter phases. Figure 57 shows a temperature-time plot for selected cooling rates with both perfectly linear and constant flux cooling. As the phase transformations occur, an offset between the curves becomes apparent. This offset reduces the effective cooling rate, which can either: increase the residence time in the bainite, ferrite, or pearlite window, which promotes further growth of these phases; or, shift the cooling line so that it passes into a different window, which will promote the growth of other phases that may not have otherwise been formed.

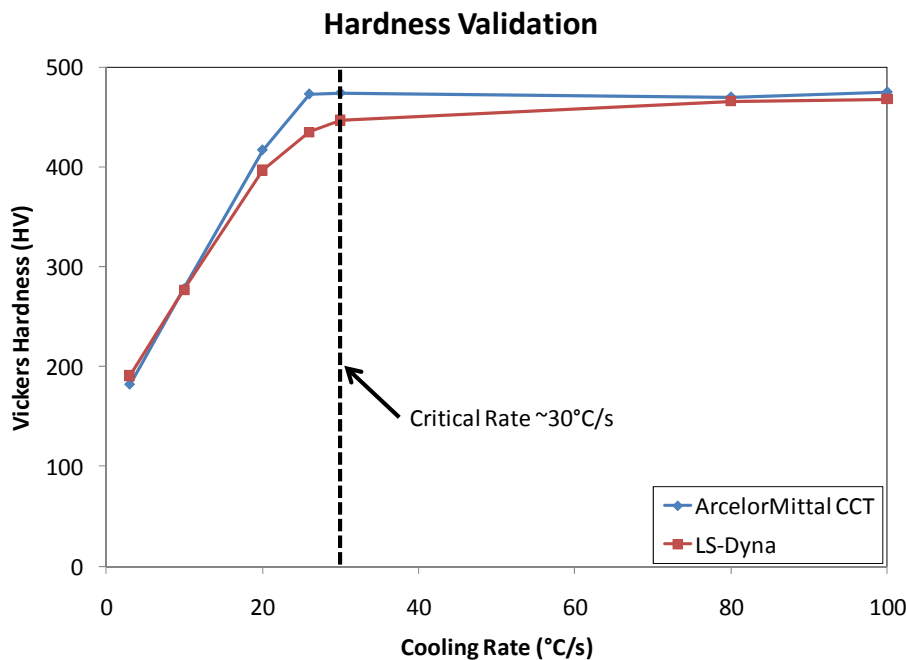


Figure 56 - Hardness Validation

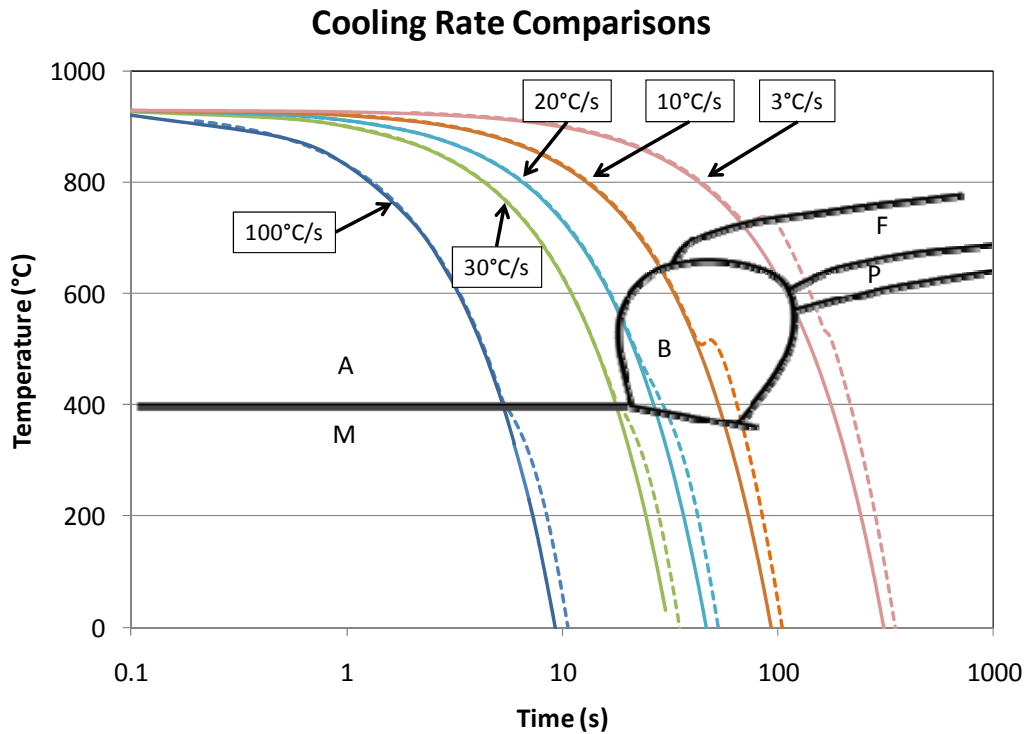


Figure 57 - Perfectly linear cooling (solid lines) and constant flux cooling (dotted lines)

### 4.3 Free Cooling Validation

The cooling of the blank in still air after the forming and quenching is an important step in the simulation. During this step, the remaining austenite in the microstructure will transform into either martensite or bainite, which is entirely based on the cooling rate of the material. The cooling of the blank occurs by heat transfer due to convection and radiation to the surroundings.

Analytical correlations are available for the heat transfer due to free convection on the upper and lower surfaces of a flat plate. These equations are given below and were taken from [32].  $Nu_L$  represents the Nusselt number, and  $Ra_L$  represents the Rayleigh number.

$$\text{Upper Surface} \quad \overline{Nu}_L = 0.15Ra_L^{\frac{1}{3}}$$

$$\text{Lower Surface} \quad \overline{Nu}_L = 0.27Ra_L^{\frac{1}{4}}$$

$$\text{Convection Coefficient} \quad \bar{h} = \overline{Nu}_L \frac{k}{L}$$

Load curves were created for the convection coefficient with respect to the surface temperature of the blank by using these equations and tabulated properties for air [32]. Radiation exchange is also an important parameter to consider at these high temperatures. The emissivity of the surface is the key parameter when defining heat transfer from a surface due to radiation. It is a difficult parameter to measure and it can vary constantly as the blank temperature changes and surface oxides form. A load curve was estimated and defined for the emissivity with respect to surface temperature. These curves for convection and emissivity can be found in Appendix F.

An experiment was performed where a blank was instrumented with three thermocouples and placed into the 930°C furnace. This was shown previously in Figure 15. When the blank reached the furnace temperature and the microstructure had fully austenitized, it was removed from the furnace and allowed to cool in still air down to room temperature. An LS-DYNA model was then run with only the blank and the convection and radiation boundary conditions applied. This was compared with the experimental cooling results, and the emissivity parameter was modified until the curves showed good agreement with each other (Figure 58).

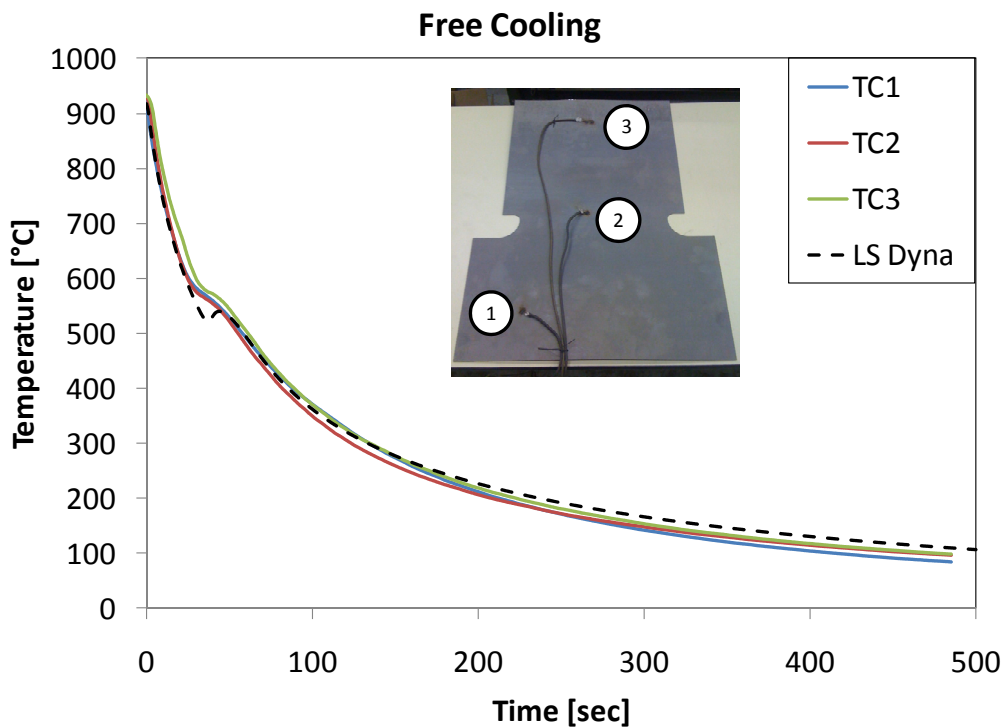


Figure 58 - Free Cooling Validation

## 4.4 Heat Transfer Coefficient

It is very difficult to accurately model the heat transfer coefficient (HTC) between the blank and the tooling. There are many factors which influence the heat flow, such as interface pressure, surface roughness, oxidation layers, die temperature, and so on. The HTC is a difficult parameter to measure, which becomes one of the greatest unknowns in the modeling of this process (discussed previously in Section 1.5.2). Work presented in [10], and a benchmarking problem in [33] has given a very good starting point in terms of the heat transfer coefficient as a function of interface pressure. However, it was found that by using these published parameters, the cooling of the blank was often over-estimated in some areas.

### 4.4.1 HTC Study

This section outlines the numerical study that was performed to attempt to improve the predicted quenching behavior in the models by modifying the HTC until “acceptable” hardness results were found. To determine the approximate range of interface pressures that will be experienced during quenching, a rough calculation was performed by taking the projected area of the blank and the tonnage applied. This gives an average pressure of 6.3 MPa over the entire blank area. Due to the fact that there will be regions of the blank which experience pressures that are either higher or lower than this, a range of 0-20 MPa was chosen for the study.

A series of parametric simulations were performed using different HTC values. After a simulation was complete, the results were analyzed and corrections were made to the HTC definitions in an effort to improve the hardness results. Three die temperatures were chosen (300°C, 350°C, and 400°C) with a four second quench to determine how the various HTC values affected the results. Figure 59 and Figure 60 show a graphical representation of the HTC for the various trials and corresponding contour plots of predicted Vickers hardness, respectively. It was found that at die temperatures of 350°C and greater, there were minimal changes with respect to the predicted hardness values for the HTC values used in the study. At 300°C, however, there were significant changes in the hardness results, which suggests that this die temperature induces a cooling rate very close to the critical rate of 30°C/s. Slight reductions in the HTC at this temperature resulted in prediction of the formation of bainite in large areas of the blank (indicated by a softer microstructure) that were originally martensite with using the baseline HTC.

As the HTC values were reduced beyond the “Final” values (Trial 5 in Figure 59), it was observed that the hardness in the cooled portion of the blank also dropped, which was not realistic based on comparison to the experimental results.

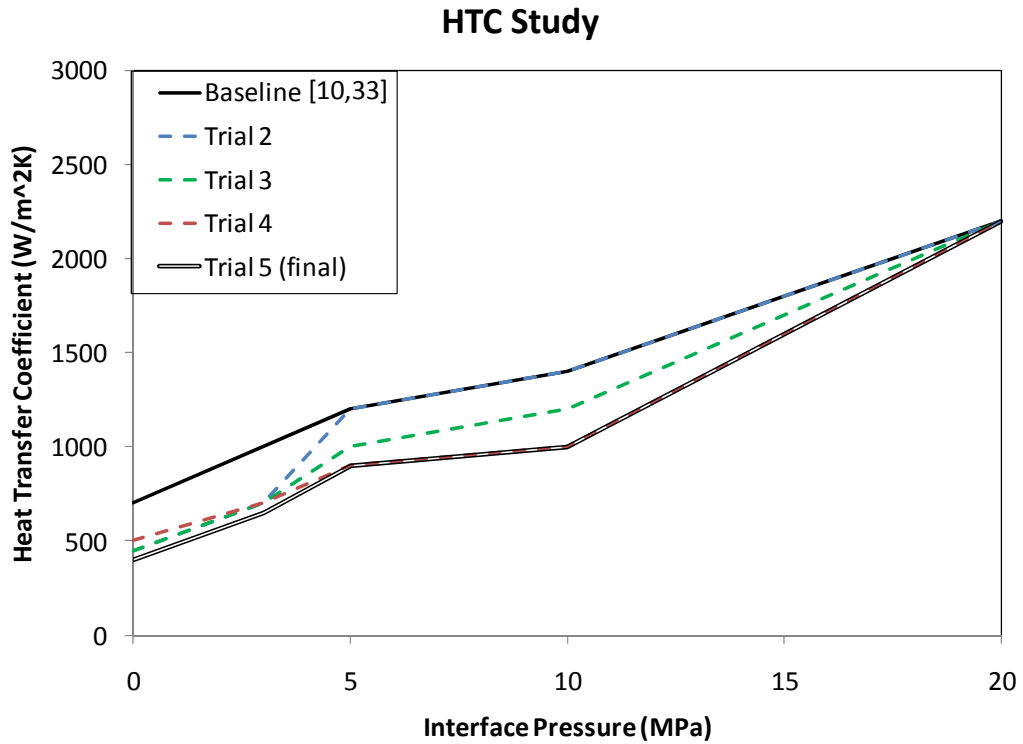


Figure 59 - HTC Study - Graph

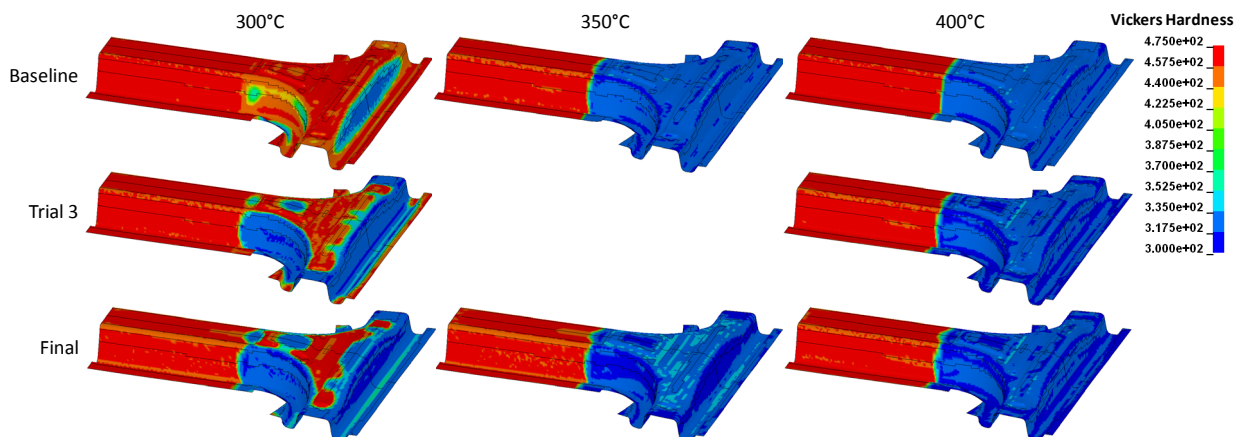


Figure 60 - HTC Study - Hardness Contour Plots for selected trials at 300°C to 400°C, showing effect of HTC on resulting predicted hardness

To quantitatively assess these results, the hardness predictions at locations H3 and H4 were compared to the experimental findings. These comparisons are shown in Figure 61 for each of the die temperatures. Locations H3 and H4 were chosen because they are located within the heated region of the tool and the hardness predictions from the model at these measurement locations differ significantly from the experiments. The experimental and numerical results for H1 and H2 (in the fully cooled region) had good agreement and are not examined in this study. From Figure 61 it is apparent that the only differences in the predicted hardness due to changes in HTC occur at location H3 for the 300°C die trial. The hardness predictions for the other die temperatures and locations are relatively constant and do not change significantly with changes in HTC, for the range considered. This can also be seen in the contour plots in Figure 60.

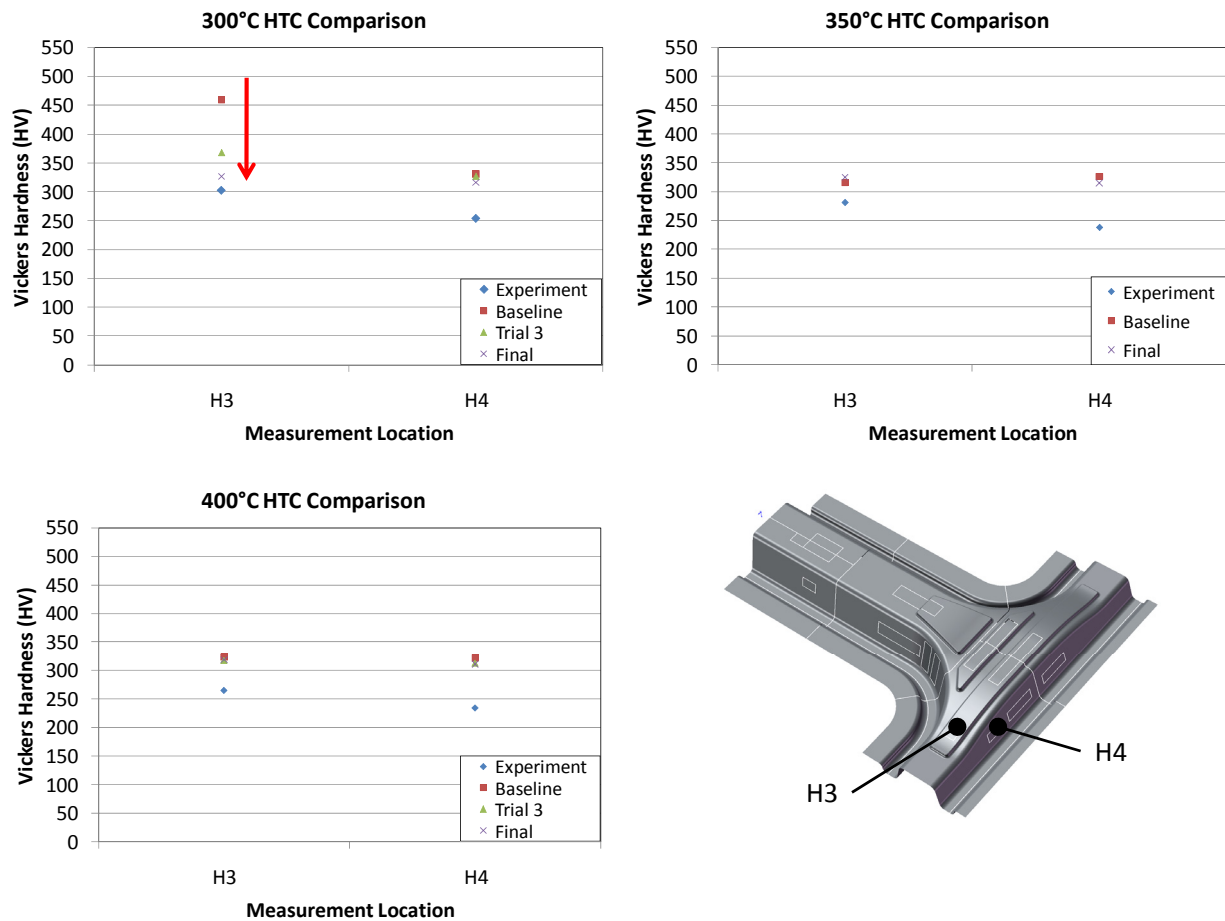


Figure 61 - HTC Study - Hardness comparison

It is apparent that despite the reduction in the HTC, the predicted hardness levels in the heated region are still lower than the experimental data. To establish a theoretical lower limit for the predicted

hardness values, a single element simulation was performed with only convection and radiation boundary conditions (similar to Section 4.3 and Figure 58), corresponding to an air cooling boundary condition which should result in much lower cooling rates than seen in the die quench operation. This air cooling simulation would represent the lowest practical cooling rate and thus the lowest practical hardness value. The temperature history and final hardness values were compared with previous single element simulation results with a 400°C die temperature and four second quench. Figure 62 shows this comparison, with the final Vickers hardness values of 277 HV for the air cooling simulation and 311 HV for the 400°C die quenching simulation. This suggests that the lowest hardness achievable from the model under practical conditions is 277 HV. Since there were actual measured hardness levels below 250 HV (Figure 61), this indicates that further work is required for the definition of this material model with heated tooling.

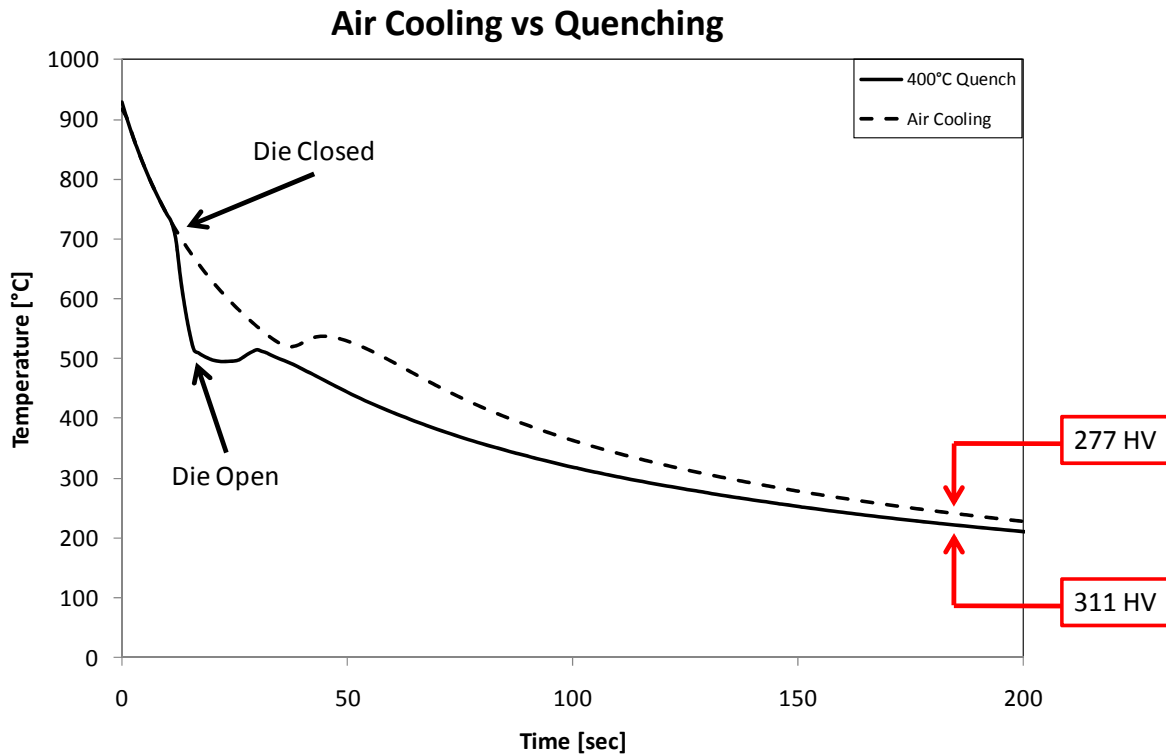


Figure 62 - Air cooling compared to 400°C die quenching

It is evident that there is still a need to perform more rigorous HTC studies, particularly by introducing a die temperature based (as well as pressure based) HTC definition. It appears that additional softening is required in the heated zone while maintaining the current hardness levels in the cooled zone. Based on

this HTC study and the range examined, a “best case” set of values are chosen. Table 5 lists the final values used for the HTC with respect to interface pressure (which was also represented in Figure 59).

**Table 5 - Heat Transfer Coefficients**

<b>Contact Pressure [MPa]</b>	<b>Heat Transfer Coefficient [W/m<sup>2</sup>K]</b>
0	400
3	650
5	900
10	1000
20	2200
40	3000

## **4.5 Numerical Results**

This section presents the results from the FE simulations. A contour plot of the predicted Vickers hardness was recorded for each die temperature and quench duration. The hardness predictions at locations H1 through H6 are also compared to the experimental results from Section 3.2. The results presented here represent a part that has been fully cooled to approximately room temperature, such that the microstructure has fully converted to the various possible phases. Results and comparison to the experiments are provided first for simulations in which the upper tool is prevented from rotating. These simulations are compared first to experiments for which the die is not shimmed to account for thermal expansion and then to the experiments at 400°C for which the die was shimmed. Finally, to further examine the effect of the rotation of the upper die induced by the thermal expansion (as illustrated in Figure 42), simulations were performed in which the thermal expansion was predicted and the upper die was allowed to rotate (Section 4.6).



### 4.5.1 Die Fully Cooled – 25°C

The results for the 25°C baseline case are presented in this section. Figure 63 shows the contour plot of Vickers hardness for both the four second and ten second quench times. The scale was chosen from 300 – 475 HV so that easy visual comparisons can be made throughout the rest of the proceeding sections.

As seen below, the 25°C die produces parts which are fully hardened and uniform.

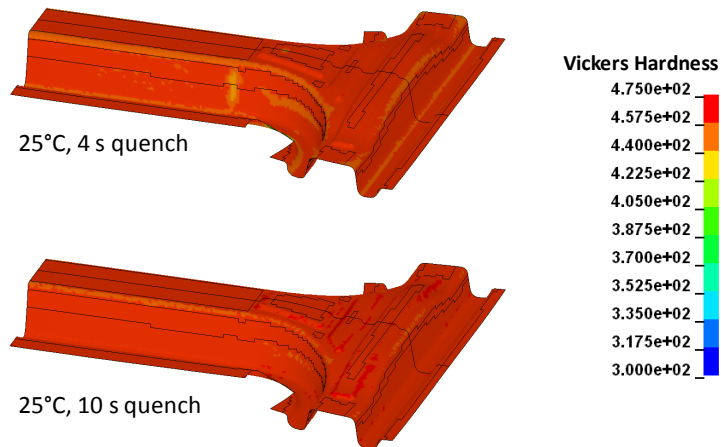


**Figure 63 - Hardness Contour Plot (25°C)**

Figure 64 presents four graphs which compare the results from the simulations to the experimental results. The hardness across all measurement locations is approximately 455 – 465 HV, which represents a fully martensitic microstructure. At measurement locations H1 to H3, the experimental results are equal to or slightly higher than the numerical results. At H4, there was the unexpected hardness drop from the experiments, which was not captured in the simulations. Measurements at H5 and H6 are in very good agreement with each other, although, the experimental data has slightly more scatter in these locations.

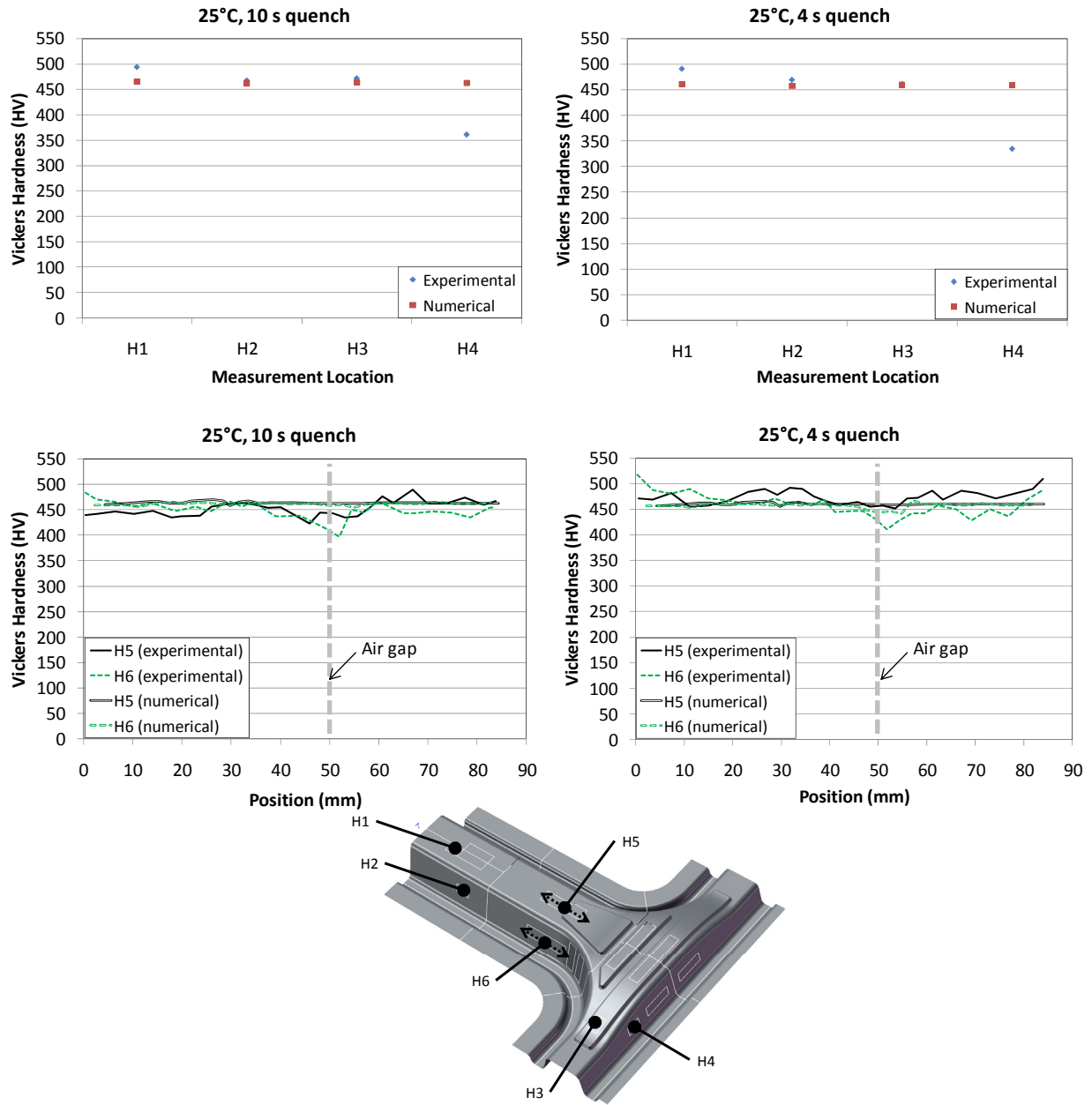
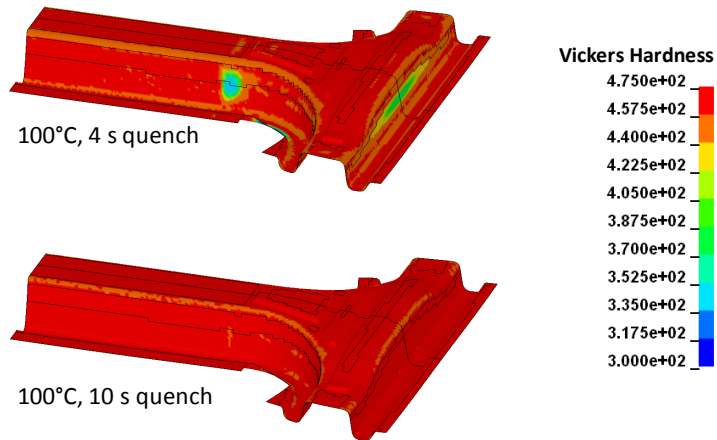


Figure 64 - Numerical Results (25°C)

#### 4.5.2 Heated Die - 100°C

Figure 65 shows a hardness plot for the 100°C die temperature. The ten second quench shows a part that is fully hardened, while the four second plot shows some areas of slight softening, mostly in the side walls.



**Figure 65 - Hardness Contour Plot (100°C)**

The numerical results for the 100°C heated die are shown below in Figure 66 with a comparison to the experiments. There is good agreement with the experimental results at measurement locations H1 through H3, which are all fully hardened. There is, however, a difference of over 100 HV at location H4. At locations H5 and H6 for the ten second quench, there is very good agreement with the experiments. The profiles are very uniform and expected to be fully martensitic across these areas. For the four second quench, there was a slight softening recorded at H6 from the experiments. The numerical results for H6 show a significantly larger softening and stronger gradient between hard and soft.

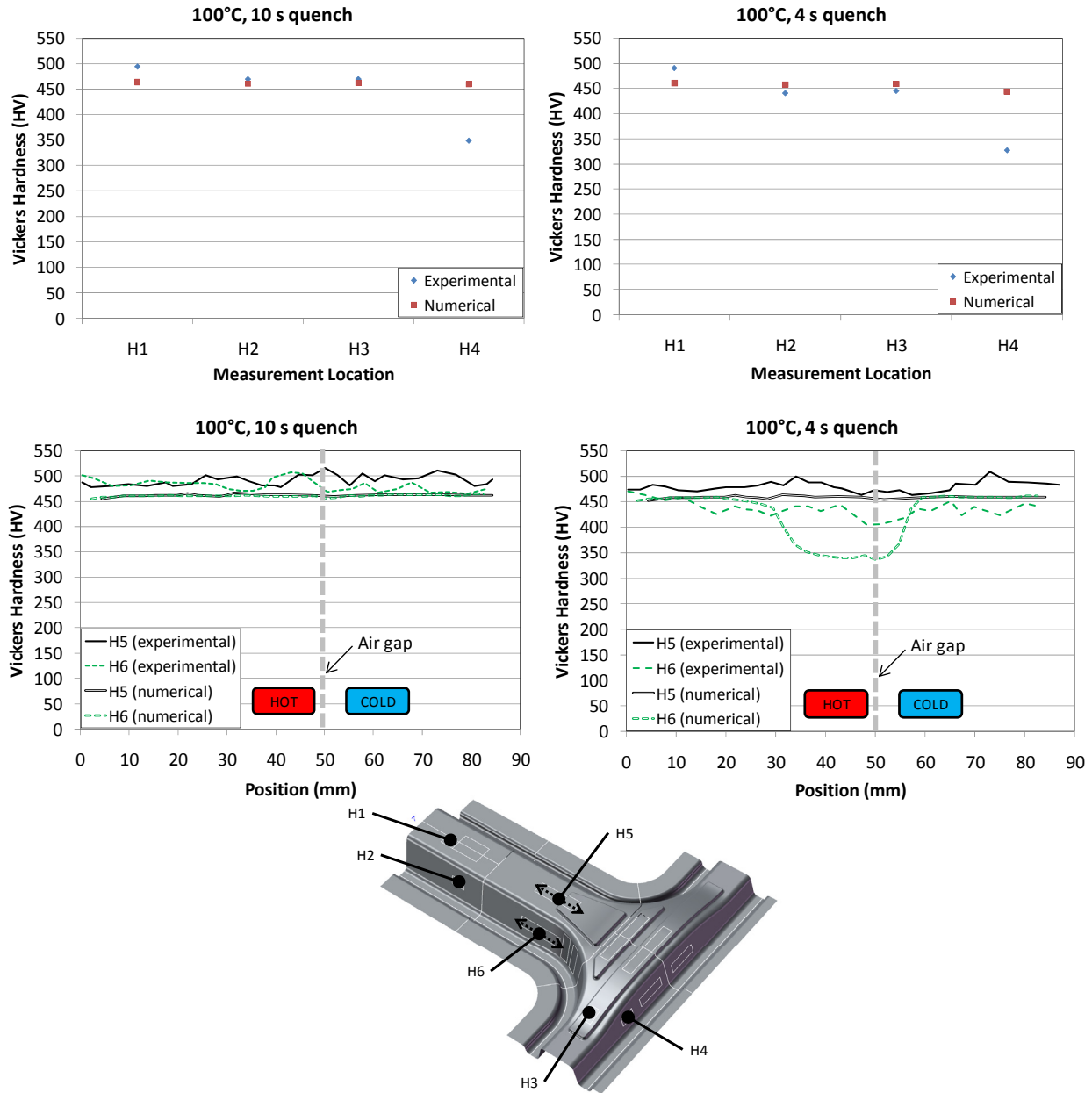
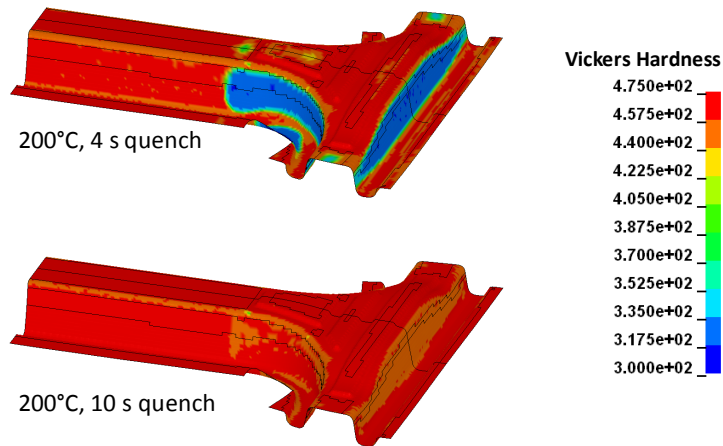


Figure 66 - Numerical Results (100°C)

#### 4.5.3 Heated Die – 200°C

Figure 67 shows the hardness contour plots for the 200°C simulation. The ten second quench is fully hardened in most locations, with very slight softening in the side walls. The four second quench is now showing large regions of soft material, however, these areas are also only in the side walls.



**Figure 67 - Hardness Contour Plot (200°C)**

The numerical and experimental results for the 200°C die are shown in Figure 68. Locations H1 through H3 show close agreement with the experiments for the ten second quench. There is an increasing gap between the experiments and the simulation at location H4, which has increased to a difference of 137 HV. For the four second quench at H4, the numerical results show a large softening down to 322 HV, which is very close to the experiments at 293 HV.

The hardness profiles H5 and H6 for the ten second quench are still in very good agreement with the experiments. The four second quench is now showing some more defined trends at H6. The experiments have shown a gradual dip down to 350 HV and fully hardened at either end. The numerical results at H6 have predicted a very soft microstructure in the heated area and a quick rise in hardness in the cooled region. There is now a dip in hardness at location H5 from the simulations near the air gap which was not seen from the experiments.

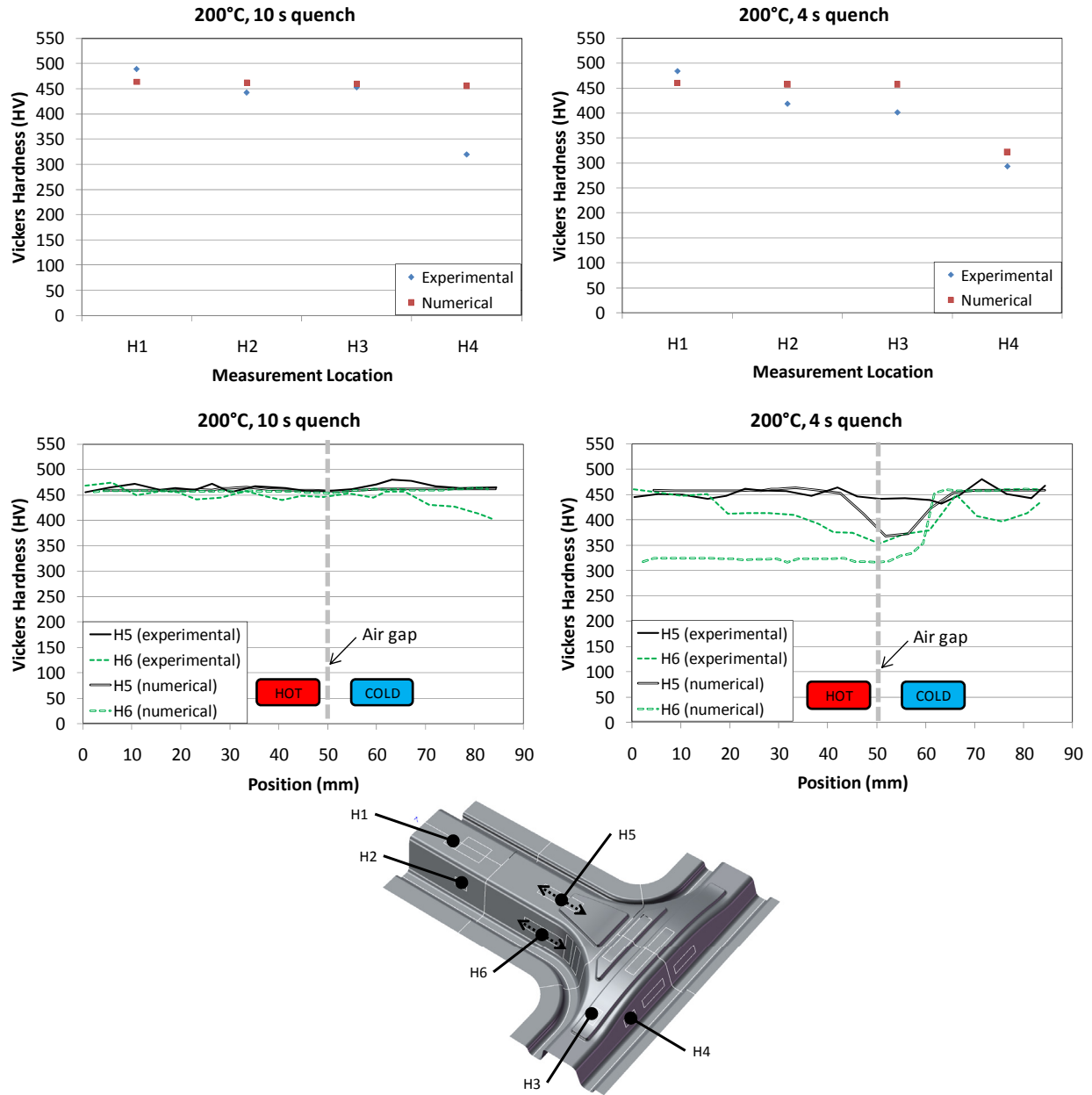
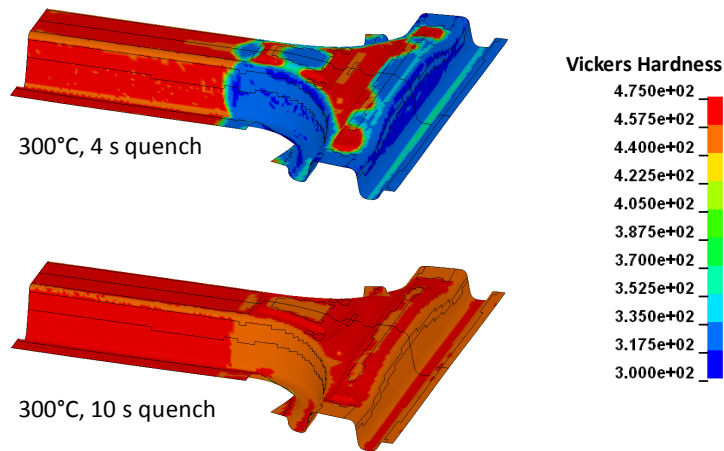


Figure 68 - Numerical Results (200°C)

#### 4.5.4 Heated Die – 300°C

The hardness plot for the two quench times at 300°C are shown in Figure 69. Much more softening is observed across the heated region for the four second quench, but there are still some patches of martensite on the top face. The ten second quench is not showing any significant softening in any areas of the part.



**Figure 69 - Hardness Contour Plot (300°C)**

Figure 70 shows the results for the 300°C simulation and experiments. There is an increasing difference between the experiments and simulations for almost all of the measurement locations. At locations H2 to H4, the softening that was measured from the experiments is not being captured to the same degree in the simulations.

The ten second quench at H5 and H6 is very uniform in the simulations and experiments, however, the simulations are predicting a slightly higher hardness on average. As mentioned previously, the experimental results for the four second quench at H5 and H6 were very unexpected, and the numerical results are showing different trends. From Figure 69 there is a small hard section along the H5 transition area, which is also seen in the curve in Figure 70 between 10 and 20 mm. This hardness trend was not observed in the experiments.

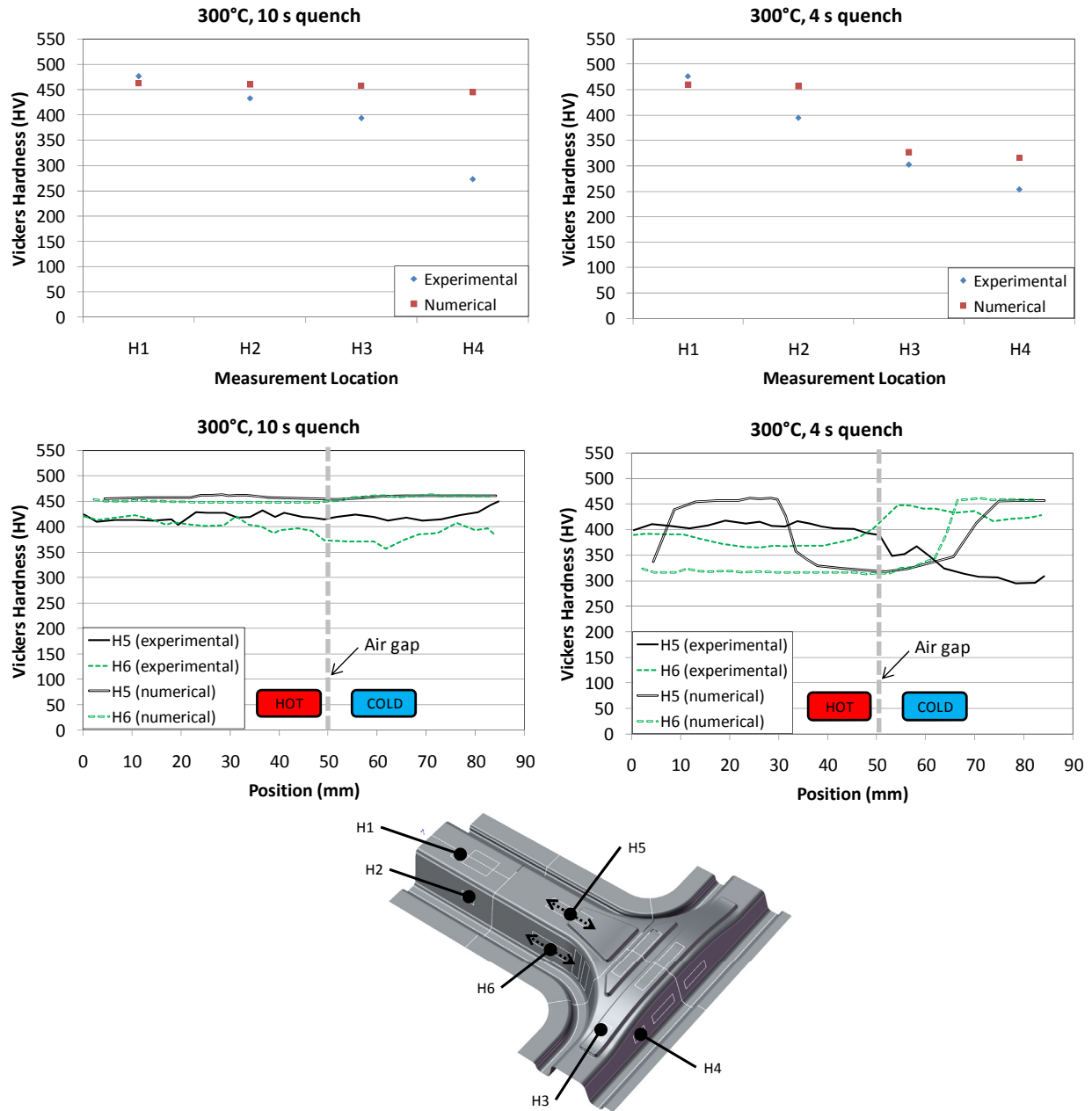
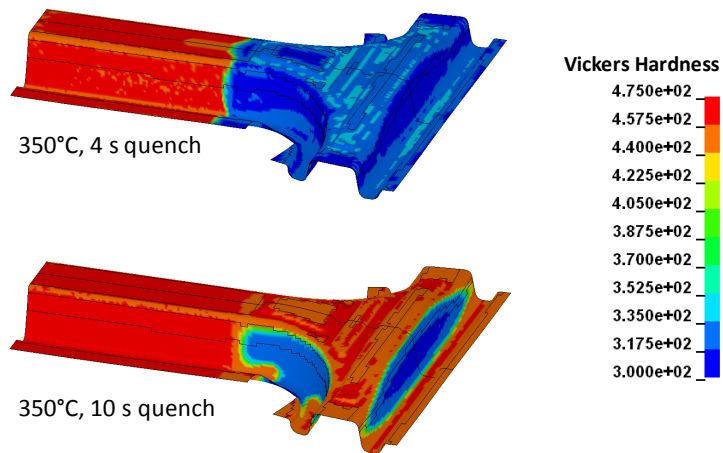


Figure 70 - Numerical Results (300°C)

#### 4.5.5 Heated Die - 350°C

Figure 71 shows the hardness contour plot for the 350°C simulations. The four second quench is almost fully softened in the heated section and significant softening is occurring in the side walls for the ten second quench as well.





**Figure 71 - Hardness Contour Plot (350°C)**

The numerical and experimental comparisons are shown below in Figure 72. The numerical results for the ten second quench are not in good agreement with the experiments at locations H2 and H3. At H4 there is a drop in hardness which is closer to the experiments, although there is still a difference of 66 HV. The simulation result at H3 for the four second quench has softened significantly and is now only 44 HV greater than the experiments.

The trend at H6 for the ten second quench is starting to show some similarities between the experiments and simulation. The experiments showed a slight upward trend between 50 and 90 mm. This trend exists in the simulation as well; although, the highs and lows are more extreme. The results for the four second quench are also aligning from 0 – 50 mm, with almost identical values. The increasing trend for H6 from the experiments is also shown in the simulation, however, with a much higher value in the cold section. The experiments showed an unexpected, decreasing trend for H5, which is not observed in the simulations.

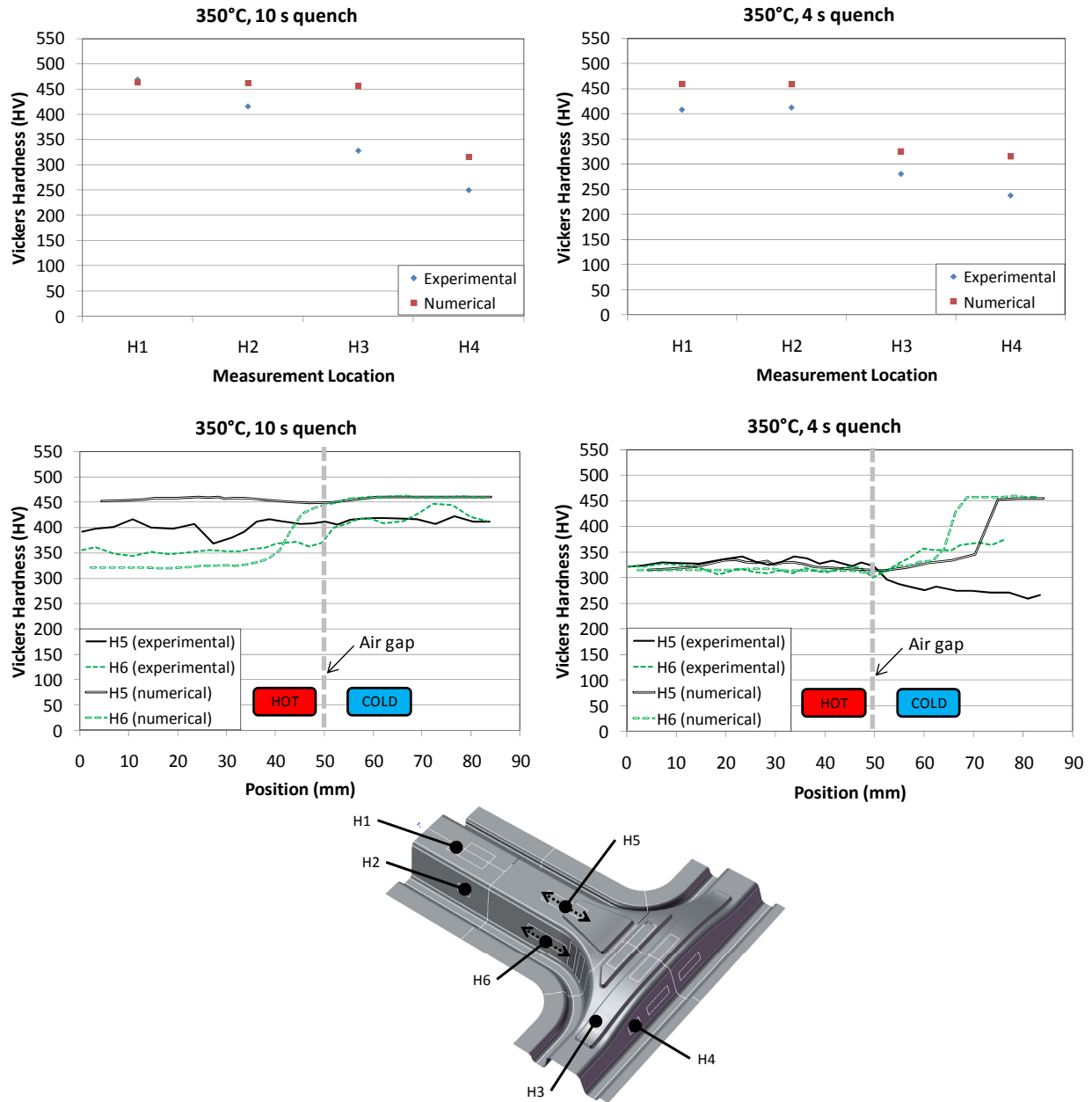
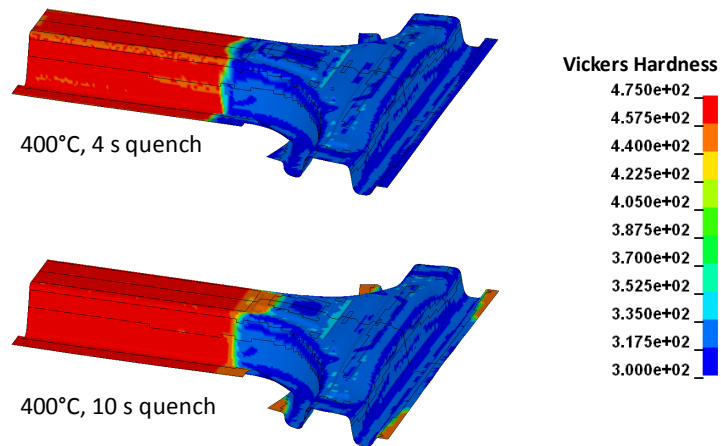


Figure 72 - Numerical Results (350°C)

#### 4.5.6 Heated Die – 400°C

The contour plots for the 400°C simulations are shown in Figure 73. At this temperature, full softening is observed for the four second quench. The ten second quench is mostly softened as well, with a small area of martensite extending into the H5 measurement location.



**Figure 73 - Hardness Contour Plot (400°C)**

Figure 74 presents the comparison of the experiments and simulations. Similar trends exist for locations H1 to H4, with the experiments being slightly softer, in general. The experimental results at H5 and H6 for the ten second quench are showing more defined trends between the heated and cooled regions of the die. The H6 curves are in very good agreement between the experiments and simulation.

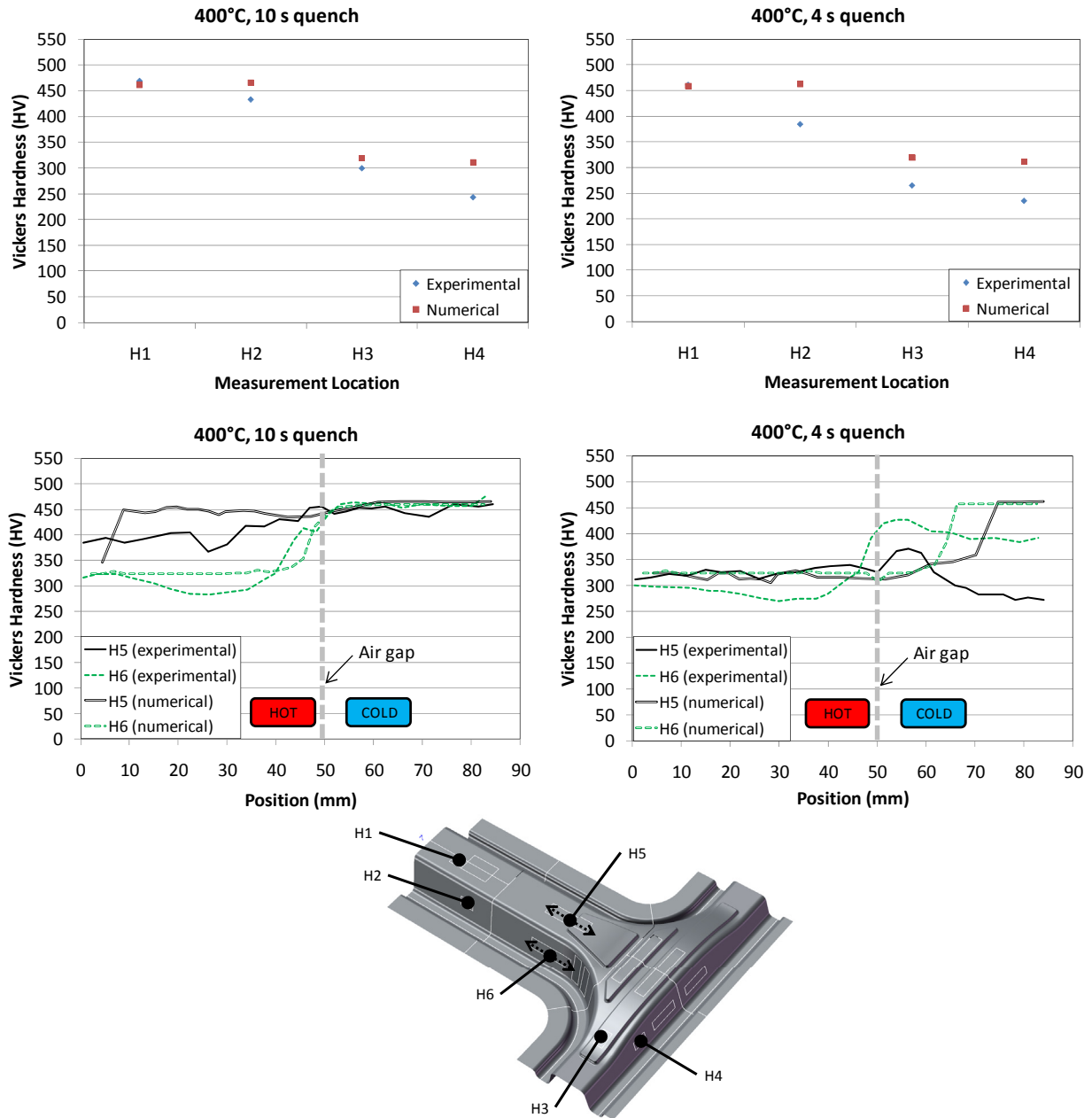


Figure 74 - Numerical Results (400°C)

#### 4.5.7 Heated Die 400°C with Shim

As described previously, a set of shims were installed beneath the dies to correct the height of the tooling at 400°C. Figure 75 shows the numerical results compared to the experimental results with the shimmed tooling. The hardness at H2 for the experiments and simulation is approximately the same. The hardness trends and magnitudes at location H5 and H6 are very similar between the experiments and simulation, although, the position where the hardness transition occurs is offset.

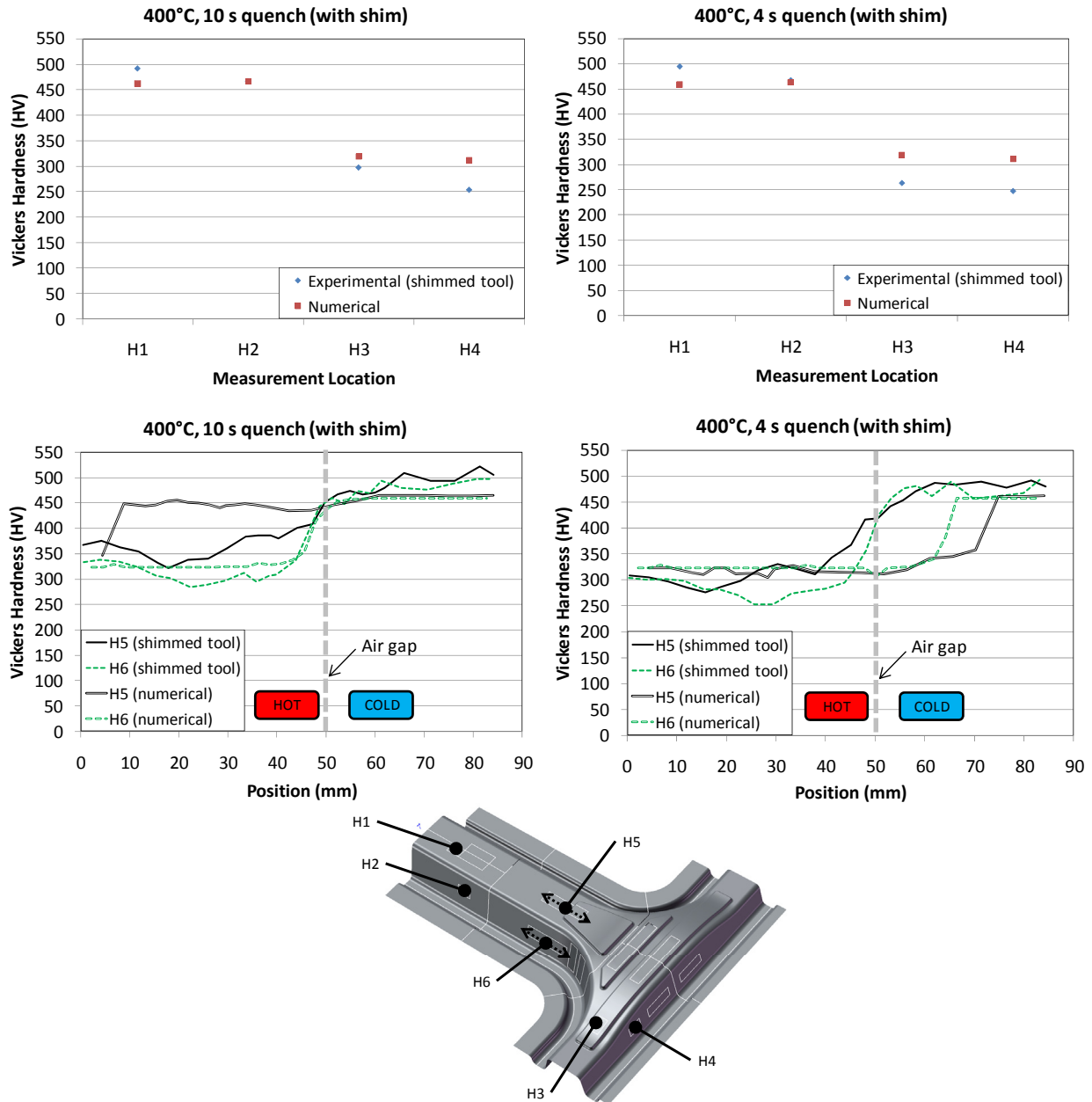
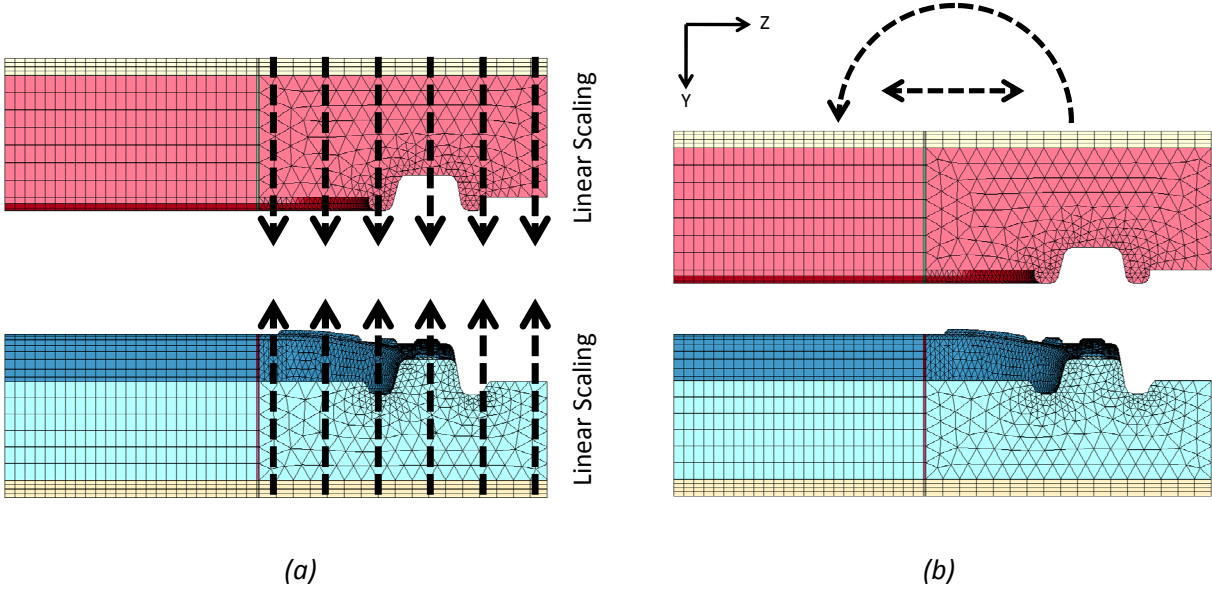


Figure 75 - Numerical Results (400°C) with shim

## 4.6 Thermal Expansion

As discussed previously, the thermal expansion of the tooling was causing problems in the experimental results. The simulations shown in the previous sections were done with tooling that was uniform and the thermal expansion was not considered. To attempt to replicate the experimental results where the tool was expanding and causing poor contact with the blank, a new set of models were developed.

To account for the expansion of the tooling, a linear scaling was applied to the heated sections of the tool such that the clearance between the top face of the hot and cold section matched the measurements from the experiments (Figure 76a). The upper tooling was also given extra degrees of freedom (DOF) to allow for slight shifting (along Z axis) and rotation (about X axis) that was observed in the experiments (Figure 76b).



**Figure 76 - Thermal Expansion (a) Uniform die scaling, (b) Addition DOF**

Simulations were performed for the three hottest die temperatures (300°C, 350°C, and 400°C), and compared to the experimental results with un-shimmed tooling.

#### 4.6.1 300°C

Figure 77 shows the Vickers Hardness contour plots for the new simulation. It shows the previous results on the left hand side (same as Figure 69) with the new results on the right hand side for ease of comparison. As expected for the four second quench, there is a large soft zone which appears in the cooled region of the die at location H5 which is due to the poor thermal contact between the blank and tooling.

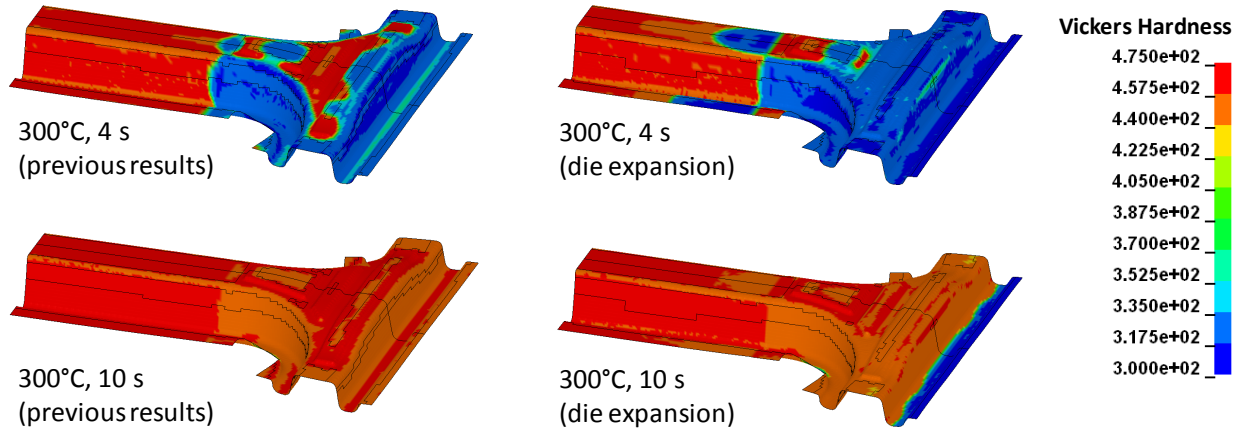


Figure 77 - Hardness Contour Plot (300°C) Thermal Die Expansion

Figure 78 shows the comparison of the experimental results with the new numerical results, at locations H5 and H6, which account for the thermal expansion (TE) of the dies. For the ten second quench, the hardness across the transition zone is very uniform for both the experimental and numerical results, although, the numerical results have an offset of approximately 50 HV higher than the experiments. For the four second quench, the softening behavior observed at H5 in the experiments is now apparent in the simulation. The hardening trend at H6 exists for the experiments and simulation, although, there are some offsets in hardness and the position where the hardening occurs.

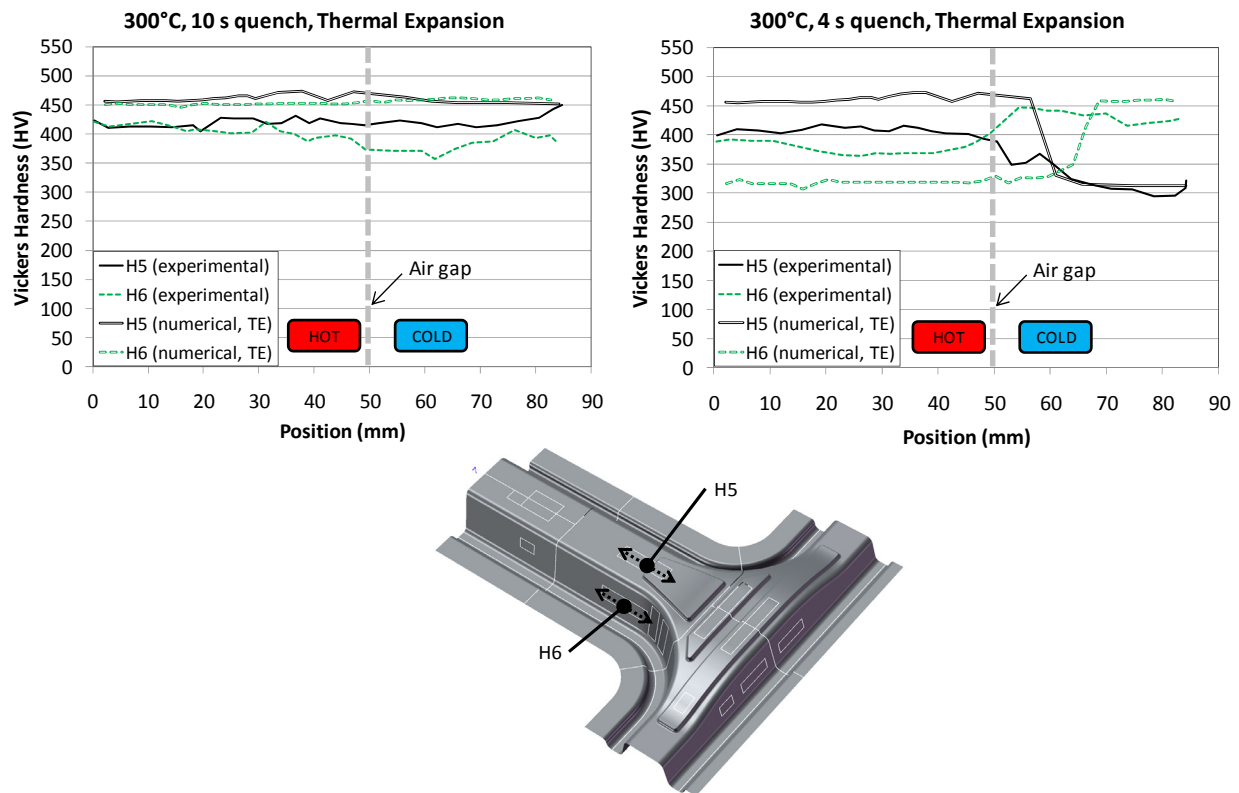


Figure 78 - Numerical Results (300°C) Thermal Die Expansion

#### 4.6.2 350°C

Figure 79 shows a similar set of contour plots as the previous section. The soft zone which appears in the cooled region for the four second quench exists here as well. It is also interesting to note the new hard region in the heated zone. This region of increased hardness is likely due to the increased interface pressure at this location due to the expanded tooling, which causes an increase in thermal conductance.



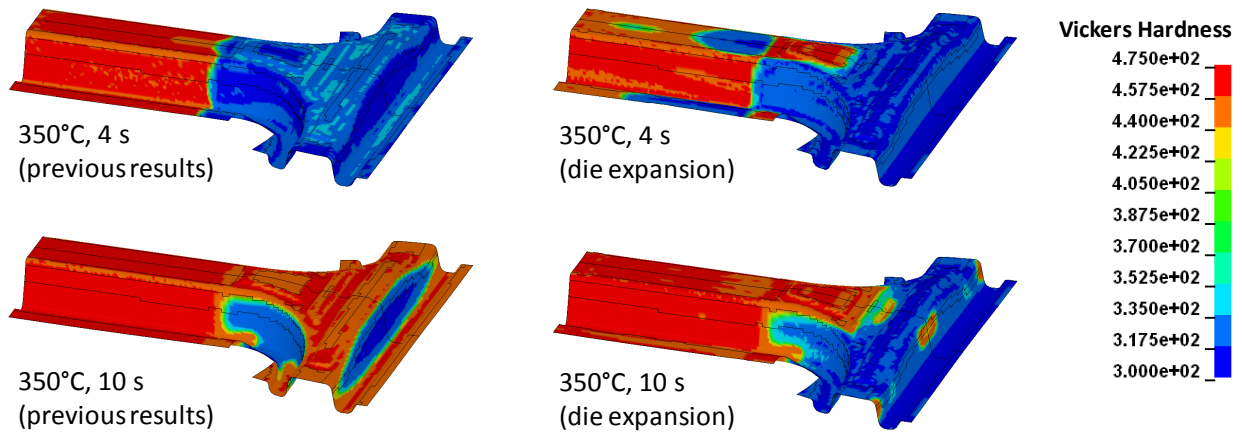


Figure 79 - Hardness Contour Plot (350°C) Thermal Die Expansion

Figure 80 shows the data across the transition zone at H5 and H6 for the new simulation. For both quench durations, similar trends between the experiments and model exist when passing from the hot to cold tooling. There are still, however, offsets in hardness and position when comparing the experimental and numerical data.

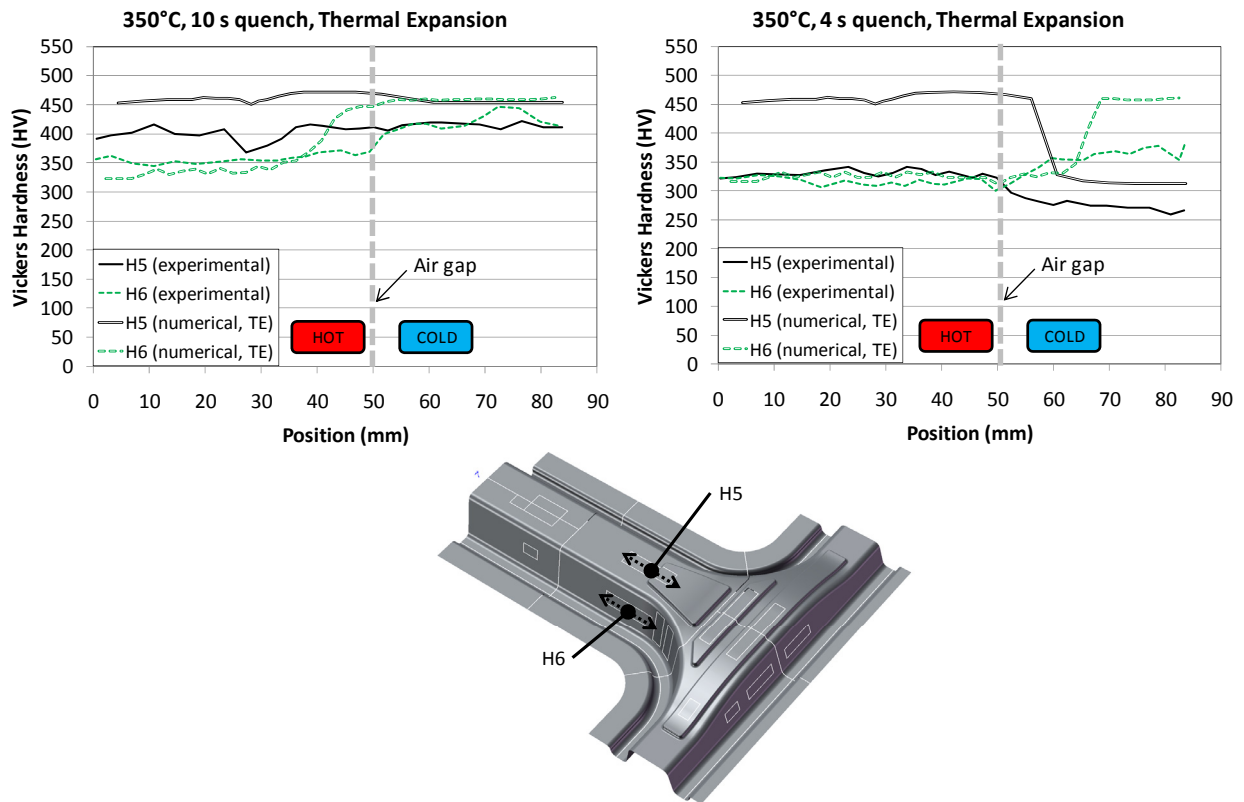


Figure 80 - Numerical Results (350°C) Thermal Die Expansion

### 4.6.3 400°C

The hardness contour plots at 400°C for the new and old simulations are shown in Figure 81. Similar to the previous sections, a large soft zone exists in the cooled part of the die for the four second quench. A small soft zone has also formed for the ten second quench, as well.

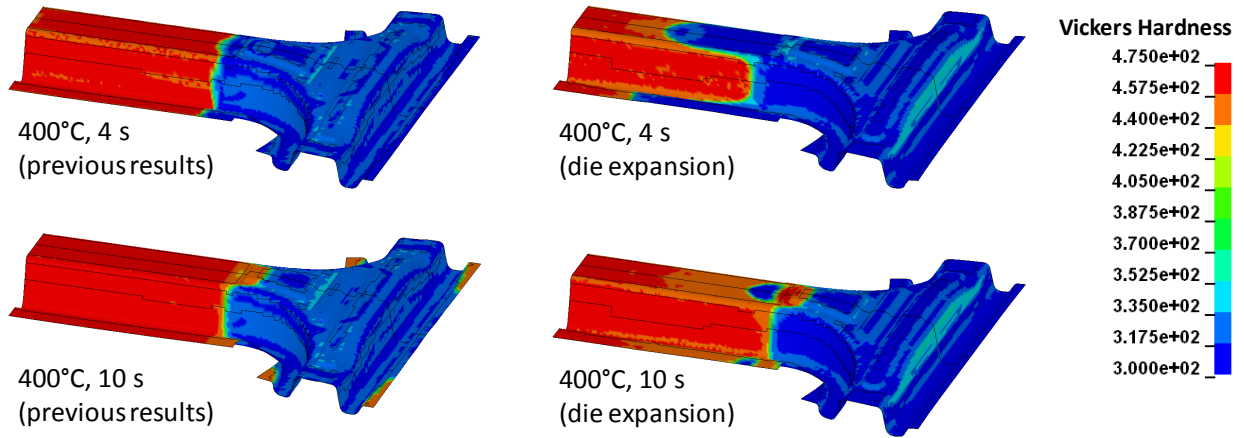


Figure 81 - Hardness Contour Plot (400°C) Thermal Die Expansion

Figure 82 shows the data across the transition zone at H5 and H6. For the ten second quench, the curves for H6 are almost identical for the numerical and experimental results. The softening trend at H5 in the simulation was not found in the experiments. For the four second quench, there is very good agreement at location H5 for the numerical and experimental data. A similar trend exists at H6, although, there is a shift in position where the hardening occurs.

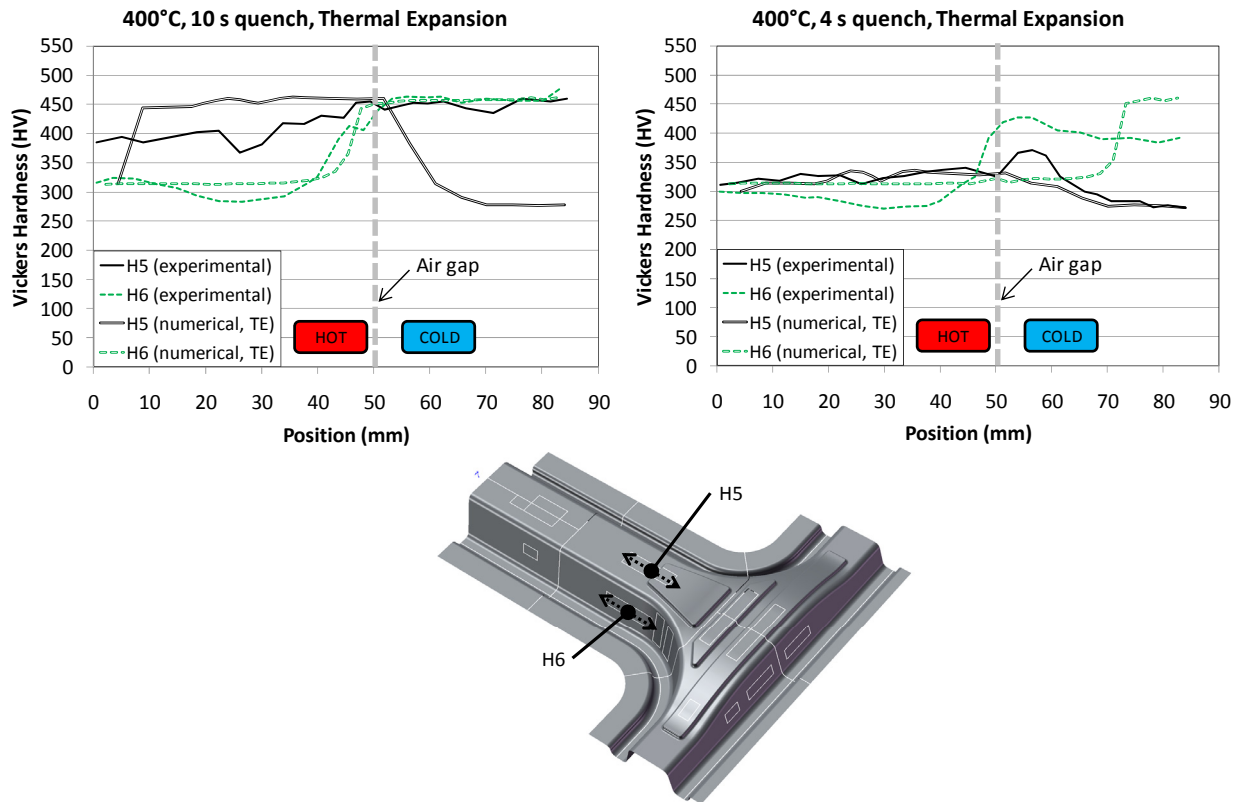


Figure 82 - Numerical Results (400°C) Thermal Die Expansion

## 5 Summary of Results

The experimental results have shown a very promising trend in terms of using the die temperature to control the final mechanical properties of the part. Figure 83 shows a summary of the experimental results for H1 through H4, for all of the heated die temperatures. Each graph represents one measurement location, and the curves illustrate the trend in hardness as the heated die temperature is increased from room temperature to 400°C. The two curves on each plot represent the different quench durations. At location H1, the hardness measurements indicate a fully martensitic microstructure for all heated die temperatures. This high hardness level is expected since H1 is located in the fully cooled region of the tooling. H2 shows a slight decrease in hardness as the heated die temperature is increased. The slight decrease in hardness may be due to the thermal expansion of the tooling, as described in previous sections. Locations H3 and H4, which are in the heated region of the tool, show a very strong softening trend as the temperature is increased. A slight offset exists between the two quench durations, which is expected. Location H3 shows the greatest softening trend between 25°C and 400°C, with a decrease in hardness of 173 HV (36% decrease) and 197 HV (43% decrease) for the ten second and four second quench, respectively. Location H4 had the lowest measured hardness of any location, dropping to 243 HV and 234 HV at 400°C for the ten second and four second quench, respectively. Die temperatures of 300°C and greater are necessary before any reasonable amount of softening occurs.

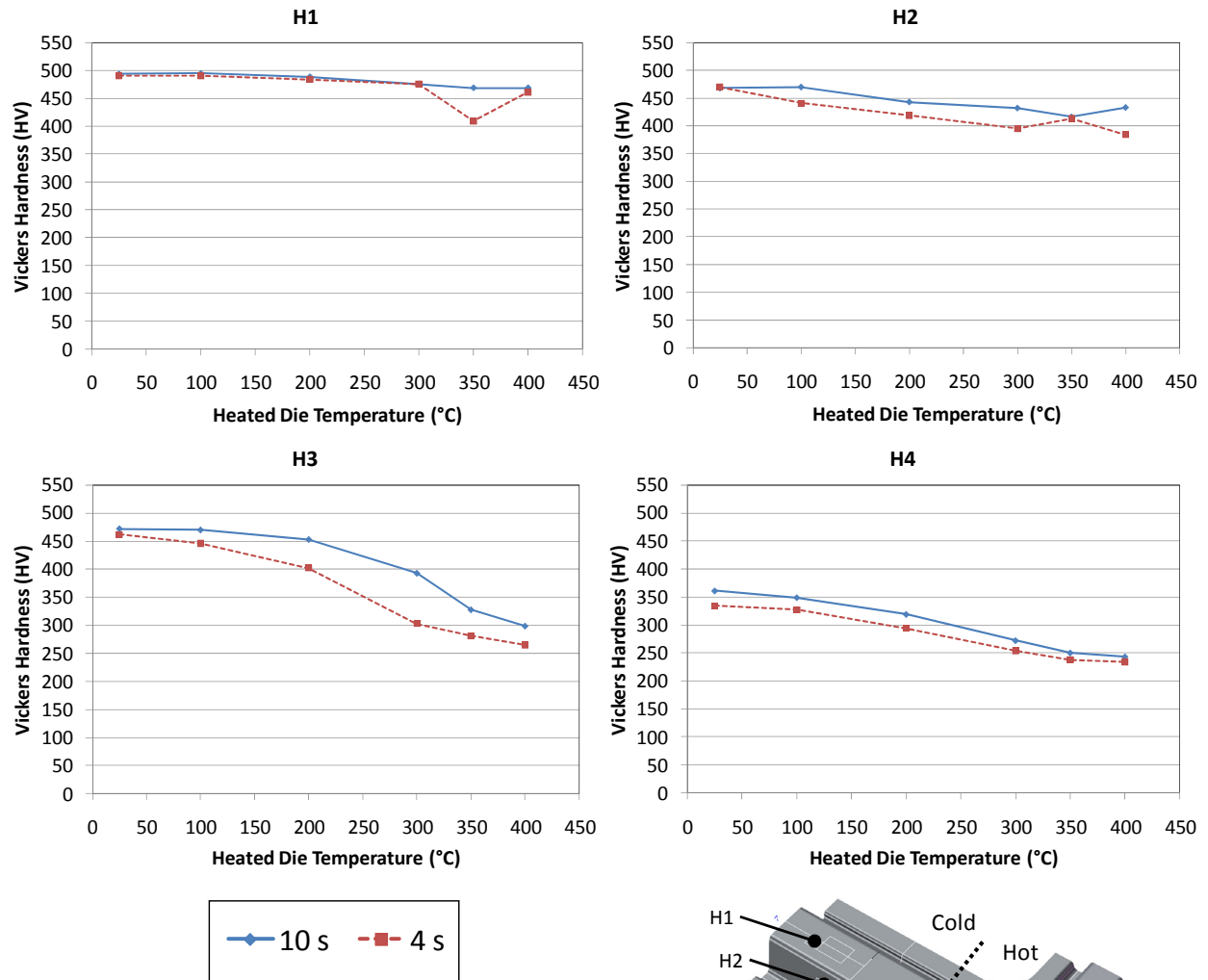


Figure 83 - Experimental Summary (H1-H4)

Figure 84 shows a set of plots for the numerical results for locations H1 to H4. The values for the 300°C, 350°C, and 400°C die temperatures were taken from the simulations where the thermal expansion of the die was taken into account. At locations H1 and H2 the hardness predictions are very constant; ranging from 457 HV to 465 HV across all heated die temperatures. At H3 and H4, there are very sharp softening trends as the temperature is increased; rather than the more gradual trends as seen in the experiments.

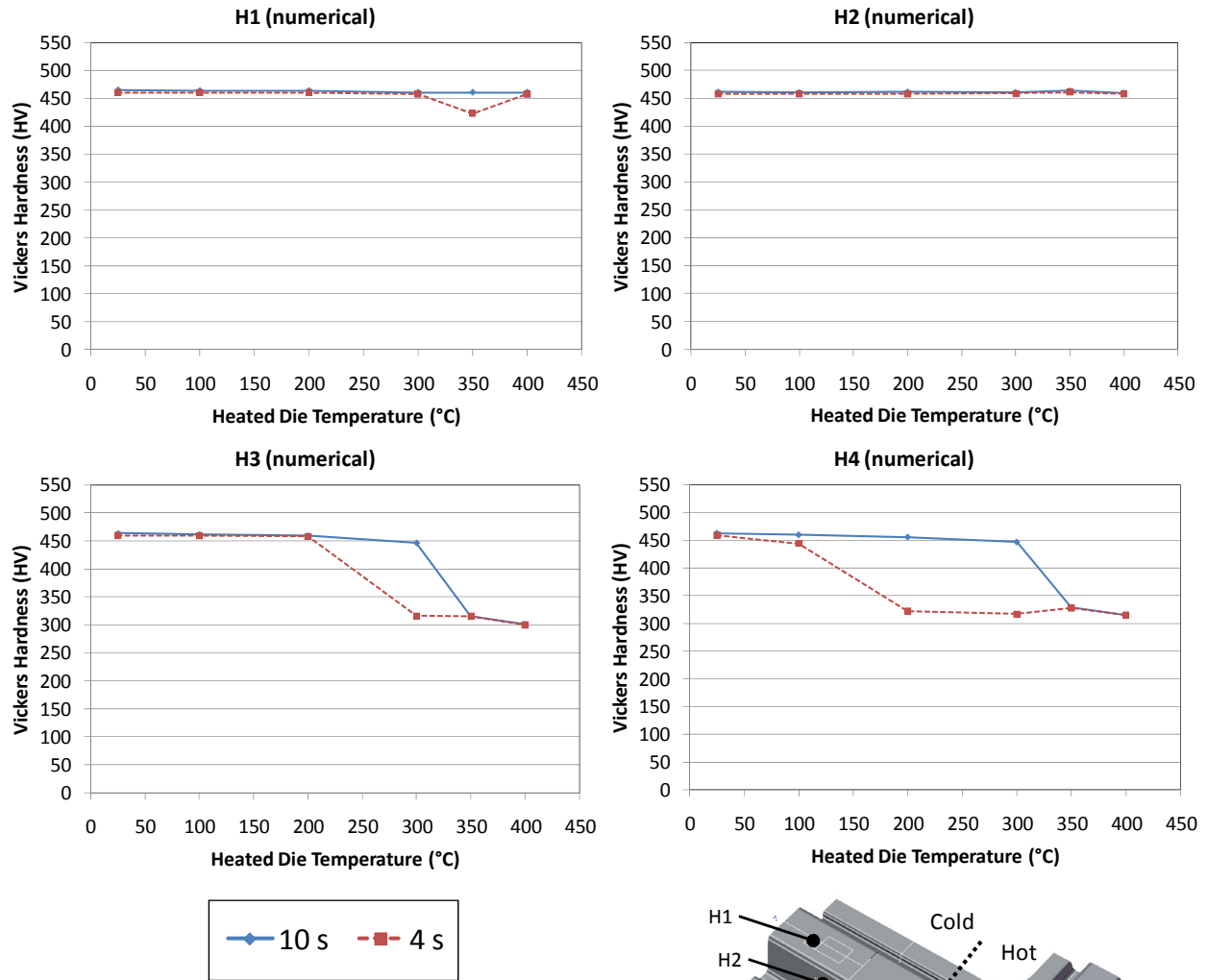


Figure 84 - Numerical Summary (H1-H4)

The *width* of the transition zone will be defined here as the distance between the fully softened and fully hardened microstructure, as measured from locations H5 and H6 (Figure 85). Figure 86 shows four plots for the experimental and numerical results at each quench duration for the 400°C heated die. The transition widths have been indicated on the graphs for measurement locations H5 and H6. The solid red line represents the H5 width and the dotted red line represents the H6 width. Only the 400°C test case is shown because this was the experiment where the tooling was shimmed to account

for the thermal expansion. From the figure, it is apparent that the experimental results have larger widths than the numerical results. The numerical models appear to have difficulty predicting the intermediate hardness values between 325 – 450 HV, which is also apparent in the contour plots from the previous sections. The transition from hard (~450 HV) to soft (~325 HV) generally occurs over very short distances, rather than the long and gradual trends measured from the experiments. There also may be differences between the actual temperature distributions of the tooling compared to the simulations, which will have an effect on the results in this region.

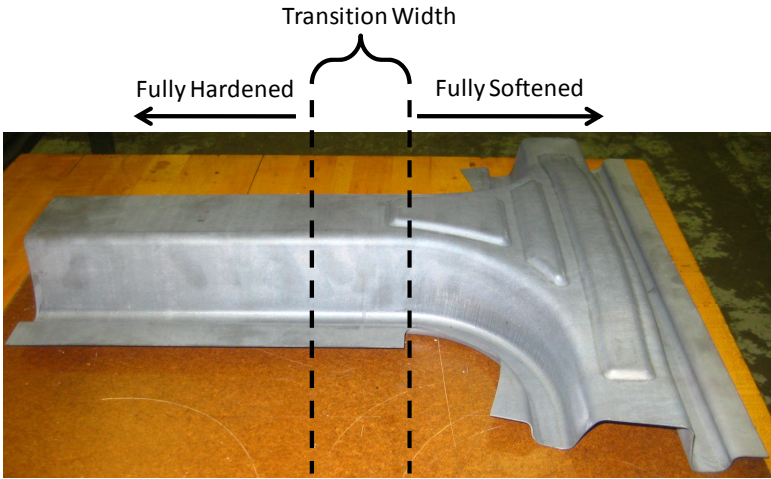
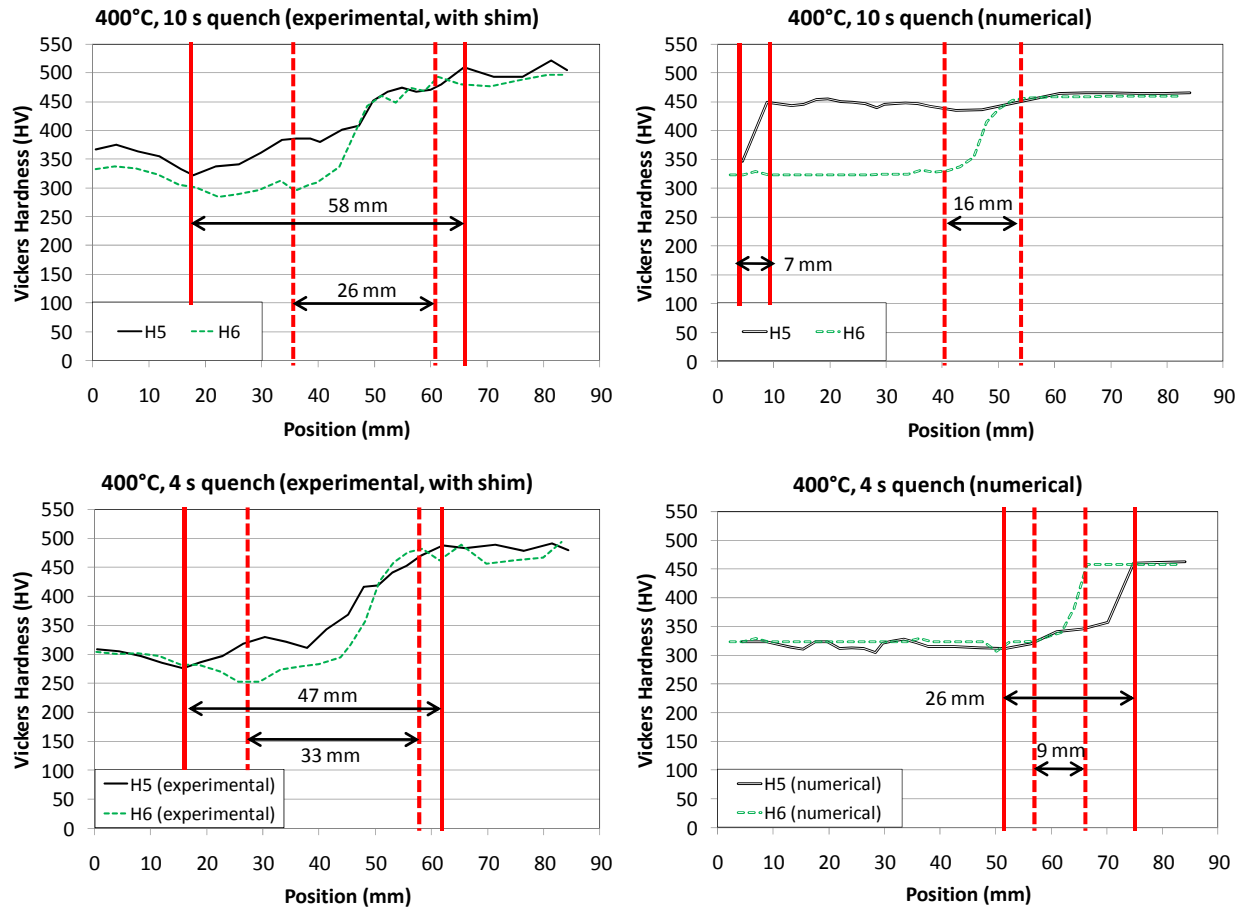


Figure 85 - Transition Zone Width Description



**Figure 86 - Transition Zone Width**

At high die temperatures, the significance of the thermal expansion of the tooling became apparent. The change in geometry of the tooling caused several contact issues between the blank and the tools, which generated unpredictable mechanical properties in the final parts. The softening which occurred in the cooled region of the tool at die temperatures above 300°C was unexpected. The poor thermal contact between the blank and the tooling caused a significant reduction in cooling rate, which resulted in a softer microstructure. It was shown that by modeling the expansion of the tool and allowing rotation of the upper tool, it was possible to predict similar trends to those observed in the experiments. This confirms the importance of thermal expansion and the need to account for this in the tooling design.



## 6 Discussion, Conclusions, and Recommendations

### 6.1 Discussion

From this work, it has been demonstrated that a significant difference in hardness between regions of a hot-formed part can be achieved using a die set with local heating to form and quench the part. The adoption of this approach within an industrial process would not require a significantly longer cycle time or significant additional capital investment. The experimental results have confirmed the hypothesis that tooling temperatures on the order of 300°C – 400°C are able to sufficiently reduce the cooling rate of the blank to below the critical rate of 30°C/s. It has also been confirmed that the use of an air gap between the heated and cooled regions of the tool, as small as 3 mm in width, is sufficient to thermally insulate the two halves of the tooling, while still allowing the part to be formed without significant gouging or dragging along these edges. It may be possible to further reduce this gap while maintaining adequate insulating behavior.

Thermal distortion of the formed part after cooling may become problematic for this process due to the elevated temperature of the part as it is removed from the tooling. There will be a large temperature gradient across the part due to the regions of fast and slow cooling and this difference may cause thermal contractions which lead to geometrical instabilities. This phenomenon has not been examined in the current work and may become increasingly important with more complicated geometries.

The prediction of the as-formed Vickers hardness has shown good agreement with the experiments in terms of predicting the softening trends with increasing die temperature. Hardness predictions for the cooled region of the tooling have shown nearly identical values to the measured Vickers hardness. There are, however, differences in the hardness results within the heated region of the tool. It is apparent that the models are generally over-predicting the hardness levels in the heated region when compared to the experimental data which suggests that the blank may be cooling faster in the model than in the experiments. This rate of cooling is directly related to the HTC which has been defined between the tooling and the blank. It is possible that individual HTC definitions must be defined for the cooled and heated tooling, so that the current HTC exists in the cooled section and a decreased HTC exists in the heated section. By creating these individual definitions, it may be possible to further improve the accuracy of the models. The original HTC definitions from the literature [10,33] were determined using

only a cooled tooling and they may not be valid when using a heated tool. Additionally, it may be necessary to modify the material model definition to achieve the desired softening behavior.

These experiments have provided a significant stepping-stone for hot forming research at the University of Waterloo. There are several opportunities to use these findings for research areas other than improving the crash behavior of hot formed parts. For example, it may be possible to locally soften regions of the part where holes are punched. This would have a two-fold effect: reducing punching force and tool wear, and softening the material to possibly reduce the notch sensitivity around the circumference of the hole. Another implementation of local die heating could be to soften the perimeter of the final part where it would be trimmed after hot forming. The final trimming stage in a hot-forming process is typically performed by laser-cutting, due to the very high strength of the material. Laser cutting is significantly slower than conventional die trimming, however, it is generally not possible to trim fully hardened hot formed parts by die cutting (in production) due to the very high tool wear. By locally softening along this trimming line it may be possible to replace laser cutting with a faster die cutting system.

For future work, it may be beneficial to start with a less complicated geometry, such as a constant cross-section hat profile. This may improve the temperature uniformity of the tooling and would decrease the time required for blank design. It may also be of interest to look further into the effect of the width of the transition zone. For a simple geometry such as a hat section, it may be possible to design multiple heated sections with a low gradient from fully cooled to fully heated. A design such as this would allow for greater control of the temperature distribution and thus a greater control of the transition width. The impact and bending behavior of a simple geometry such as this could be easily tested in a 3- or 4-point bending apparatus. Axial crush tests may also be performed for a constant cross-section part such as this.

## **6.2 Conclusions**

The following conclusions can be drawn from this work:

### **6.2.1 Experiments**

- The use of cartridge heaters to increase the die temperature has proven to be an effective method for significantly reducing the cooling rate of the blank such that the softer daughter phases are formed. At a heated die temperature of 400°C, Vickers hardness measurements

ranged from 461 HV in the cooled region down to 234 HV in the heated region. This represents a reduction in hardness of 49%.

- Die temperatures of approximately 300°C and greater are necessary to reduce the cooling rate of the blank such that noticeable softening occurs.
- The transition zone width (distance between the fully hardened and fully softened microstructure) is on the order of 25-60 mm for the 400°C die temperature, depending on quench duration and measurement location.
- Thermal expansion of the tooling is a critical parameter which must be accounted for in the design and manufacture of the tooling. The expansion can cause regions of the blank to lose contact with the tool and significantly change the expected outcome. Interestingly, the intentional introduction of thermal expansion-induced geometric variation could also be used as another method for reducing the cooling rate of the blank in local regions, to form a softer microstructure.

### **6.2.2 Simulations**

- The use of advanced numerical modeling techniques with the sophisticated hot forming material model of Åkerström [1] has been successfully implemented and is able to predict the trends in Vickers hardness as the blank is subjected to various die temperatures. In the cooled section of the part, the hardness predictions demonstrated very good agreement to the experimental results. In the heated region, however, the exact magnitude of hardness values do not match the measured data, although the overall softening trends are captured and can be used to approximate the final microstructure of the part.
- The transition zone width predicted in the simulations (distance between the fully hardened and fully softened microstructure) is very narrow compared to the experiments. This may be due to differences of the die temperature gradient between the experiments and simulations.

## **6.3 Recommendations**

The following recommendations are proposed for future studies:

### **6.3.1 Experiments**

- The investigation into using die temperatures above 400°C should be examined. This would require higher powered cartridge heaters (or other heating methods) and also the use of insulation around the outside surfaces of the tooling to minimize heat loss to the surroundings.

- Tooling should be designed for each specific die temperature to account for thermal expansion. When several temperatures are desired, different tools or inserts should be used.
- Improved die mounting and fixturing should be developed to allow for thermal expansion of the tools without the need for re-alignment before every set of trials.
- A chamfer or radius should be machined into the tooling along the air gap to reduce any dragging or gouging of the blank as it is formed over this area.
- An automated blank transfer system should be implemented into the press to improve repeatability. Also, the addition of alignment pins would ensure more consistent part placement into the die.
- An ejector system should be added to the tool to remove the part from the die to improve the repeatability of the time at which the quenching process is interrupted.
- The effect of multi-zone furnace heating on the final microstructure should be examined. Using this approach in conjunction with a heated tool may provide additional softening.
- Additional tool sections with heat control to widen the transition zone, using a simplified geometry (ie. a hat section), should be considered. This approach could be used to control the width of the transition zone between fully hard and fully soft.
- Investigations into the effect of thermal distortion on the final parts should be considered. Large gradients between the cooled and heated regions of the blank may cause geometric instabilities.

### **6.3.2 Simulations**

- An in-depth study of the Heat Transfer Coefficient (HTC) between the blank and the tooling should be performed to improve the simulation results. It is possible that a temperature-based (as well as pressure-based) HTC may improve the results through the heated section of the tooling with respect to the experiments. It may also be necessary to modify the constitutive model definition to capture the softening behavior that was seen in the experiments.
- Further numerical work regarding strain measurements, thickness reduction, and friction should be performed.
- Investigations into the use of forming limit data should be performed to improve the simulation predictions in terms of failure and wrinkling.
- It would be beneficial to develop a more consolidated model which is able to capture the entire process in one simulation (rather than several), but still maintain reasonable computation times.

This may be possible by controlling the mass-scaling as a function of time or by using explicit/implicit switching techniques.

## References

- [1] P. Åkerström, "Doctoral Thesis: Modelling and Simulation of Hot Stamping," Luleå University of Technology, 2006.
- [2] M. Jonsson, "Press hardening, from innovation to global technology," *Hot Sheet Metal Forming of High Performance Steel*, Kassel, Germany: 2008, pp. 253-265.
- [3] T. Altan, "Hot-stamping boron-alloyed steels for automotive parts, Part I : Process methods and uses," *Metal Forming*, 2006, pp. 40-41.
- [4] M. Geiger, M. Merklein, and C. Hoff, "Basic investigations on the hot stamping steel 22MnB5," *Advanced Materials Research*, vol. 6, 2005, pp. 795-802.
- [5] R. Kolleck, R. Veit, M. Merklein, J. Lechler, and M. Geiger, "Investigation on induction heating for hot stamping of boron alloyed steels," *CIRP Annals - Manufacturing Technology*, vol. 58, 2009, pp. 275-278.
- [6] H. Karbasian and A.E. Tekkaya, "A review on hot stamping," *Journal of Materials Processing Technology*, vol. 210, Nov. 2010, pp. 2103-2118.
- [7] M. Maikranz-Valentin, U. Weidig, U. Schoof, H.-helmut Becker, and K. Steinhoff, "Components with Optimised Properties due to Advanced Thermo-mechanical Process Strategies in Hot Sheet Metal Forming," *Steel Research International*, vol. 79, 2008, pp. 92-97.
- [8] ArcelorMittal, "Steels for hot stamping, Product Catalog," 2010.
- [9] D.W. Fan, H.S. Kim, S. Biroasca, and B.C. De Cooman, "Critical review of hot stamping technology for automotive steels," *Proceedings of Materials Science and Technology (MS&T)*, 2007, pp. 99-110.
- [10] M. Merklein and J. Lechler, "Determination of Material and Process Characteristics for Hot Stamping Processes of Quenchenable Ultra High Strength Steels with Respect to a FE-based Process Design," *SAE Int'l Journal of Materials and Manufacturing*, vol. 1, 2008, pp. 411-426.
- [11] A. Barcellona and D. Palmeri, "Effect of Plastic Hot Deformation on the Hardness and Continuous Cooling Transformations of 22MnB5 Microalloyed Boron Steel," *Metallurgical and Materials Transactions A*, vol. 40, Feb. 2009, pp. 1160-1174.
- [12] M. Merklein and J. Lechler, "Investigation of the thermo-mechanical properties of hot stamping steels," *Journal of Materials Processing Technology*, vol. 177, Jul. 2006, pp. 452-455.
- [13] T. Altan, "Hot-stamping boron-alloyed steels for automotive parts, Part II," *Metal Forming*, 2007, pp. 14-15.

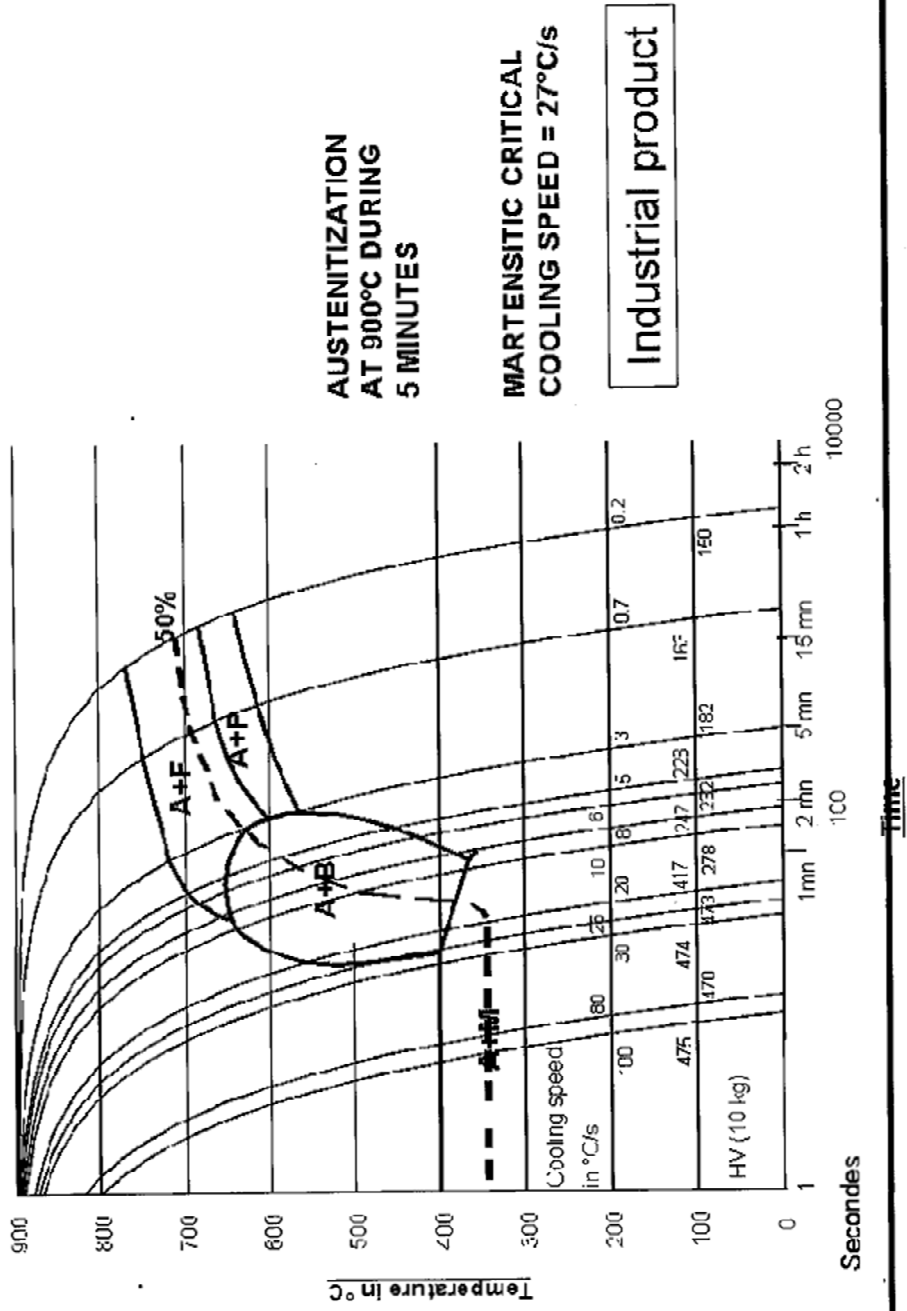
- [14] P. Hein and J. Wilsius, "Status and Innovation Trends in Hot Stamping of USIBOR 1500 P," *Steel Research International*, vol. 2, 2008, pp. 85-91.
- [15] G.T. Eldis, "A critical review of data sources for isothermal transformations and continuous cooling transformation diagrams.," *Hardenability Concepts with Applications to Steel*, 1978, pp. 126-157.
- [16] ArcelorMittal - Private Communication with R. Soldaat, "Usibor 1500P CCT Diagram," 2009.
- [17] D.R. Askeland and P.P. Phule, *The Science and Engineering of Materials, 4th Ed.*, 2003.
- [18] R. Kolleck, R. Veit, H. Hofmann, and F.-J. Lenze, "Alternative heating concepts for hot sheet metal forming," *Hot Sheet Metal Forming of High-Performance Steel*, Kassel, Germany: 2008, pp. 239-246.
- [19] B.-A. Behrens, S. Hubner, and M. Demir, "Conductive heating system for hot sheet metal forming," *Hot Sheet Metal Forming of High-Performance Steel*, Kassel, Germany: 2008, pp. 63-68.
- [20] K. Mori and Y. Okuda, "Tailor die quenching in hot stamping for producing ultra-high strength steel formed parts having strength distribution," *CIRP Annals - Manufacturing Technology*, vol. 59, 2010, pp. 291-294.
- [21] D.D. Múnera, A. Pic, D. Abou-khalil, and F. Shmit, "Innovative Press Hardened Steel Based Laser Welded Blanks Solutions for Weight Savings and Crash Safety Improvements," *SAE International Journal of Materials and Manufacturing*, vol. 1, 2008, pp. 472-479.
- [22] D.D. Múnera, F. Pinard, and L. Lacassin, "Very and Ultra High Strength Steels Based Tailored Welded Blanks: A Step Further Towards Crashworthiness Improvement," *2006 SAE World Congress*, vol. 115, 2006, pp. 796-804.
- [23] T. Stoehr, J. Lechler, and M. Merklein, "Investigations on different strategies for influencing the microstructural properties with respect to partial hot stamping," *Hot Sheet Metal Forming of High-Performance Steel*, 2009, pp. 273-281.
- [24] T. Labudde and W. Bleck, "Formability characterisation of press hardened steels," *Hot Sheet Metal Forming of High-Performance Steel*, 2009, pp. 127-135.
- [25] B. Casas, D. Latre, N. Rodriguez, and I. Valls, "Tailor made tool materials for the present and upcoming tooling solutions in hot sheet metal forming," *Hot Sheet Metal Forming of High-Performance Steel*, 2008, pp. 23-35.
- [26] R. George, A. Bardelcik, and M. Worswick, "Localized Die Temperature Control for Tailored Properties in Hot Forming of Boron Steels - Numerical Study," *IDDRG*, Golden, CO: 2009, pp. 131-139.
- [27] LSTC, *LS-Dyna Keyword User's Manual v971*, 2007.

- [28] G. Bergman, "Doctoral Thesis: Modelling and Simulation of Simultaneous Forming and Quenching," Luleå University of Technology, 1999.
- [29] A. Shapiro, "How to use LS-OPT for Parameter Estimation - hot stamping and quenching applications," *8th European LS-DYNA Users Conference*, 2011.
- [30] A. Bardelcik, C.P. Salisbury, S. Winkler, M.A. Wells, and M.J. Worswick, "Effect of cooling rate on the high strain rate properties of boron steel," *International Journal of Impact Engineering*, vol. 37, 2010, pp. 694-702.
- [31] J.O. Hallquist, *LS-DYNA Theory Manual*, 2006.
- [32] F. Incropera, D. Dewitt, T. Bergman, and A. Lavine, *Fundamentals of Heat and Mass Transfer, 6th Edition*, 2007.
- [33] "Continuous press hardening benchmark problem BM03," *NUMISHEET 2008 Benchmark*, 2008.



**Appendix A - Usibor® 1500P CCT**

# CCT Diagram for average composition (C=0,22%)



**arcelor MITAL**

## **Appendix B – LS-DYNA Material Model**

## MAT\_UHS\_STEEL

This is the input deck for material 244 (\*MAT\_UHS\_STEEL). The material model is developed both for shell and solid models. It is mainly suited for hot stamping processes where phase transformations are crucial. It has five phases and it is assumed that the blank is fully austenitized before cooling. The basic constitutive model is based on the work done by Åkerström et al (2007).

**WARNING:** This material model currently only works for cooling from the austenization temperature. Do not use it for heating up from room temperature. The initial temperature of the blank must be set to the austenization temperature which must be greater than the largest value used for any of the ferrite, pearlite, or bainite phase start temperatures.

### Card format

Card 1	1	2	3	4	5	6	7	8
Variable	MID	RO	E	PR	TUNIT	CRSH	PHASE	
Type	I	F	F	F	F	I	I	
Defaults	none	none	none	none	3600	0	0	

Card 2	1	2	3	4	5	6	7	8
Variable	LCY1	LCY2	LCY3	LCY4	LCY5	KFER	KPER	B
Type	I	I	I	I	I	F	F	F
Defaults	none	none	none	none	none	0.0	0.0	0.0

Card 3	1	2	3	4	5	6	7	8
Variable	C	Co	Mo	Cr	Ni	Mn	Si	V
Type	F	F	F	F	F	F	F	F
Defaults	0.0	0.0	0.0	0.0	0.0	0.0	0.0	0.0

Card 4	1	2	3	4	5	6	7	8
Variable	W	Cu	P	Al	As	Ti		
Type	F	F	F	F	F	F		
Defaults	0.0	0.0	0.0	0.0	0.0	0.0		

Card 5	1	2	3	4	5	6	7	8
Variable	THEXP1	THEXP5	LCTH1	LCTH5	TREF	LAT1	LAT5	
Type	F	F	I	I	F	F	F	
Defaults	0.0	0.0	none	none	273.15	0.0	0.0	

Card 6	1	2	3	4	5	6	7	8
Variable	QR2	QR3	QR4	ALPHA	GRAIN			
Type	F	F	F	F	F			
Defaults	0.0	0.0	0.0	0.0	0.0			

Card 7	1	2	3	4	5	6	7	8
Variable	PLMEM 2	PLMEM 3	PLMEM 4	PLMEM 5	STRC	STRP		
Type	I	F	F	F	F	F		
Defaults	0.0	0.0	0.0	0.0	0.0	0.0		

<b>Variable</b>	<b>Description</b>	<b>Baseline value</b>
MID	Material ID, a unique number has to be chosen.	
RO	Material density	7830 Kg/m <sup>3</sup>
E	Youngs' modulus: GT.0.0: constant value is used LT.0.0: temperature dependent Youngs' modulus given by load curve ID = -E	100.e+09 Pa [1]
PR	Poisson's ratio	0.30 [1]
A	Material parameter $a$ in $(T_k - T)^a \exp(-Q/RT)$ . Usually a value of 2 or 3 is recommended.	3.
TUNIT	Number of time units per hour. Default is seconds, that is 3600 time units per hour. It is used only for hardness calculations.	3600.
CRSH	Switch to use a simple and fast material model but with the actual phases active. EQ.0: The original model were phase transitions and trip is used. EQ.1: A more simpler and faster version is active. To use this the NIPS and/or NIPH on *DATABASE_EXTENT_BINARY must be set to 12 or greater. Please see <b>remark 5</b> below for more information.	0
PHASE	Switch to exclude middle phases from the simulation. EQ.0: All phases ACTIVE default) EQ.1: pearlite and bainite ACTIVE EQ.2: bainite ACTIVE EQ.3: ferrite and pearlite ACTIVE EQ.4: ferrite and bainite ACTIVE EQ.5: NO ACTIVE middle phases (only austenite -> martensite)	0
LCY1	Load curve ID for austenite hardening (stress versus eff. pl. str.)	100 [5]
LCY2	Load curve ID for ferrite hardening (stress versus eff. pl. str.)	200 [5]
LCY3	Load curve ID for pearlite hardening (stress versus eff. pl. str.)	300 [5]
LCY4	Load curve ID for bainite hardening (stress versus eff. pl. str.)	400 [5]
LCY5	Load curve ID for martensite hardening (stress versus eff. pl. str.)	500 [5]

KFERR	Correction factor for boron in the ferrite reaction.	1.9e+05 [2]
KPEAR	Correction factor for boron in the pearlite reaction.	3.1e+03 [2]
B	Boron [weight %]	0.003 [2, 4]
C	Carbon [weight %]	0.23 [2, 4]
Co	Cobolt [weight %]	0.0 [2, 4]
Mo	Molybdenum [weight %]	0.0 [2, 4]
Cr	Chromium [weight %]	0.21 [2, 4]
Ni	Nickel [weight %]	0.0 [2, 4]
Mn	Manganese [weight %]	1.25 [2, 4]
Si	Silicon [weight %]	0.29 [2, 4]
V	Vanadium [weight %]	0.0 [2, 4]
W	Tungsten [weight %]	0.0
Cu	copper [weight %]	0.0
P	Phosphorous [weight %]	0.013
Al	Aluminium [weight %]	0.0
As	Arsenic [weight %]	0.0
Ti	Titanium [weight %]	0.0
THEXP1	Coefficient of thermal expansion in austenite	25.1e-06 1/K [7]
THEXP5	Coefficient of thermal expansion in martensite	11.1e-06 1/K [7]
LCTH1	Load curve for the thermal expansion coefficient for austenite: LT.0.0: curve ID = -LA and TREF is used as reference temperature GT.0.0: curve ID = LA	0
LCTH5	Load curve for the thermal expansion coefficient for martensite: LT.0.0: curve ID = -LA and TREF is used as reference temperature GT.0.0: curve ID = LA	0
TREF	Reference temperature for thermal expansion. Used if and only if LA.LT.0.0 or/and LM.LT.0.0	293.15
LAT1	Latent heat for the decomposition of austenite into ferrite, pearlite and bainite.	590.e+06 J/m <sup>3</sup> [2]
LAT5	Latent heat for the decomposition of austenite into martensite	640.e+06 J/m <sup>3</sup> [2]

QR2	Activation energy divided by the universal gas constant for the diffusion reaction of the austenite-ferrite reaction: $Q2/R$ . $R = 8.314472$ [J/mol K].	11575. K [3] = (23000 cal/mole)*(4.184 J/cal) / (8.314 J/mole*K)
QR3	Activation energy divided by the universal gas constant for the diffusion reaction for the austenite-pearlite reaction: $Q3/R$ . $R=8.314472$ [J/mol K].	13840. K [3]
QR4	Activation energy divided by the universal gas constant for the diffusion reaction for the austenite-bainite reaction: $Q4/R$ . $R=8.314472$ [J/mol K].	13588. K [3]
ALPHA	Material constant for the martensite phase. A value of 0.011 means that 90% of the available austenite is transformed into martensite at 210 degrees below TSMART, whereas a value of 0.033 means a 99.9% transformation.	0.011
GRAIN	ASTM grain size number for austenite, usually a number between 7 and 11.	8
PLMEM2	Memory coefficient for the plastic strain that is carried over from the austenite. A value of 1 means that all plastic strains from austenite is transferred to the ferrite phase and a value of 0 means that nothing is transferred.	0
PLMEM3	Memory coefficient for the plastic strain that is carried over from the austenite. A value of 1 means that all plastic strains from austenite is transferred to the pearlite phase and a value of 0 means that nothing is transferred.	0
PLMEM4	Memory coefficient for the plastic strain that is carried over from the austenite. A value of 1 means that all plastic strains from austenite is transferred to the bainite phase and a value of 0 means that nothing is transferred.	0
PLMEM5	Memory coefficient for the plastic strain that is carried over from the austenite. A value of 1 means that all plastic strains from austenite is transferred to the martensite phase and a value of 0 means that nothing is transferred.	0

STRC	Effective strain rate parameter C. STRC.LT.0.0: load curve id = -STRC STRC.GT.0.0: constant value STRC.EQ.0.0: strain rate NOT active	0
STRP	Effective strain rate parameter P. STRP.LT.0.0: load curve id = -STRP STRP.GT.0.0: constant value STRP.EQ.0.0: strain rate NOT active	0

**Remark 1:** History variables 1-7 include the different phases, the Vickers hardness and the yield stress. Set NEIPS = 7 (shells) or NEIPH = 7 (solids) on \*DATABASE\_EXTENT\_BINARY.

History variable	
1	Amount austenite
2	Amount ferrite
3	Amount pearlite
4	Amount bainite
5	Amount martensite
6	Vickers hardness
7	Yield stress

**Remark 2:** To exclude a phase from the simulation, set the start temperature of that phase to zero

**Remark 3:** Note that both strain rate parameters must be set to include the effect. It is possible to use a temperature dependent load curve for both parameters simultaneously or for one parameter keeping the other constant.

**Remark 4:** TUNIT is time units per hour and is only used for calculating the Vicker Hardness, as default it is assumed that the time unit is seconds. If other time unit is used, for example milli seconds, then TUNIT must be changed to  $TUNIT = 3.6 \cdot 10^6$

**Remark 5:** With the CRSH = 1 option it is now possible to transfer the material properties from a hot stamping simulation (CRSH = 0) into another simulation. The CRSH = 1 option reads a *dynain* file from a simulation with CRSH = 0 and keeps the amount of austenite, ferrite, pearlite, bainite and martensite constant. This will allow steels with inhomogeneous strength to be analysed in, for example, a crash simulation. The speed with the CRSH=1 option is comparable with \*MAT\_024.



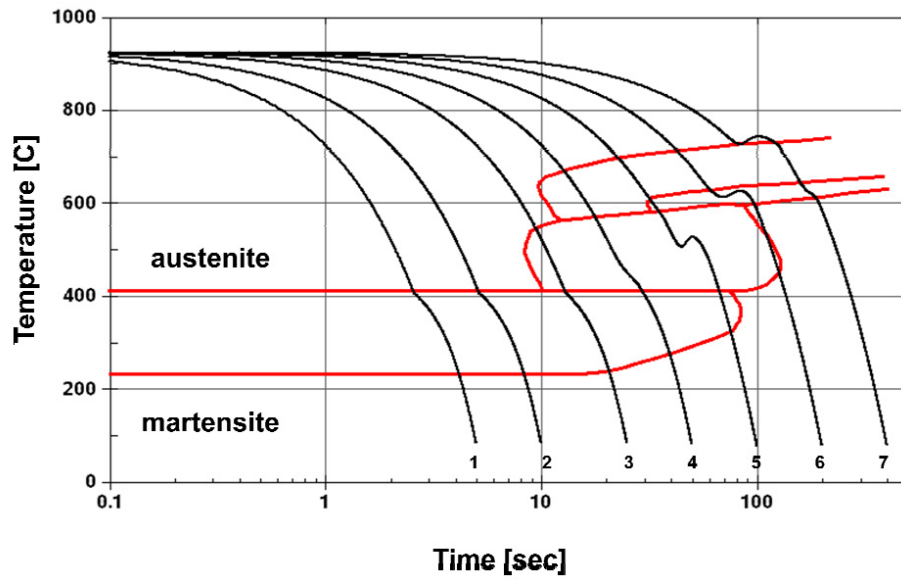
## References

1. Numisheet 2008 Proceedings, The Numisheet 2008 Benchmark Study, Chapter 3, Benchmark 3, Continuous Press Hardening, Interlaken, Switzerland, Sept. 2008.
2. P. Akerstrom & M. Oldenburg, "Austenite Decomposition During Press hardening of a Boron Steel – Computer Simulation and Test", Journal of Material processing technology, 174 (2006), pp399-406.
3. D.F. Watt, "An Algorithm for Modelling Microstructural Development in Weld heat-Affected Zones (Part A) Reaction Kinetics", Acta metal. Vol. 36., No. 11, pp. 3029-3035, 1988.
4. ThyssenKrupp Steel, "Hot Press hardening Manganese-boron Steels MBW", product information Manganese-boron Steels, Sept. 2008.
5. Sjostrom & Akerstrom (1982)
6. Malek Naderi, "Hot Stamping of Ultra High Strength Steels", Doctor of Engineering Dissertation, Technical University Aachen, Germany, 2007.
7. P. Akerstrom, "Numerical Implementation of a Constitutive model for Simulation of Hot Stamping", Division of Solid Mechanics, Lulea University of technology, Sweden.
8. Malek Naderi, "A numerical and Experimental Investigation into Hot Stamping of Boron Alloyed Heat treated Steels", Steel research Int. 79 (2008) No. 2.

## Boron steel composition from the literature.

	HAZ code	Akerstrom (2)	Naderi (8)	ThyssenKrupp(4) (max amount)
B		0.003	0.003	0.005
C	0.168	0.23	0.230	0.250
Co				
Mo	0.036			0.250
Cr	0.255	0.211	0.160	0.250
Ni	0.015			
Mn	1.497	1.25	1.18	1.40
Si	0.473	0.29	0.220	0.400
V	0.026			
W				
Cu	0.025			
P	0.012	0.013	0.015	0.025
Al	0.020			
As				
Ti			0.040	0.05
S		0.003	0.001	0.010

**CCT Diagram for 22MnB5 from Naderi [6]  
Cooling curves 1-7 calculated using LS-DYNA.**



	Cooling Rate [C/sec]	Vickers Hardness LS-DYNA	Vickers Hardness M. Naderi [6]
1	200	478	---
2	100	472	471
3	40	459	428
4	20	376	383
5	10	273	240
6	5	174	184
7	2.5	172	165

\*KEYWORD

\$

\$ UNITS: ton - mm - sec - N - MPa

\$

\*MAT\_UHS\_STEEL

\$	MID	RHO	E	PR	TUNIT	CRSH	PHASE	
	10	7.83e-9	1.00e+05	0.3	3600.0	0	0	
\$	LCY1	LCY2	LCY3	LVY4	LCY5	KFER	LPER	B
	100	200	300	400	500	1.9e5	3.1e3	0.004
\$	C	Co	Mo	Cr	Ni	Mn	Si	V
	.22	0.	0.02	.200	0.02	1.23	.25	0.008
\$	W	Cu	P	Al	As	Ti		
	0.	0.03	0.008	0.03	0.	0.037		
\$	THEXP1	THEXP2	LCTH1	LCTH2	TREF	LAT1	LAT2	
	26.E-6	11.E-6	0	0	293.15	590.e+00	640.e+00	
\$	QR2	QR3	QR4	ALPHA	GRAIN			
	11322	17300	15039	0.011	6.8			
\$	PLMEM2	PLMEM3	PLMEM4	PLMEM5	STRC	STRP		
	0.0	0.0	0.0	0.0	0.0	0.0		

\$ Austenite hardening curve

\*DEFINE\_CURVE

\$#	lcid	sidr	sfa	sfo	offa	offo	dattyp
-----	------	------	-----	-----	------	------	--------

	100	0	1.000000	1.000000			
--	-----	---	----------	----------	--	--	--

\$#		a1		o1			
-----	--	----	--	----	--	--	--

		0.000		111.5000000			
	5.0000002e-04			111.6999969			
	0.0010000			111.9000015			
	0.0015000			112.0999985			
	0.0020000			112.3000031			
	0.0050000			113.5000000			
	0.0100000			115.4000015			
	0.0150000			117.3000031			
	0.0200000			119.1999969			
	0.0250000			121.0000000			
	0.0300000			122.8000031			
	0.0350000			124.5000000			
	0.0400000			126.0999985			
	0.0450000			127.8000031			
	0.0500000			129.3999939			
	0.0600000			132.3999939			
	0.0700000			135.3000031			
	0.0800000			138.0000000			
	0.0900000			140.6000061			
	0.1000000			143.1000061			
	0.1100000			145.3999939			
	0.1300000			149.6999969			
	0.1500000			153.6000061			
	0.1700000			157.1000061			
	0.1900000			160.3000031			
	0.2100000			163.1000061			
	0.2300000			165.6999969			
	0.2500000			168.0000000			
	0.2700000			170.0000000			
	0.2900000			171.8999939			
	0.3100000			173.5000000			
	0.3300000			175.0000000			
	0.3500000			176.3999939			
	0.3700000			177.6000061			
	0.3900000			178.6999969			
	0.4100000			179.6999969			
	0.4300000			180.6000061			
	0.4500000			181.3999939			
	0.4700000			182.1000061			

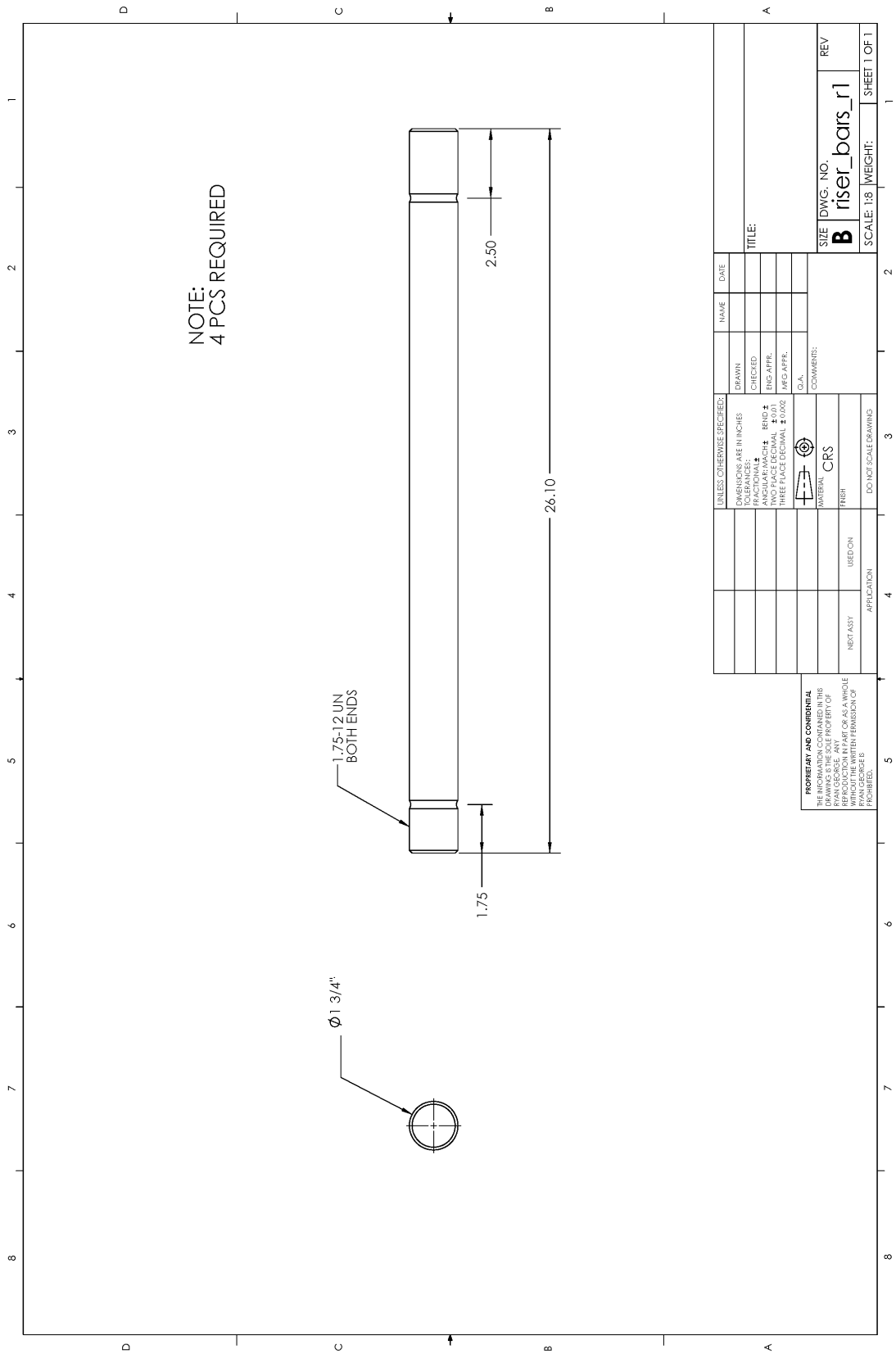
```

0.4900000      182.6999969
0.5000000      183.0000000
$ Ferrite hardening curve
*DEFINE_CURVE
$#   lcid      sidr      sfa      sfo      offa      offo      dattyp
      200        0  1.000000  1.000000
$#           a1           o1
      0.000      180.0000000
      0.020      285.0000000
      0.0400000  342.0000000
      0.0600000  371.0000000
      0.0800000  400.0000000
      0.1000000  428.0000000
      0.1200000  442.0000000
      0.1400000  457.0000000
      0.2000000  485.0000000
      0.3000000  542.0000000
$ Pearlite hardening curve
*DEFINE_CURVE
$#   lcid      sidr      sfa      sfo      offa      offo      dattyp
      300        0  1.000000  1.000000
$#           a1           o1
      0.000      371.0000000
      0.020      568.0000000
      0.060      615.0000000
      0.080      771.0000000
      0.100      800.0000000
      0.120      828.0000000
      0.140      842.0000000
      0.160      857.0000000
      0.200      865.0000000
$ Bainite hardening curve
*DEFINE_CURVE
$#   lcid      sidr      sfa      sfo      offa      offo      dattyp
      400        0  1.000000  1.000000
$#           a1           o1
      0.000      657.0000000
      0.010      940.0000000
      0.020      960.0000000
      0.060     1071.0000000
      0.080     1128.0000000
      0.100     1171.0000000
      0.120     1200.0000000
      0.140     1228.0000000
      0.160     1242.0000000
      0.180     1250.0000000
      0.200     1256.0000000
$ Martensite hardening curve
*DEFINE_CURVE
$#   lcid      sidr      sfa      sfo      offa      offo      dattyp
      500        0  1.000000  1.000000
$#           a1           o1
      0.0        750.0
      0.01       1406.25
      0.02       1656.25
      0.03       1781.25
      0.045      1968.75
      0.05       2031.25
      0.06       2062.50
*END

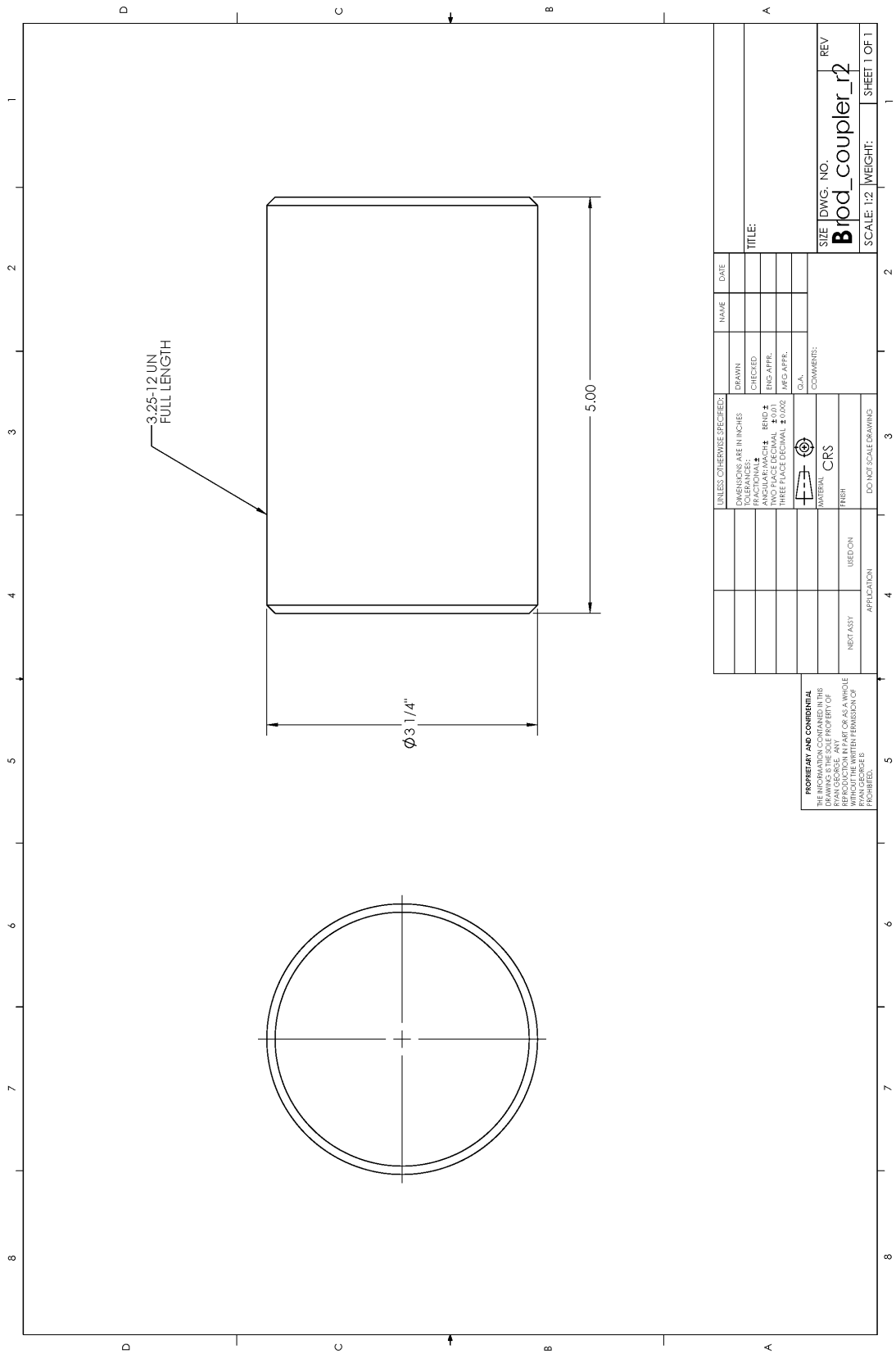
```

**Appendix C – Press Modification CAD**







UNLESS OTHERWISE SPECIFIED:		NAME	DATE
DRAWN			
CHECKED			
ENG. APPR.			
DATE			
UNLESS OTHERWISE SPECIFIED:		COMMENTS:	
DIMENSIONS ARE IN INCHES			
TOLERANCES:			
FRACTIONAL ± 0.005			
DECIMAL ± 0.010			
THREE PLACE DECIMAL ± 0.002			
ANGLE ± 0.002			
FINISH			
CRS			
DO NOT SCALE DRAWING			
APPLICATION			
NEXT ASSY			
USED ON			
<p>PROPRIETARY AND CONFIDENTIAL</p> <p>THIS INFORMATION CONTAINED IN THIS DRAWING IS THE PROPERTY OF RYAN GEORGE ANY REPRODUCTION OR TRANSMISSION OF THIS INFORMATION IN ANY FORM OR BY ANY MEANS WITHOUT THE WRITTEN PERMISSION OF RYAN GEORGE IS PROHIBITED.</p>		<p>SIZE DWG. NO.</p> <p><b>B</b> riser_bars_r1</p> <p>SCALE: 1:8 WEIGHT:</p>	<p>REV</p> <p>SHEET 1 OF 1</p>



3.25-12 UN  
FULL LENGTH

$\varnothing 3 \frac{1}{4}$ "

5.00

UNLESS OTHERWISE SPECIFIED:		DRAWN	NAME	DATE
DIMENSIONS ARE IN INCHES		CHECKED		
FRACTIONAL DIMENSIONS: 1/16, 1/8, 1/4, 3/8, 1/2, 5/8, 3/4, 7/8				
DECIMAL DIMENSIONS: 0.0005, 0.001, 0.002, 0.005, 0.010, 0.015, 0.030, 0.050, 0.100, 0.150, 0.300, 0.500				
TOLERANCES: ±0.001, ±0.002, ±0.005, ±0.010, ±0.015, ±0.030, ±0.050				
SURFACE FINISH: UNLESS OTHERWISE SPECIFIED, ALL SURFACES SHALL BE FINISHED TO A MAXIMUM RUGHOSS OF 32 RMS				
MATERIAL:  CRS				
FINISH:  FRB				
DO NOT SCALE DRAWINGS				
NEXT ASSY		APPLICATION		
<p><b>PROPRIETARY AND CONFIDENTIAL</b></p> <p>THE INFORMATION CONTAINED IN THIS DRAWING IS THE PROPERTY OF RYAN GEORGE ANY REPRODUCTION OR TRANSMISSION OF THIS INFORMATION WITHOUT THE WRITTEN PERMISSION OF RYAN GEORGE IS PROHIBITED.</p>		<p>SIZE DWG. NO. REV</p> <p><b>Brod_coupler_r2</b></p> <p>SCALE: 1:2 WEIGHT: SHEET 1 OF 1</p>		





## Appendix D – Press Operation Procedures

This appendix outlines the procedures for operating the press and hydraulics to form a part. **Please read and understand the entire section before attempting to do anything.**

The LabView program was written by Neil Griffett, and the wiring and controls were performed by Andy Barber.

**Note:** Before forming a part, ensure that the die has been aligned properly as outlined in section 3.1 of this thesis.

**Safety Note:** Always ensure die stops are in position before reaching within the press.

### Manual Operation:

1. Hydraulics & Controller. Open the main hydraulic valve which feeds the Hot Forming press and accumulators. Ensure the MTS FlexTest SE controller is on. If not, please contact a lab technician for assistance.
2. Status & Setpoint. Check to see if the Status Menu is active, if not, press the Status Button. Press the Setpoint Button to activate the setpoint dialog.

### MTS FlexTest SE Controller



Status Menu

Setpoint button

Status Button

3. Turn on the Hydraulic Power Unit (HPU) to “Low”. The pump should turn on. Now turn the HPU to “High”. To turn on the servo valve (to start moving the press), turn the Hydraulic Servo Module (HSM) to “Low”. Turning to “High” is not necessary.

## MTS FlexTest SE Controller

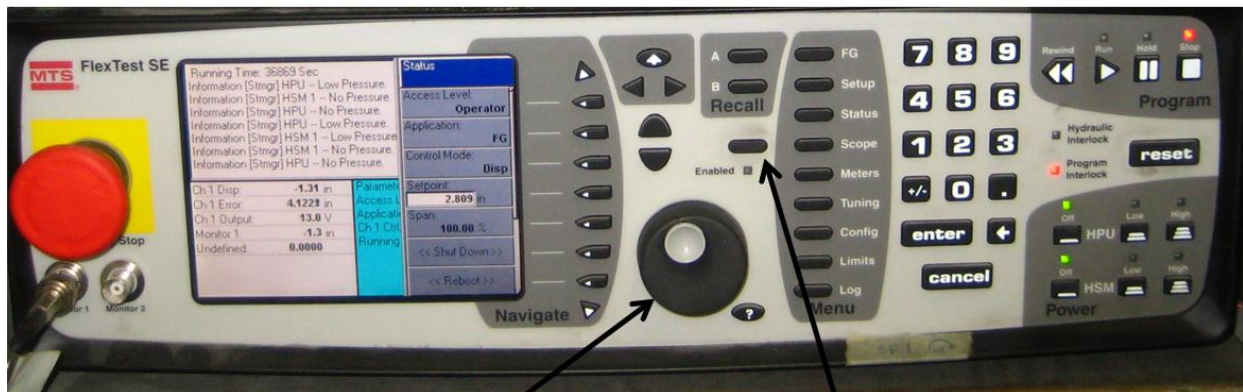


HPU controls

HSM controls

4. Manually operate the press. Press the “Enabled” button to turn on/off manual setpoint control. Turn the dial to move the press up or down.

## MTS FlexTest SE Controller



Setpoint dial

Enabled

5. To turn off the press, first set both the HPU and HSM to “Low”. Then turn the HSM “Off” and then the HPU to “Off”. The press is essentially “locked out” and work may be performed within. **Note: Move the slide to fully open or fully closed before turning the HSM off. If this is not done, the press will “bang” and you might wet yourself.**

### Automatic Operation:

1. Follow the same instructions as outlined in “Manual Operation” to turn the HPU and HSM on. Move the press slide all the way to the top. Press “Reset” to reset all of the interlocks. Press “Run” on the Program Controls to enable the controller to automatic operation. The controller is now waiting on signals from the LabView program.

## MTS FlexTest SE Controller

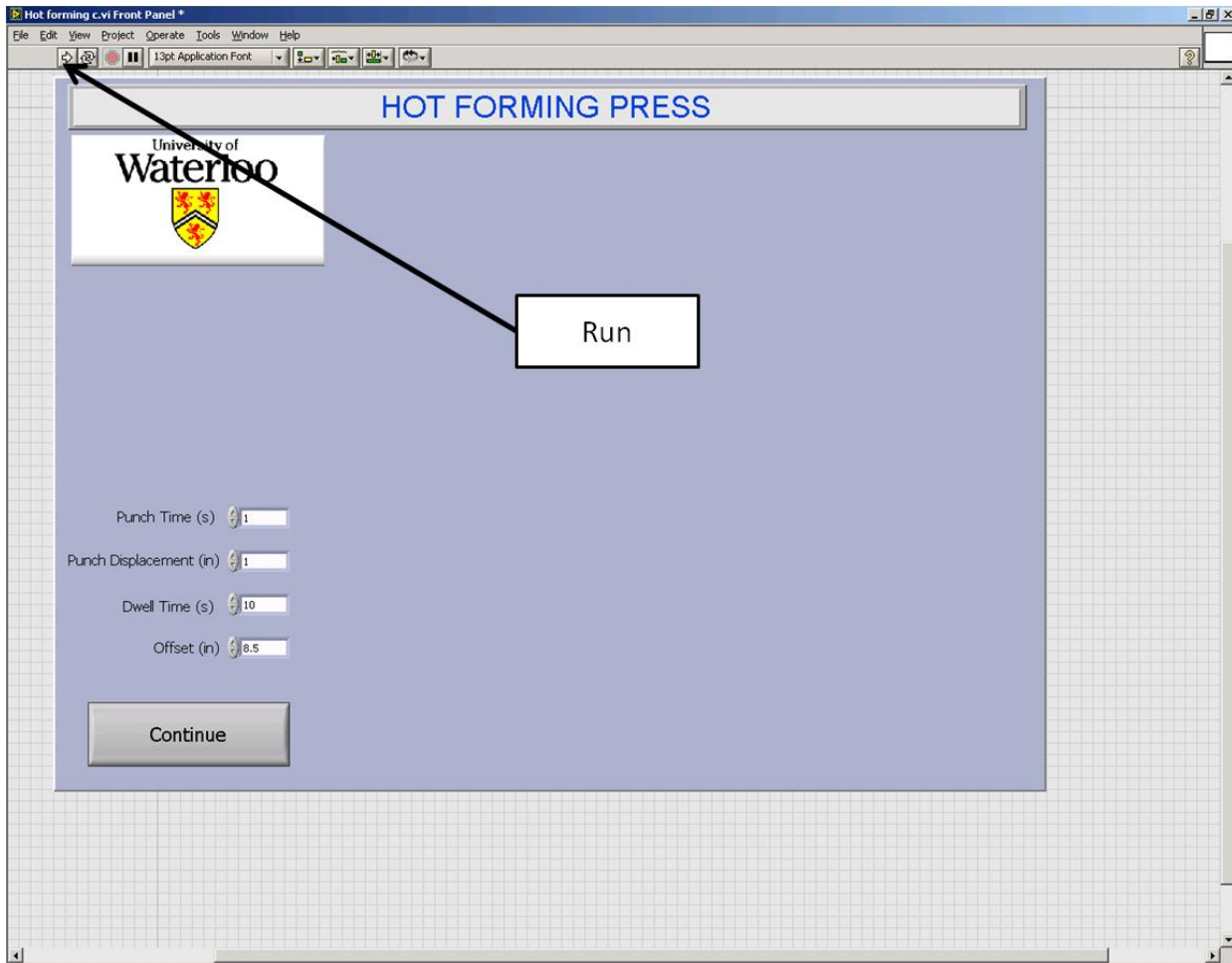


Program Controls

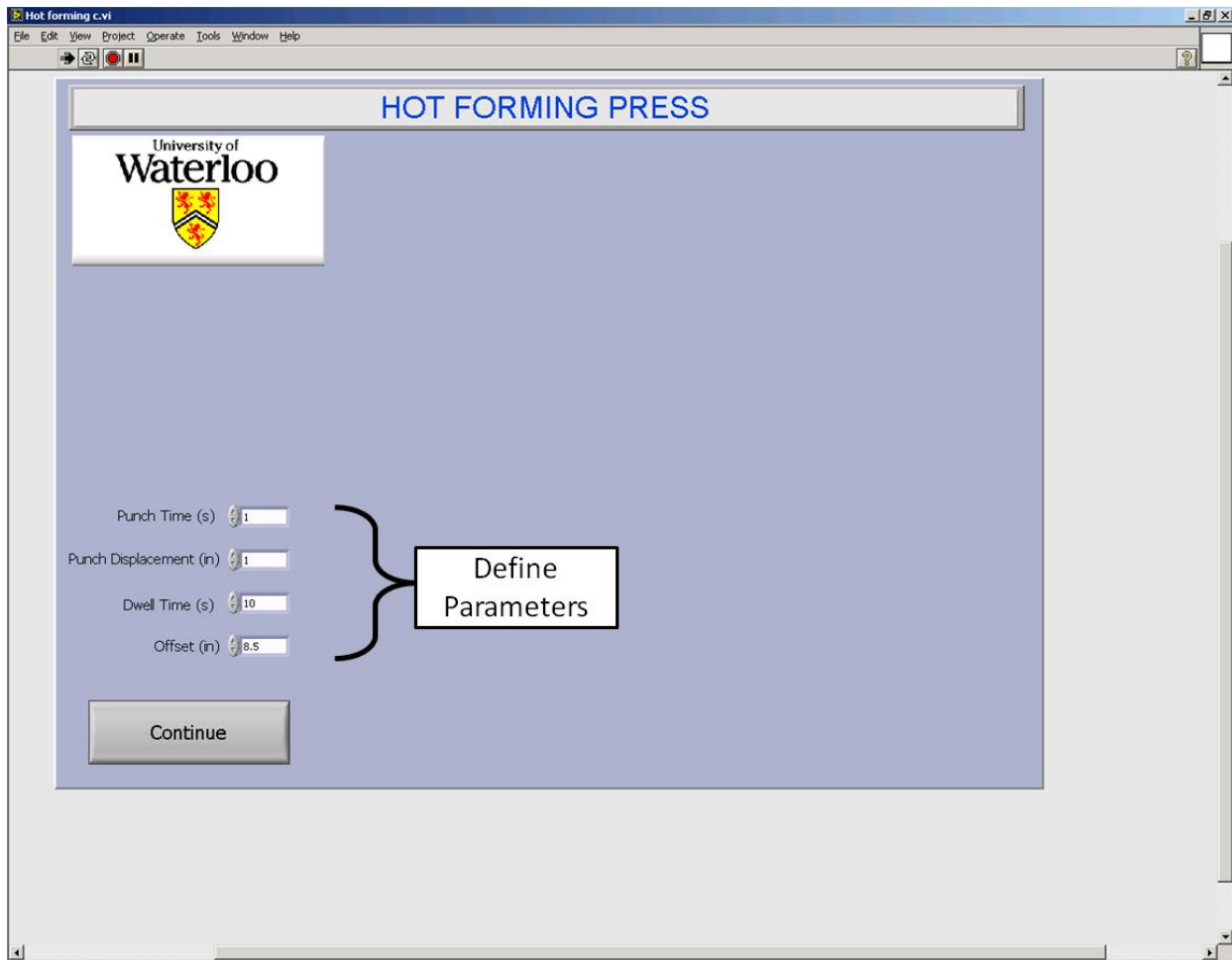
Interlock status

Reset

2. Open the "Hot Forming" LabView program on the desktop. Press the "Run" button to activate the program and to enter in the required parameters.



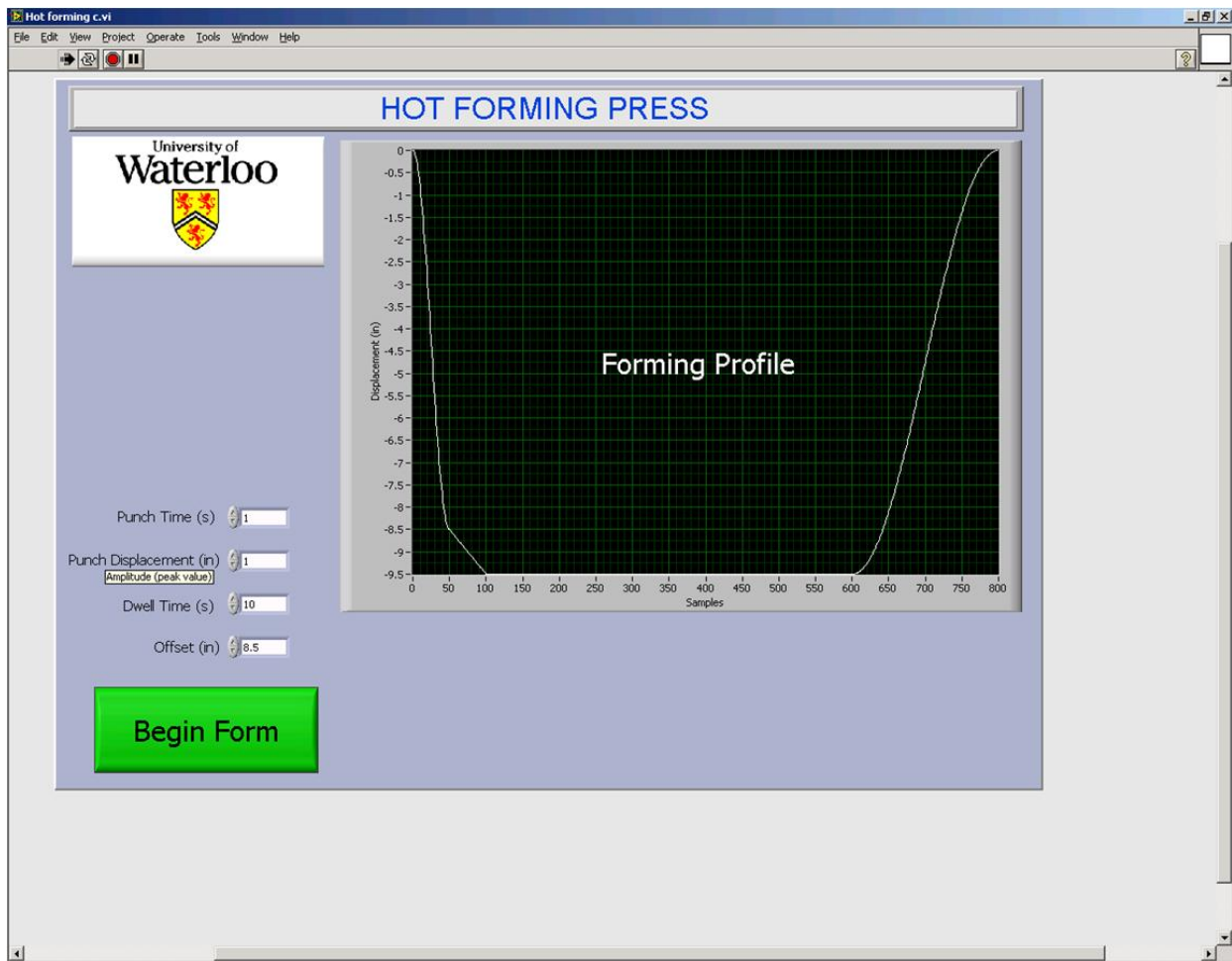
3. Define the parameters for the press speed and displacement. "Offset" is the initial displacement of the punch to move it as quickly as possible to the working height. This displacement always occurs over the period of 1 second. The "Punch Displacement" is the final stroke of the punch to bring it fully closed. This displacement will occur over the amount of time defined in "Punch Time". The "Dwell" parameter is the amount of time the press will be fully closed before opening back to the home position (position = 0). There is currently no user control of the speed of the punch retraction. Press "Continue" when ready to proceed.



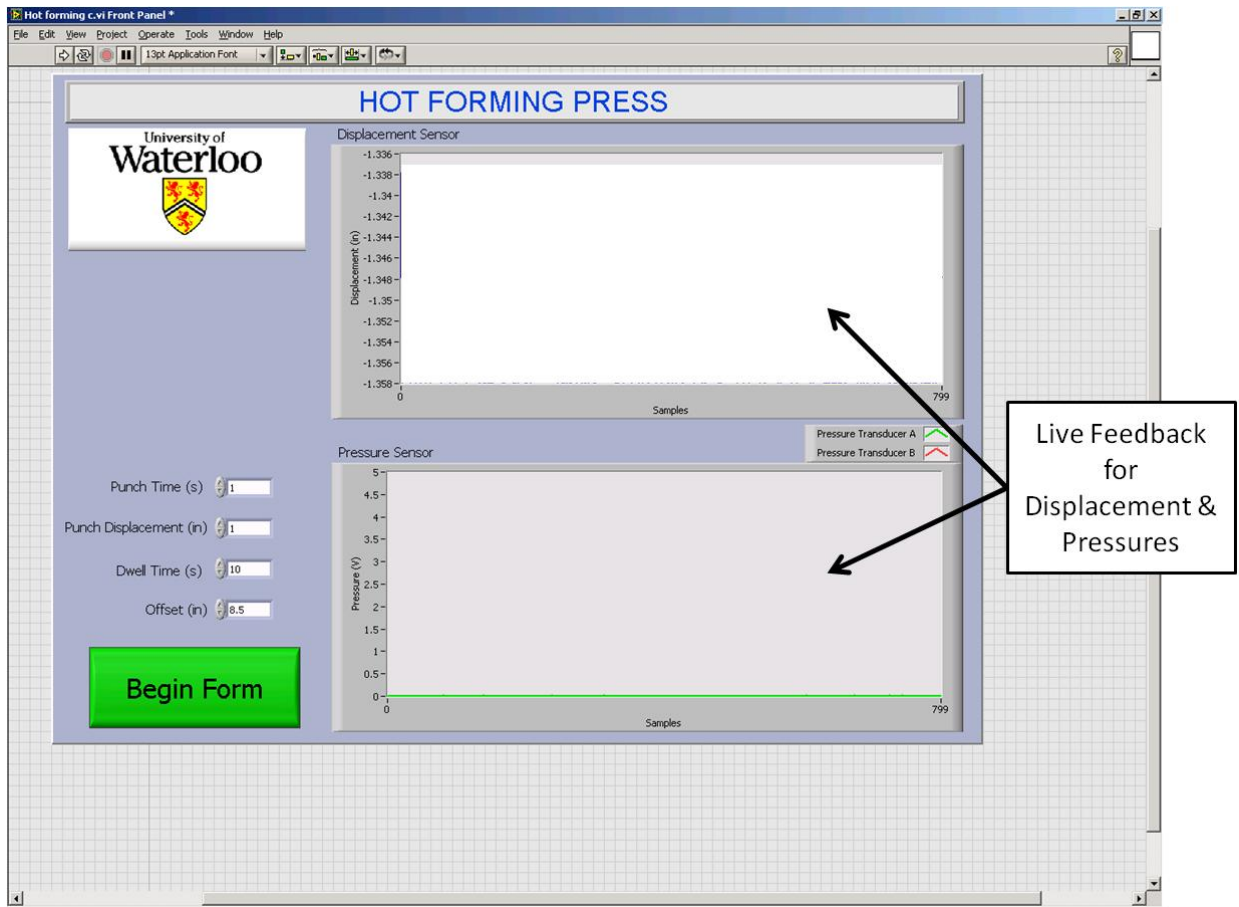
4. **Warning: Pressing "Begin Form" will cause the punch to move very quickly. Do not press it until you are absolutely ready.** You will see a graph of the Forming Profile which represents the punch Displacement vs Time, for reference. When you are ready to form the part, there are two options to choose from:
  - a. Place the blank into the tooling via the transfer system and ensure the transfer cart is in its locked position. Press the "Begin Form" button and the press will actuate and form the part. This is the slowest method, as it requires you to go to the computer to press the button. If time is critical (ie. Hot forming experiments), this may not be the preferred option.



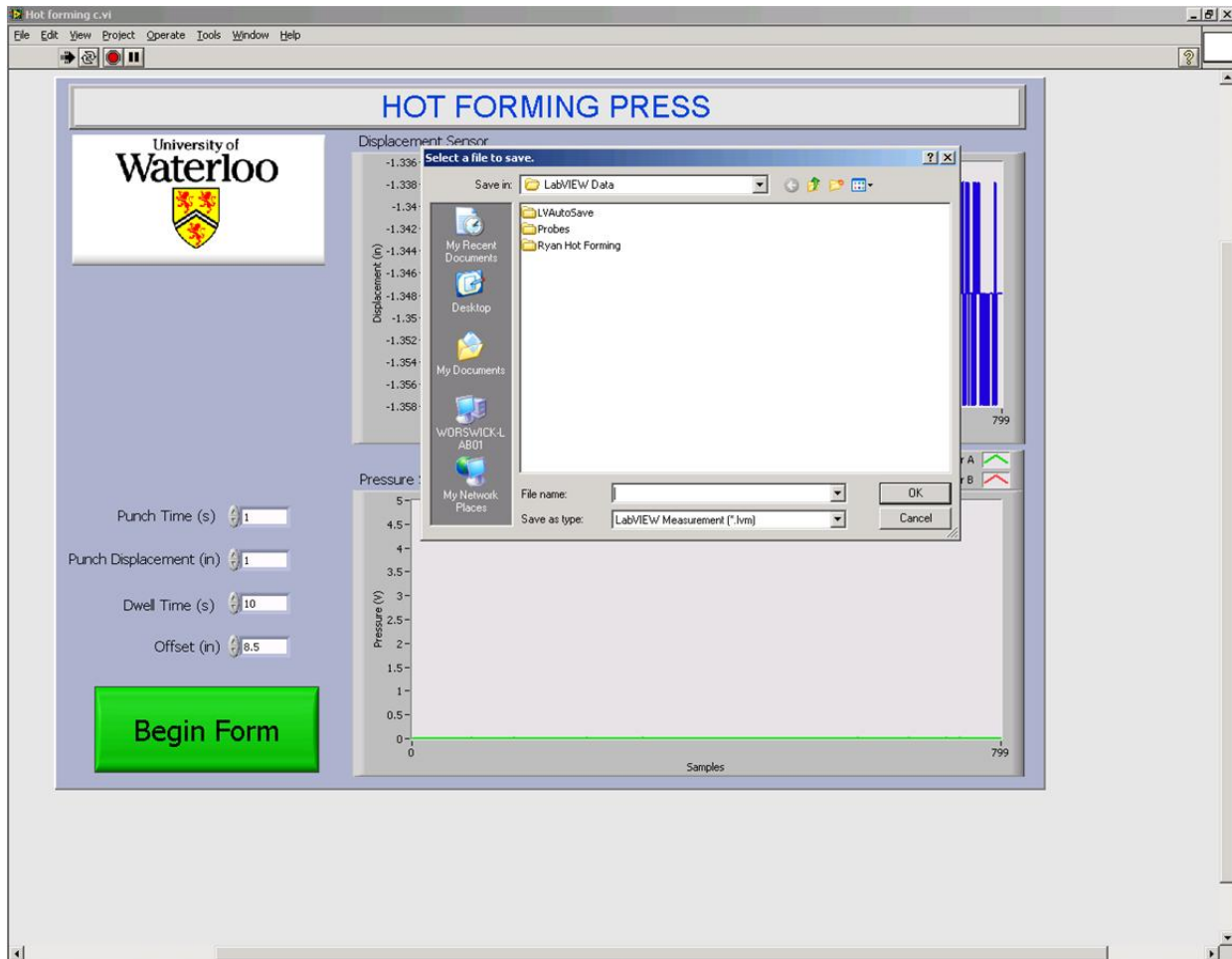
- b. If timing is more important, move the transfer cart out of the locked position to deactivate the microswitch. There is a microswitch which tells LabView if the cart is in the home position. Press the “Begin Form” button. Note that the press will not actuate until the cart is back in home position and the microswitch is tripped. Use the transfer cart to place the blank into the tooling and move the transfer cart back to the home position. The press will actuate and form the part. This microswitch is in place to ensure that the press does not actuate while the transfer cart is inside the press. **Note: When in manual control mode, it is still very possible to damage the cart or anything else between the tools!**



5. While the punch is moving and the program is running, there will be a live feedback on the screen which shows the punch displacement and the pressure readings from the two transducers.



- After the program has finished, a “Save” dialog will appear to save the displacement and pressure data to a text file. Note that the sampling rate is currently 50 samples per second. To form another part, simply press the “Run” button in step 2 and continue. To finish testing, simply exit the LabView program and follow the instructions in Manual Operation above to turn off the hydraulics.



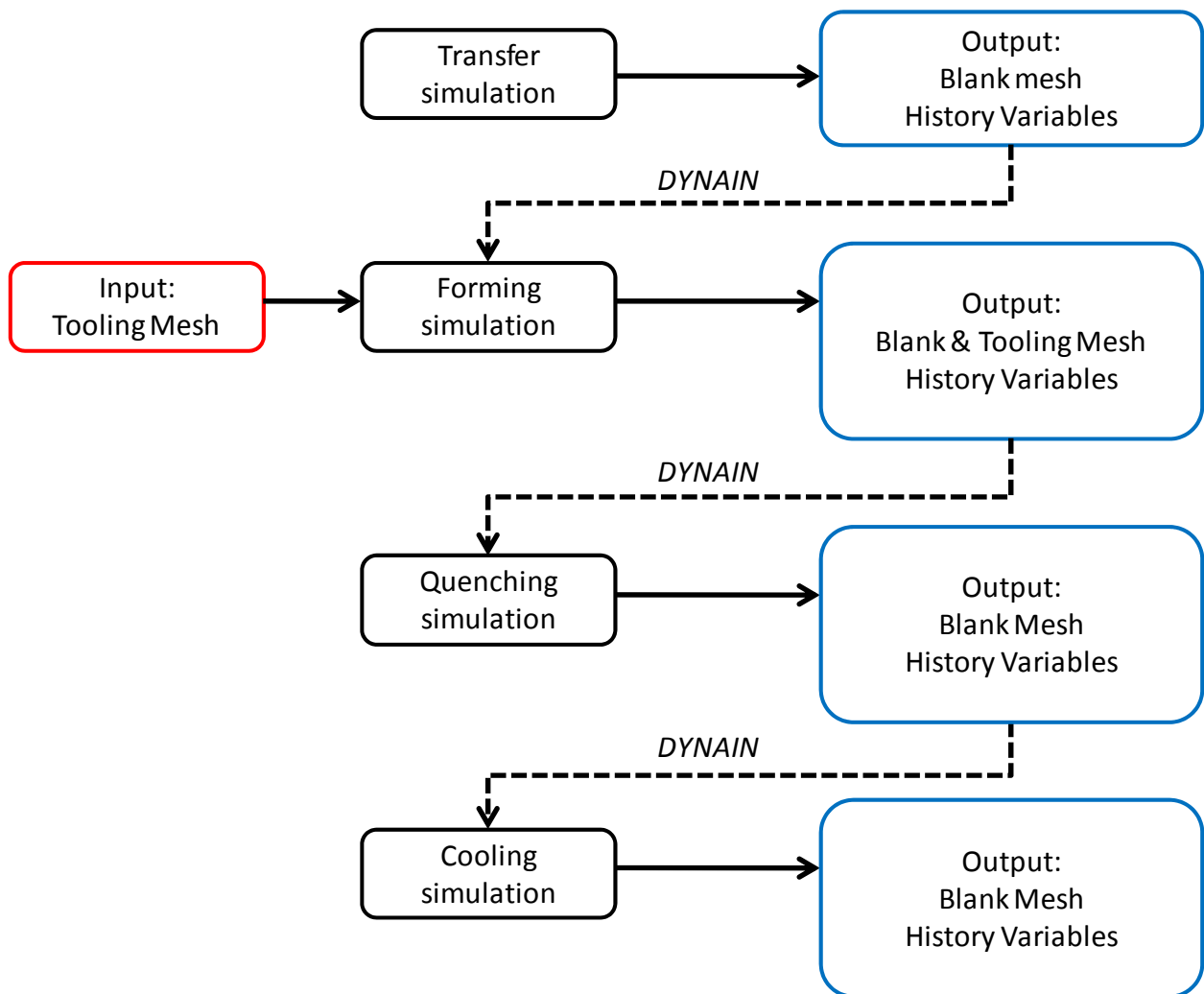
**Additional Notes:**

- The Light Curtain will trip the “Program Interlock” feature, and must be reset if planning to run in automatic mode.
- While the press is running the program, tripping the light curtain or moving the transfer cart out of the home position will cause the press to open.



## **Appendix E – LS-DYNA Simulation Steps**

This appendix outlines in more details the simulation steps performed in LS-DYNA. A total of four simulations are performed for a given trial. Refer to the flowchart below for a visual representation. The first simulation is a free-air cooling simulation where the blank loses temperature due to convection and radiation while it passes from the furnace to the press. The final temperature and all other history variables for the blank are passed to the Forming Simulation through the DYNAIN file. During the forming simulation, the tooling mesh and boundary conditions are introduced and the blank undergoes significant deformation to the final shape. All data from the blank and tooling is passed to the next simulation. During the Quenching Simulation the full tonnage is applied to the blank and it is quenched for 4 or 10 seconds, depending on the trial. After this simulation, the tooling is no longer required, and only the data for the blank is passed on. The final simulation is the cooling of the formed and quenched blank down to room temperature due to convection and radiation from the air.



## **Appendix F – Convection and Radiation Parameters**

The following graph represents the convective heat transfer coefficient,  $h$ , and surface emissivity,  $\epsilon$ , as a function of blank temperature. This curve is input to LS-DYNA for the purposes of free-air cooling of the blank. The convection coefficient was calculated using standard equations as given in [32], and the emissivity was used to calibrate the numerical and experimental cooling results.

